SAFEGUARD OF MITOSIS: THE SPINDLE CHECKPOINT

APPROVED BY SUPERVISORY COMMITTEE

_____
Hongtao Yu, Ph.D. (Mentor)

_____
Zhijian “James” Chen, Ph.D. (Chair)

_____
Melanie H. Cobb, Ph.D.

_____
Luke Rice, Ph.D.

DEDICATION

I would like to acknowledge my mentor Dr. Hongtao Yu for his terrific guidance and continuous support. His dedication to scientific researches and his envision of sciences have largely influenced my understanding and altitudes towards scientific researches. He works closely with every student and postdoc in the lab, discussing the details of experiment designs and data analyses. He also gives opportunities to everyone in lab, encouraging them to pursue their own interests independently. I have learned a lot from him about how to become independent and how to be a great scientist. I would also like to thank my thesis committee, Dr. Zhijian "James" Chen, Dr. Melanie Cobb, and Dr. Luke Rice, for their great support and thoughtful advice on my graduate work. In addition, I want to thank all faculty members of the Pharmacology Department at UT Southwestern, for their generous courtesy and helpful discussions.

I would like to acknowledge all the current Yu lab members, as well as several former lab members. Soonjoung Kim has been a great and helpful benchmate. We has discussed and even debated on all aspects of our projects, from technical troubleshoots to future directions. I have been working with Haishan Gao on several projects. He has been always generous and helpful. I have also learned a lot from Bing Li to design and perform sophisticated biochemical assays.

I would like to thank my parents as well as my girlfriend. Their bestowed loves and numerous supports have encouraged me to move forward, even in the hardest time of my life. I could not have accomplished any without their bolster.

SAFEGUARD OF MITOSIS: THE SPINDLE CHECKPOINT

by

ZHEJIAN JI

DISSERTATION

Presented to the Faculty of the Graduate School of Biomedical Sciences

The University of Texas Southwestern Medical Center

In Partial Fulfillment of the Requirements

For the Degree of

DOCTOR OF PHILOSOPHY

The University of Texas Southwestern Medical Center

Dallas, Texas

December, 2016

Copyright

by

ZHEJIAN JI, 2016

All Rights Reserved

SAFEGUARD OF MITOSIS: THE SPINDLE CHECKPOINT

ZHEJIAN JI

The University of Texas Southwestern Medical Center, 2016

Supervising Professor: HONGTAO YU, Ph.D.

In mitosis, the kinetochore-microtubule attachment is under surveillance by the spindle checkpoint to ensure the fidelity of chromosome segregation. Defects in the checkpoint could lead to aneuploidy, which has been implicated in cancers, birth defects, and other human diseases. In presence of kinetochores that are not attached or improperly attached to microtubules, the checkpoint signals to assemble the mitotic checkpoint complex (MCC), which consists of BubR1–Bub3, Mad2, and Cdc20. The diffusible MCC inhibits the ubiquitin ligase activity of the anaphase-promoting complex or cyclosome bound to its co-activator Cdc20 (APC/C^{Cdc20}) to arrest cells in mitosis. Nevertheless, it remains unknown how the checkpoint monitors the status of the kinetochore-microtubule attachment. Neither is clear how MCC is assembled in an active checkpoint signaling. My graduate work has answered these two questions by revealing the critical functions of a checkpoint kinase, monopolar spindle 1 (Mps1), in both attachment sensing and checkpoint signaling.

Of kinetochore proteins, the KMN network acts as both a critical microtubule receptor and a signaling platform for the spindle checkpoint. The human KMN contains the kinetochore null 1 complex (Knl1C), the minichromosome instability 12 complex (Mis12C), and the nuclear division cycle 80 complex (Ndc80C). In my first project, I have shown that the non-kinase domain of Mps1 directly binds to Ndc80C through two independent interactions. Both interactions involve the microtubule-binding surfaces of Ndc80C and are directly inhibited by microtubules. Elimination of one such interaction in human cells causes checkpoint defects expected from a failure in detecting unattached kinetochores. This competition between Mps1 and microtubules for Ndc80C binding thus constitutes a direct mechanism for unattached kinetochore detection.

The next question is how the kinetochore-associated Mps1 kinase rules the checkpoint signaling. At kinetochore, Mps1 phosphorylates the scaffolding protein Knl1. Phosphorylated Knl1 (pKnl1) recruits checkpoint complexes budding uninhibited by benomyl 1–3 (Bub1–Bub3) and Bub1-related protein in complex with Bub3 (BubR1–Bub3) to kinetochores. My following work has demonstrated that Mps1 promotes the inhibition of APC/C^{Cdc20} by MCC components in vitro through phosphorylating Bub1 and mitosis arrest deficiency 1 (Mad1). Phosphorylated Bub1 (pBub1) binds with Mad1–Mad2. Phosphorylated Mad1 (pMad1) directly interacts with Cdc20. Mutations of Mps1 phosphorylation sites in Bub1 or Mad1 abrogate the spindle checkpoint in human cells. Therefore, Mps1 promotes checkpoint activation through a pKnl1-pBub1-pMad1 phosphorylation cascade, in which phosphorylation of upstream components enables binding of downstream ones. We propose that this sequential multi-target phosphorylation cascade allows Mps1 to amplify checkpoint signals and makes the

checkpoint highly responsive to Mps1, which itself is regulated by kinetochore-microtubule attachment.

Taken together, my graduate work has solved two long-standing questions in spindle checkpoint regulation. Accordingly, Mps1 recognizes the unattached kinetochores via its non-kinase domain, while activates the checkpoint signaling through its kinase activity. The dual function of Mps1 couples checkpoint activation with unattached kinetochore detection, making checkpoint under the control of kinetochore-microtubule attachment.

TABLE OF CONTENTS

PRIOR PUBLICATIONS

Ji, Z.*, Gao, H.*, Jia, L., Li, B., and Yu, H. (2016). A sequential multi-target Mps1 phosphorylation cascade promotes spindle checkpoint signaling. *Submitted*.

Ji, Z., Gao, H., and Yu, H. (2015). CELL DIVISION CYCLE. Kinetochore attachment sensed by competitive Mps1 and microtubule binding to Ndc80C. Science *348*, 1260-1264.

Ji, Z., and Yu, H. (2014). A protective chaperone for the kinetochore adaptor Bub3. Developmental cell *28*, 223-224.

Wu, N., Kong, X., **Ji, Z.**, Zeng, W., Potts, P.R., Yokomori, K., and Yu, H. (2012). Scc1 sumoylation by Mms21 promotes sister chromatid recombination through counteracting Wapl. Genes & development *26*, 1473-1485.

LIST OF FIGURES

LIST OF DEFINITIONS

AAA – ATPases Associated with diverse cellular Activities
ABBA – motif in cyclin A, BubR1, Bub1, and Acm1
APC/C – anaphase-promoting complex
B56 – protein phosphatase 2A 56-kDa regulatory subunit
Bir – baculovirus inhibitor of apoptosis protein repeat
BSA – bovine serum albumin
Bub1 – budding uninhibited by benomyl 1
Bub3 – budding uninhibited by benomyl 3
BubR1 – Bub1-related 1
CBB – Coomassie brilliant blue
CCAN – Constitutive centromere-associated network
Cdc20 – cell division cycle 20
Cdh1 – Cdc20 homolog 1
Cdk1 – cyclin-dependent kinase 1
Cdt1 – chromatin licensing and DNA replication factor 1
CENP – centromere protein
CH domain – calponin homology domain
CM – conserved motif
CPC – chromosome passenger complex
CREST – calcinosis, Raynaud's phenomenon, esophageal dysmotility, sclerodactyly, telangiectasia
CTD – C-terminal domain
C-Mad2 – closed Mad2
D box – destruction box
DAPI – 4',6-diamidino-2-phenylindole
Dsn1 – dosage suppressor of NNF1
GLEBS – Gle2-binding sequence
GTB – general tubulin buffer
Hec1 – highly expressed in cancer 1
I-Mad2 – intermediate Mad2
INCENP – inner centromere protein
IPTG – isopropyl β-D-1-thiogalactopyranoside
ITC – isothermal titration calorimetry
K_d – dissociation constant
KEN box – lysine-glutamate-asparagine motif
KI motif – lysine-isoleucine motif
KMN network – complex of Knl1C, Mis12C, and Ndc80C

Knl1 – kinetochore null 1
KT – kinetochore
Mad1 – mitotic arrest deficiency 1
Mad2 – mitotic arrest deficiency 2
MCC – mitotic checkpoint complex
MELT – methionine-glutamate-leucine-threonine motif
MIM – Mad2-interacting motif
Mis12 – minichromosome instability 12
Mps1 – monopolar spindle 1
MR – middle-region motif
MST – microscale thermophoresis
MT – microtubule
MTBD – microtubule-binding domain
Ndc80C^{bonsai} – a miniaturized Ndc80C comprising mostly the head domains of its four subunits
Nnf1 – necessary for nuclear function 1
Nsl1 – Nnf1 synthetic lethal 1
NTE – N-terminal extension
Nuf2 – Nuclear filament-containing protein 2
O-Mad2 – open Mad2
PCR – polymerase chain reaction
Phe box – phenylalanine-containing motif
Plk1 – polo-like kinase 1
PP1 – protein phosphatase 1
PP2A – protein phosphatase 2A
RING – really interesting new gene
RLK – arginine-leucine-lysine motif
ROD – Rough deal homolog
RVSF – arginine-valine-serine-phenylalanine motif
RWD – RING finger-containing proteins, WD-repeat-containing proteins, and yeast DEAD (DEXD)-like helicases
RZZ – Rod-Zwilch-ZW10 complex
Ska – spindle-kinetochore associated protein
Spc24 – spindle component 24
Spc25 – spindle component 25
TPR – tetratricopeptide repeat
TRIP 13 – Thyroid receptor-interacting protein 13
Uba1 – Ubiquitin-activating enzyme E1
UbcH10 – Ube2C, Ubiquitin-conjugating enzyme E2 C
Ube2S – Ubiquitin-conjugating enzyme E2 S

CHAPTER I: INTRODUCTION

Cell division is an essential process for proliferation and development of all cellular organisms. During eukaryotic cell division, the duplicated chromosomes are segregated evenly into two daughter cells through their kinetochore-mediated attachment to microtubules. To ensure the fidelity of chromosome segregation, the kinetochore-microtubule attachment is closely monitored by a surveillance mechanism called the spindle checkpoint (Foley and Kapoor, 2013; Jia et al., 2013; Musacchio, 2015; Sacristan and Kops, 2015). It senses kinetochores that are not attached or improperly attached to spindle microtubules, and delays anaphase onset until all kinetochores are correctly attached. Errors in this process could cause precocious chromosome separation and lead to aneuploidy, which has been implicated in cancer, birth defects, and other human diseases (Gorbsky, 2015; Holland and Cleveland, 2012).

ARCHITECTURE OF KINETOCHORE

Kinetochore is a multi-protein complex assembled at centromeric chromatins. It functions as a bridge to connect centromeric DNA with spindle microtubules (Cleveland et al., 2003). Although DNA at the centromeres do not share a sequence-wise similarity across species, the centromeric chromatics are featured by nucleosomes containing a centromere-specific histone H3 variant, CENP-A (Earnshaw and Rothfield, 1985). Deposition of CENP-A nucleosome is not only required but also sufficient to assemble a

functional kinetochore at any chromosome regions (Heun et al., 2006; Mendiburo et al., 2011; Saffery et al., 2000). Kinetochore can be further divided into inner kinetochore and outer kinetochore.

Inner Kinetochore

The inner kinetochore recognizes CENP-A nucleosomes (Foltz et al., 2006; Okada et al., 2006). It consists of a constitutive centromere-associated network (CCAN), containing CENP-C, -H, -I, -K, -L, -M, -N, -O, -P, -Q, -R, -S, -T, -U, -W, and -X. Besides CENP-C, the rest of CCAN components can be grouped into following sub-complexes: CENP-LN, CENP-HIKM, CENP-TWSX, and CENP-OPQUR. CCAN is deposited after DNA replication, and remains localized at centromeres throughout the cell cycle.

CENP-C and CENP-LN preferentially interacts with the CENP-A nucleosome, not the H3 nucleosome (Carroll et al., 2010; Carroll et al., 2009; Weir et al., 2016). They further recruit CENP-HIKM (Basilico et al., 2014; Klare et al., 2015). In addition, CENP-C directly interacts with CENP-LN (McKinley et al., 2015; Weir et al., 2016), suggesting the formation of a six-subunit tight complex, CENP-CHIKMLN. Importantly, the larger complex of CENP-CHIKMLN binds to CENP-A nucleosomes at a higher affinity comparing to CENP-C or CENP-LN alone (Weir et al., 2016), indicative of a cooperative binding in the CENP-A recognition. CENP-TWSX forms a structure similar to the histone fold, and binds to DNA independent of other CCAN components (Nishino et al., 2012). Nevertheless, the deposition of CENP-TWSX relies on CENP-A (Hori et al., 2008). Moreover, it has been shown that the kinetochore recruitment of CENP-TWSX requires CENP-C and CENP-HIKM (Basilico et al., 2014; Carroll et al., 2010).

Therefore, CENP-CHIKMLN directs the inner kinetochore assembly at the centromeres by recognizing the CENP-A nucleosomes and facilitating the recruitment of other CCAN components (Figure 1-1).

Outer Kinetochore and KMN

On the basis of the inner kinetochore, the outer kinetochore is assembled in order to engage with spindle microtubules. The KMN network is an evolutionarily conserved complex located at the outer kinetochores. It consists of the Knl1 complex (Knl1C), the Mis12 complex (Mis12C), and the Ndc80 complex (Ndc80C). Knl1C contains Knl1 (also known as AF15q14/CASC5/Blinkin, SPC105 in budding yeast, SPC7 in fission yeast, and SPC105R in fly) and Zwint. Mis12C contains Mis12, Nnf1, Nsl1, and Dsn1. Ndc80C contains Hec1 (also named Ndc80), Nuf2, Spc24, and Spc25 (Figure 1-1). The KMN network acts both as a critical microtubule receptor and a signaling platform for spindle checkpoint (Foley and Kapoor, 2013; Jia et al., 2013; Kim and Yu, 2015; Sacristan and Kops, 2015) (See the next sections on kinetochore-microtubule attachment and spindle checkpoint activation). Unlike CCAN, the outer kinetochore is only assembled and recruited during mitosis.

Mis12C is a major hub that lies at the juncture of the inner and outer kinetochores. It binds directly with Knl1 and Ndc80C, as well as CENP-C (Cheeseman et al., 2006; Screpanti et al., 2011). Recent structural analyses reveal that the four subunits of Mis12C form a “Y”-shape helical bundle (Dimitrova et al., 2016; Petrovic et al., 2016). The N-terminal head and connector of Mis12C bind to CENP-C, and are required for the kinetochore recruitment of Mis12C. The Mis12C–CENP-C binding is auto-inhibited by a

flexible loop at the N-terminus of Dsn1. Such an inhibition can be relieved by Aurora B-mediated phosphorylation of the Dsn1 loop (Kim and Yu, 2015). Thus the Aurora B activity promotes the assembly of KMN at kinetochore. The C-terminal tails of Nsl1 and Dsn1 anchor Mis12C to Knl1 and Ndc80C, respectively, in line with the previously reported requirement of the C-terminal region of Nsl1 and Dsn1 in the kinetochore recruitment of Knl1 and Ndc80C (Malvezzi et al., 2013; Petrovic et al., 2010).

The Knl1 subunit is an over 200-kDa protein. The majority region of Knl1 is unstructured, except the C-terminal RWD domain, which interacts with the Nsl1 subunit of Mis12C (Petrovic et al., 2014). This Knl1 RWD–Nsl1 interaction is critical for the kinetochore localization of Knl1 during mitosis. Although Knl1 has a poor sequence similarity among homologs across species, its function and relevant motifs are conserved. At the N-terminal Knl1, there are two PP1-binding motifs (Liu et al., 2010; Rosenberg et al., 2011), as well as two KI motifs that can directly bind with the TPR domains of Bub1 and BubR1 (Kiyomitsu et al., 2007; Krenn et al., 2012). The middle region of Knl1 is composed of multiple MELT motifs. In mitosis, Mps1 phosphorylates the MELT motifs and creates docking sites to recruit Bub1–Bub3 and BubR1–Bub3 to kinetochores (London et al., 2012; Primorac et al., 2013; Shepperd et al., 2012; Yamagishi et al., 2012). Besides the RWD domain, the C-terminal Knl1 contains a putative coiled-coil domain, which has been implicated to bind with Zwint (Kiyomitsu et al., 2007), although the functionality of this interaction has not been characterized.

Ndc80C contains four subunits, each of which has a globular head domain and a long coiled-coil stem (Ciferri et al., 2008). The four coiled-coil stems tightly form a stable complex, whereas the head domains are responsible to interact with binding

partners. The Hec1–Nuf2 heads directly bind with microtubules through the N-terminal tail of Hec1 and the calponin-homology (CH) domains of Hec1 and Nuf2 (Alushin et al., 2012; Ciferri et al., 2008). The Spc24–Spc25 heads directly bind to either Dsn1 of Mis12C or CENP-T in order for Ndc80C to localize to kinetochores (Bock et al., 2012; Malvezzi et al., 2013; Schleiffer et al., 2012). Phosphorylation of CENP-T by Cdk1 enhances its association with Ndc80C (Nishino et al., 2013). Since Dsn1 and CENP-T bind to the same pocket of Spc24–Spc25 head, the Mis12C binding and CENP-T binding are mutually exclusive (Malvezzi et al., 2013; Nishino et al., 2013). There are likely two distinct pools of Ndc80C at kinetochores: one incorporated into KMN that is anchored by CENP-C, and the other bound directly to CENP-T. Both pools of Ndc80C may contribute to the Ndc80C-mediated kinetochore-microtubule attachment.

THE KINETOCHORE-MICROTUBULE ATTACHMENT

KMN Acts as A Microtubule Receptor

The KMN network is a major microtubule receptor at kinetochores (Foley and Kapoor, 2013). A proper kinetochore-microtubule attachment requires the persistent localization of Ndc80C at kinetochore. Ndc80C binds to microtubule through the N-terminal tail of Hec1 and the two CH domains of Hec1 and Nuf2 (Alushin et al., 2012; Ciferri et al., 2008). Deletion or mutation of any of the three greatly compromises microtubule binding, and results in severe chromosome misalignment in cells (Alushin et al., 2012; Zaytsev et al., 2014).

The kinetochore-microtubule attachment is fine tuned by Aurora B kinase throughout mitosis. Aurora B can phosphorylate multiple sites at the N-terminal tail of Hec1, which compromises the Ndc80C-microtubule interaction (Cheeseman et al., 2006; Welburn et al., 2010). Increasing phosphorylation of the Hec1 tail by Aurora B progressively weakens microtubule binding with Ndc80C (Zaytsev et al., 2015; Zaytsev et al., 2014). The phosphorylation of Hec1 tail is high in early mitosis, disfavoring the kinetochore-microtubule binding; whereas it rapidly reduces once the chromosome achieves bi-orientation to stabilize the kinetochore-microtubule attachment (DeLuca et al., 2011). This Hec1 tail phosphorylation is critical for the error correction activity of Aurora B.

Aside from the globular head and the coiled-coil, Hec1 has an internal loop close to the kink region of Ndc80C. Deletion of this Hec1 loop does not cause obvious conformation change according to the electron microscopic analysis (Zhang et al., 2012). Despite being away from the microtubule-binding sites at the Hec1–Nuf2 head, the Hec1 loop is crucial for chromosome alignment (Hsu and Toda, 2011; Maure et al., 2011; Varma et al., 2012; Zhang et al., 2012). This could be due to a direct involvement of Hec1 loop in microtubule binding. Alternatively, the loop may indirectly contribute to the kinetochore-microtubule attachment by recruiting other microtubule-binding factors. In line with the second hypothesis, several studies have attributed the requirement of Hec1 loop to its ability in recruiting its binding partner, such as the Ska complex or the replication licensing protein Cdt1 (Varma et al., 2012; Zhang et al., 2012). But the interaction between the Hec1 loop and the Ska complex was not well established. Neither is clear how Cdt1 contributes to the kinetochore-microtubule attachment. Future work is

needed to decipher functions of the Hec1 loop in microtubule binding and chromosome alignment.

C. elegans Knl-1 has microtubule-binding activity through its N-terminal region. It synergizes with Ndc80C, in context of KMN, to bind with microtubules (Cheeseman et al., 2006). There is no evidence, however, showing the microtubule-binding activity of Knl1 is conserved in other organisms. Moreover, the binding of Knl1 to microtubule appears to be dispensable for load-bearing attachment in *C. elegans* (Espeut et al., 2012). Instead, the N-terminal region of Knl1 contributes to checkpoint silencing through binding to phosphatases.

Indirect Functions of KMN in Microtubule Attachment

KMN not only establishes the direct interactions with microtubules, but also stabilizes the kinetochore-microtubule attachment indirectly by recruiting protein phosphatases to dephosphorylate the Hec1 tail. Knl1 recruits PP1 directly through the N-terminal RVSF motif (Liu et al., 2010). Interestingly, the Knl1 RVSF–PP1 interaction is negatively regulated by Aurora B (Liu et al., 2010). The phosphorylation by Aurora B at the Serine residue of RVSF prevents from PP1 binding. Additionally, Knl1 recruits PP2A to kinetochores through BubR1. Mps1-phosphorylated Knl1 recruits Bub1 and BubR1 (London et al., 2012; Shepperd et al., 2012; Yamagishi et al., 2012). The phosphorylation of BubR1 by Plk1 enables a direct interaction between BubR1 and B56 subunit of PP2A (Suijkerbuijk et al., 2012b; Wang et al., 2016). The accumulation of both PP1 and PP2A can oppose the Aurora B-mediated phosphorylation at the Hec1 tail therefore stabilize the kinetochore-microtubule attachment.

Aside from the recruitment of protein phosphatases to counteract with Aurora B, KMN also recruits other microtubule-binding proteins to strengthen the kinetochore-microtubule attachment. One of the well-known examples is the plus end-directed kinesin protein CENP-E. CENP-E is recruited to kinetochores by the kinetochore-associated Bub1 and BubR1 (Chen, 2002; Johnson et al., 2004). Inactivation of CENP-E leads to unstable kinetochore-microtubule attachment, and results in chromosome missegregation (Kim et al., 2010; Putkey et al., 2002).

Ndc80C is also required for the kinetochore localization of the Ska complex (Welburn et al., 2009), although the recruiting mechanism is still lacking. The Ska complex contains three subunits: Ska1, Ska2, and Ska3. The N-terminal regions of Ska1 and Ska3, together with Ska2, form a three-helical bundle. Two copies of each subunit then assemble into a "W"-shape hetero-hexamer (Jeyaprakash et al., 2012). Each of Ska1 and Ska3 contains a C-terminal microtubule-binding domain (MTBD) that binds with microtubule through electrostatic interactions (Abad et al., 2014). Earlier work has shown that the Ska complex is able to bind with the curved microtubule, suggestive of a key function in recognizing microtubule plus-ends (Welburn et al., 2009). The role of the Ska complex as a microtubule-binding partner, however, has been challenged by a recent study. Sivakumar and coworkers have demonstrated that MTBD of the Ska complex is not essential for chromosome alignment, but rather is crucial for the kinetochore recruitment of protein phosphatase 1 in order to timely silence the spindle checkpoint (Sivakumar et al., 2016). It is possible that the previously observed defects in chromosome alignment caused by depletion of the Ska complex is due to a hyper-active spindle checkpoint, rather than the lack of microtubule-Ska interaction.

A recent study of the budding yeast kinetochores has identified a TOG protein, Stu2, as a key component required for the load-bearing activity of kinetochores (Miller et al., 2016). Stu2 is likely to be recruited to kinetochores through its direct binding with Ndc80C. Only the Stu2-containg kinetochores can tightly bind to microtubules with a continuous pulling force. Therefore Stu2 renders kinetochores able to associate with the shrinking microtubule plus ends.

FUNCTIONS OF KINETOCHORE IN CHECKPOINT ACTIVATION

The activation of spindle checkpoint requires a set of checkpoint proteins, including Mps1, Bub1, Bub3, BubR1, Mad1, and Mad2. They have been initially identified in yeast, and later found conserved in most eukaryotic species. Mps1 and Bub1 are two checkpoint kinases, while BubR1 is believed to be a pseudokinase (Suijkerbuijk et al., 2012a). Especially, Mad3, the yeast homolog of BubR1, does not contain a kinase domain. The Bubs and Mads proteins form three constitutive complexes: Bub1–Bub3, BubR1–Bub3, and Mad1–Mad2. In mitosis, all checkpoint proteins need to be recruited to kinetochores in order to activate the spindle checkpoint.

In presence of unattached or improperly attached kinetochores, Mps1 acts as a master kinase to initiate the checkpoint signaling (Liu and Winey, 2012). The checkpoint signal is transduced by the Bubs and Mads proteins. Several mitotic kinases, such as Cdk1, Aurora B, and Plk1, also modulate the checkpoint signaling by regulating the checkpoint proteins. The downstream effectors of spindle checkpoint include BubR1–

Bub3 and Mad2, which work concomitantly to inhibit the APC/C co-activator, Cdc20, by assembling the mitotic checkpoint complex (MCC). Mad2 can adopt two native conformations: a latent open conformer (O-Mad2), and an active closed conformer (C-Mad2) (Luo et al., 2002; Luo et al., 2004; Sironi et al., 2002). When Mad2 is bound with its partner like Mad1 or Cdc20, it adopts the closed conformation. In human cells, O-Mad2 is converted to C-Mad2 by the active spindle checkpoint signaling, whereas C-Mad2 is turned back to O-Mad2 by the checkpoint-silencing factors $p31^{comet}$ and an AAA-ATPase, Trip13 (Eytan et al., 2014; Ye et al., 2015).

Kinetochore Recruitment of Mps1

Mps1 is an evolutionarily conserved kinase, whose kinase activity is indispensable for checkpoint activation in organisms from yeast to man (Abrieu et al., 2001; Dorer et al., 2005; Hardwick et al., 1996; Kang et al., 2007; Stucke et al., 2002). In early mitosis, Mps1 is recruited to kinetochores in an Ndc80C-dependent manner (Martin-Lluesma et al., 2002; Stucke et al., 2002). In metaphase when most sister chromatids are properly attached by spindle microtubules, Mps1 is released from the kinetochores (Dou et al., 2003). Furthermore, Mps1 is asymmetrically distributed at the kinetochore pair with monotelic attachment (Nijenhuis et al., 2013). It is preferentially enriched at the unattached kinetochores comparing to the kinetochores that are attached by microtubules. Thus, microtubule attachment can release Mps1 from kinetochores.

The kinetochore localization of Mps1 requires an N-terminal extension (NTE) (Nijenhuis et al., 2013). Deletion of NTE abolishes Mps1 localization at kinetochores. Moreover, Mps1 localization is negatively regulated by its own kinase activity, indicative

of a negative feedback regulation (Hewitt et al., 2010; Jelluma et al., 2010; Santaguida et al., 2010). Additionally, the kinase activity of centromeric Aurora B promotes the kinetochore recruitment of Mps1 (Saurin et al., 2011). The mechanism how the kinetochore localization is regulated by these two kinases remains elusive.

Mps1 kinase activity is enhanced by a transphosphorylation at the activation loop, which is required for its checkpoint functions (Kang et al., 2007). It has been proposed that the kinetochore enrichment of Mps1 stimulates its kinase activity by facilitating the transphosphorylation.

Kinetochore Recruitment of CPC (Aurora B)

The chromosome passenger complex (CPC) consists of Aurora B, INCENP, Borealin, and Survivin (Ruchaud et al., 2007). In early mitosis, CPC is predominantly located at inner centromere. The kinetochore-associated Bub1 phosphorylates T120 of histone H2A at its C-terminal tail (Kawashima et al., 2010). The phosphorylated H2A then binds to Shugosin, which can further recruit CPC through its interaction with Survivin (Kawashima et al., 2007; Liu et al., 2015). In parallel, another mitotic kinase Haspin phosphorylates histone H3 at T3 residue (Kelly et al., 2010; Wang et al., 2010). The phosphorylated H3 directly binds to the Bir domain of Survivin, thus contributes to the recruitment of CPC. The two epigenetic markers, phospho-H2A and phospho-H3, therefore coordinate the CPC localization at inner centromere (Yamagishi et al., 2010). As discussed earlier, Aurora B phosphorylates several key components of KMN, such as the RVSF motif of Knl1, the Dsn1 loop of Mis12C, and the Hec1 tail of Ndc80C (Kim and Yu, 2015; Liu et al., 2010; Welburn et al., 2010) (Cheeseman et al., 2006; Welburn et

al., 2010). These Aurora B-mediated phosphorylation events play key roles in assembly of outer kinetochores, correction of erroneous attachment, and strengthening spindle checkpoint. A gradient model has been proposed, where Aurora B is recruited and activated at inner centromere, and diffuses to kinetochore to phosphorylate substrates (Lampson and Cheeseman, 2011). It is likely that a minor pool of CPC exists at outer kinetochore in order to anchor Aurora B with its substrates. This kinetochore pool of CPC, if exist, is expected to be suppressed by tension-generating microtubule attachment.

Kinetochore Recruitment of Bub1–Bub3 and BubR1–Bub3

Bub1, BubR1 and Bub3 are checkpoint proteins downstream of Mps1. Their kinetochore recruitment depends on Knl1 (Kiyomitsu et al., 2007). The TPR domains of Bub1 and BubR1 can directly bind to the KI motifs at the N-terminal Knl1 (Bolanos-Garcia et al., 2011; Kiyomitsu et al., 2011; Krenn et al., 2012). But the TPR–KI interaction plays a marginal role in the kinetochore targeting of Bub1 and BubR1 proteins in human cells (Krenn et al., 2012). Instead, the kinetochore targeting of Bub1 and BubR1 rely on Bub3, Mps1, and the repetitive MELT motifs in the middle region of Knl1. Mps1 phosphorylates MELT and creates docking sites for Bub1–Bub3 and BubR1–Bub3 (London et al., 2012; Primorac et al., 2013; Shepperd et al., 2012; Yamagishi et al., 2012). Aside from being recruited directly through Bub3 and the MELT motifs, BubR1 can also bind to Bub1, which serves as an indirect mechanism for the kinetochore recruitment of BubR1 (Overlack et al., 2015; Zhang et al., 2015). Thus there are two pools of BubR1 at kinetochores, the Knl1 MELT-bound pool and the Bub1-associated pool. A recent study has suggested the Bub1-bound pool of BubR1 supports chromosome

alignment, whereas BubR1 directly recruited by MELT stimulates checkpoint signaling (Zhang et al., 2016).

Kinetochore Recruitment of Mad1 and Mad2

Mad1 contains a coiled-coil N-terminal region and a C-terminal domain (CTD) folding into a structure related to RWD domain (Kim et al., 2012). Mad1 is constitutively associated with C-Mad2 to form a stable complex of Mad1–C-Mad2 throughout the cell cycle. The CTD of Mad1 forms a homodimer (Kim et al., 2012). Thus a hetero-tetramer of Mad1 and C-Mad2 is the prevalent form of Mad1–Mad2 complex.

In mitosis, Mad1–Mad2 is recruited to kinetochores in response to checkpoint signaling. The kinetochore localization of Mad1 depends on Mps1 and Ndc80C (Martin-Lluesma et al., 2002). In yeast, Bub1 recruits Mad1 to kinetochores through a direct interaction with the C-terminal domain of Mad1 (Brady and Hardwick, 2000; London and Biggins, 2014; Mora-Santos et al., 2016). The kinetochore recruitment of Bub1 and the Bub1–Mad1 interaction both involve Mps1-mediated phosphorylation. In metazoans, although Bub1 still contributes to the kinetochore localization of Mad1, the majority of Mad1 at kinetochore is recruited through the metazoan-specific RZZ complex (Karess, 2005; Kim et al., 2012; Vleugel et al., 2015). RZZ is composed of Rod, ZW10, and Zwilch. The recruitment of RZZ relies on Ndc80C as well as an inner kinetochore component CENP-I (Matson and Stukenberg, 2014; Samejima et al., 2015). In *C.elegans*, the RZZ-binding protein Spindly interacts with Mad1 and modulates the kinetochore localization of Mad1 (Yamamoto et al., 2008). In human cells, a similar hierarchy of

RZZ, Spindly and Mad1 may exist, although no evidence illustrating the physical interactions among the three has been reported.

Mad1 prefers to accumulate at unattached kinetochores. On the kinetochores that are attached with microtubule, Mad1 is released from kinetochore through a dynein-dependent poleward transport mechanism (Griffis et al., 2007; Howell et al., 2001). Spindly directly interacts with the dynein-dynactin complex and anchors them to RZZ and Mad1 at the kinetochore. The dynein-mediated minus-end transportation thus strips Spindly from the kinetochore in cohort of Mad1 and RZZ (Gassmann et al., 2010). This removal mechanism of Mad1 constitutes an important step for spindle checkpoint silencing. The Spindly mutant that does not bind with dynein blocks the Mad1 release from microtubule-attached kinetochores and delays the silencing of checkpoint signaling (Gassmann et al., 2010). Similarly, ectopic targeting Mad1 to kinetochore by artificial tethering Mad1 with Mis12 causes spontaneous mitotic arrest in the absence of microtubule poisons (Maldonado and Kapoor, 2011). This is due to a persistent checkpoint signaling and requires MCC components. Interestingly, the mitotic arrest induced by Mis12-Mad1 fusion protein still depends on Mps1 kinase activity, suggesting Mps1 has a critical function at checkpoint signaling downstream of Mad1 recruitment.

Besides the Mad1-bound Mad2, a cytosolic pool of Mad1-free Mad2 is required for checkpoint signaling (Chung and Chen, 2002). The conformational activation of the cytosolic Mad2 is crucial for Cdc20 binding and checkpoint activation. When spindle checkpoint is activated, the cytosolic O-Mad2 needs to be recruited to kinetochores through the Mad1–C-Mad2 complex in order for activation. The O-Mad2 binds to the Mad1-bound C-Mad2, forming an O-C Mad2 dimer. Dimerization with C-Mad2 induces

a subtle conformation change of O-Mad2 and turns it into an intermediate conformer (I-Mad2). Although I-Mad2 represents an intermediate state during the O-to-C conversion, the structural analysis reveals that I-Mad2 folds into a conformation largely identical to O-Mad2 (Hara et al., 2015). Therefore, the major conformational activation of Mad2 occurs after its association with Mad1–Mad2 at kinetochores. In cells, the kinetochore recruitment of O-Mad2 requires the kinase activity of Mps1 (Hewitt et al., 2010).

Kinetochore Recruitment of Cdc20

In mitosis, Cdc20 is recruited to kinetochores in order to interact with Mad2. It has been reported that the internal Phe boxes (phenylalanine-containing box, also known as ABBA motif) of both Bub1 and BubR1 contribute to the kinetochores localization of Cdc20, although the contribution of BubR1 is controversial with conflicting evidence showing BubR1 is not at all required for Cdc20 localization at kinetochores (Di Fiore et al., 2015; Diaz-Martinez et al., 2015; Han et al., 2014). Nevertheless, it has been further demonstrated that the Cdc20-binding region of Bub1 is critical for checkpoint activation (Di Fiore et al., 2015; Vleugel et al., 2015). Therefore, the Bub1-mediated kinetochore recruitment of Cdc20 is important for spindle checkpoint activation.

INHIBITION OF APC/C^{CDC20}

APC/C is a multi-subunit ubiquitin ligase, related to the Cullin-RING family of ubiquitin ligases. APC/C can recruit two ubiquitin conjugating E2 enzymes, UbcH10 and Ube2S (Garnett et al., 2009; Tang et al., 2001b; Williamson et al., 2009). UbcH10 is recruited by

the sub-complex of APC2 (contains Cullin-homology domain) and APC11 (contains RING-homology domain). Ube2S is recruited through APC2 and APC4 (Chang et al., 2015). UbcH10 is responsible for ubiquitin chain initiation, while Ube2S elongates the K11-specific ubiquitin chain (Garnett et al., 2009; Williamson et al., 2009). For substrate recognition, APC/C requires either of the two co-activators, Cdc20 and Cdh1 (Cdc20 homolog 1). In mitosis, the Cdk-dependent phosphorylation of APC/C enables Cdc20 binding (Fang et al., 1998b; Kraft et al., 2003), while the phosphorylation of Cdh1 by Cdks prevents Cdh1 from binding with APC/C (Zachariae et al., 1998). Thus Cdc20 and Cdh1 activate APC/C at different cell cycle stages: Cdc20 activates APC/C from early mitosis to metaphase-anaphase transition; Cdh1 activates APC/C from late anaphase to G1. Cdc20 contributes to APC/C-dependent ubiquitination by recognizing degron-containing substrates. Most of Cdc20 substrates contain either the destruction box (D box) or the lysine-glutamate-asparagine box (KEN box) or both. The spindle checkpoint inhibits APC/C^{Cdc20} in at least two parallel ways: MCC assembly and Cdc20 phosphorylation.

APC/C^{Cdc20} Inhibition by MCC

MCC is composed of BubR1–Bub3, C-Mad2, and Cdc20. While BubR1, Mad2 and Cdc20 form the core of MCC, Bub3 is not required for the core MCC formation (Sczaniecka et al., 2008), but may contribute to the MCC assembly by stabilizing the Bub1 and BubR1 proteins and recruiting them to kinetochores. The structural analysis of fission yeast core MCC reveals the molecular interactions among the three subunits. In MCC, Mad2 adopts the closed formation and embraces the Mad2-interacting motif at the

N-terminal tail of Cd20. The first KEN box (KEN1) at the N-terminus of BubR1 occupies the KEN-binding site of Cdc20, preventing Cdc20 from binding with any KEN box-containing substrates (Chao et al., 2012).

For a long period in the past, it was believed that MCC inhibits APC/C by sequestering Cdc20 from substrate recognition. Except KEN1 that is required for MCC assembly, however, BubR1 contains several other Cdc20-interacting motifs scattered at its N-terminal and middle region: Phe1, D1, KEN2, Phe2 and D2. The functions of the other Cdc20-interacting motifs were not characterized. Work from the Pines group has demonstrated that MCC can suppress APC/C that is pre-bound with Cdc20. This suppression requires D1 and KEN2 of BubR1 (Izawa and Pines, 2015). Furthermore, structural analyses of APC/C^{Cdc20} bound with MCC have elucidated the underlying molecular interactions (Alfieri et al., 2016; Yamaguchi et al., 2016). In the complex structure, the KEN-, D-, and Phe-binding sites of both APC/C-bound Cdc20 ($Cdc20^{APC/C}$) and MCC-incorporated Cdc20 ($Cdc20^{MCC}$) are connected with electron densities, which have been assigned to the other Cdc20-interacting motifs of BubR1. $Cdc20^{MCC}$ is bound with KEN1, Phe2 and D2; while $Cdc20^{APC/C}$ is bound with D1, Phe1 and KEN2. Such an extensive binding of BubR1 to both Cdc20 molecules blocks the Cdc20-mediated recruitment of all KEN- and D-box-containing substrates. In addition, the TPR of BubR1 binds to APC2 and results in a conformational change of APC2, preventing APC2-dependent recruitment of UbcH10. Collectively, MCC inhibits APC/C^{Cdc20} through blocking both substrate recognition and UbcH10 recruitment.

APC/C^{Cdc20} Inhibition by Cdc20 Phosphorylation

The ultimate target of the spindle checkpoint is APC/C^{Cdc20}. The checkpoint has developed a parallel pathway, other than MCC formation, to inhibit APC/C. Such an MCC-independent mechanism involves the phosphorylation of Cdc20. The checkpoint kinase Bub1 can phosphorylate Cdc20 at S153, which inhibits APC/C in vitro (Tang et al., 2004). In human cells, however, Bub1 kinase activity is not strictly required for checkpoint activation (Jia et al., 2016), suggesting this Bub1-mediated phosphorylation of Cdc20 S153 might be redundant in checkpoint-active cells. Interestingly, Cdk1-mediated phosphorylation of Bub1 establishes a direct interaction with Plk1 (Qi et al., 2006). Since Bub1 also binds with Cdc20 through Phe and KEN, Bub1 scaffolds a Plk1-mediated phosphorylation of Cdc20 N-terminal tail. The Plk1-phosphorylated Cdc20, once bound with APC/C, inhibits the Ube2S-dependent ubiquitin-chain elongation (Jia et al., 2016). This parallel pathway still requires the Mps1-dependent kinetochore recruitment of Bub1 and Cdc20, but might be independent of BubR1, Mad1 and Mad2. Considering the fact that the APC/C^{Cdc20}–MCC does not block Ube2S recruitment and function, this MCC-independent APC/C inhibition mechanism may compensate with the MCC-mediated APC/C inhibition. The combined action of the two leads to a compete inhibition of APC/C and arrest cells in mitosis.

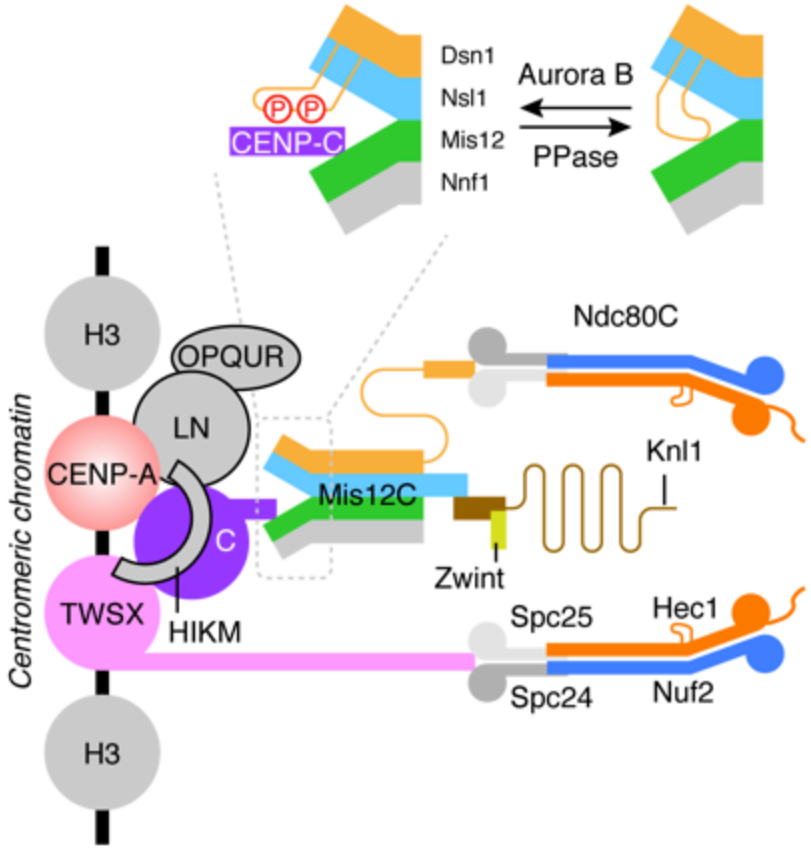

Figure 1-1. Organization of kinetochore at the centromere.

The CENP-A nucleosome is recognized by a set of CENP proteins, which constitute the inner kinetochore. The inner kinetochore sets foundation for the assembly of outer kinetochore mainly through CENP-C and CENP-T. CENP-T directly binds to the Spc24–Spc25 head domains of Ndc80C. CENP-C binds to the head and connector regions of Mis12C, which can further recruit Knl1 and Ndc80C through Nsl1 and Dsn1 subunits. Knl1, Mis12C, and Ndc80C form the KMN network. The CENP-C–Mis12C interaction is auto-inhibited by a Dsn1 loop. Aurora B-mediated phosphorylation of the Dsnl1 loop can relieve the inhibition, promote CENP-C binding, and facilitate the kinetochore recruitment of KMN.

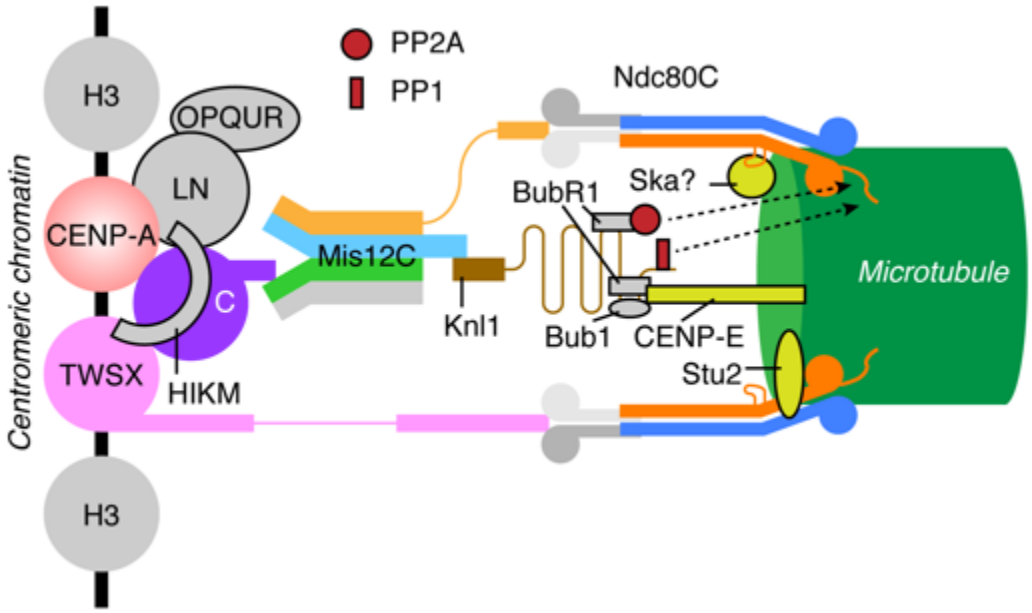

Figure 1-2. The kinetochore-microtubule attachment.

Ndc80C binds laterally with the microtubules. Knl1 recruits the protein phosphatases (PP1 and PP2A) through Bub1 and BubR1 to dephosphorylate (dash arrows) the Hec1 tail in order to stabilize the Ndc80C-microtubule interaction. Additional microtubule-binding proteins, like CENP-E, Stu2, and the Ska complex, are recruited by KMN to strengthen the kinetochore-microtubule attachment. The conformational changes of Ndc80C-bound CENP-T and Dsn1 under the microtubule-pulling force are speculations.

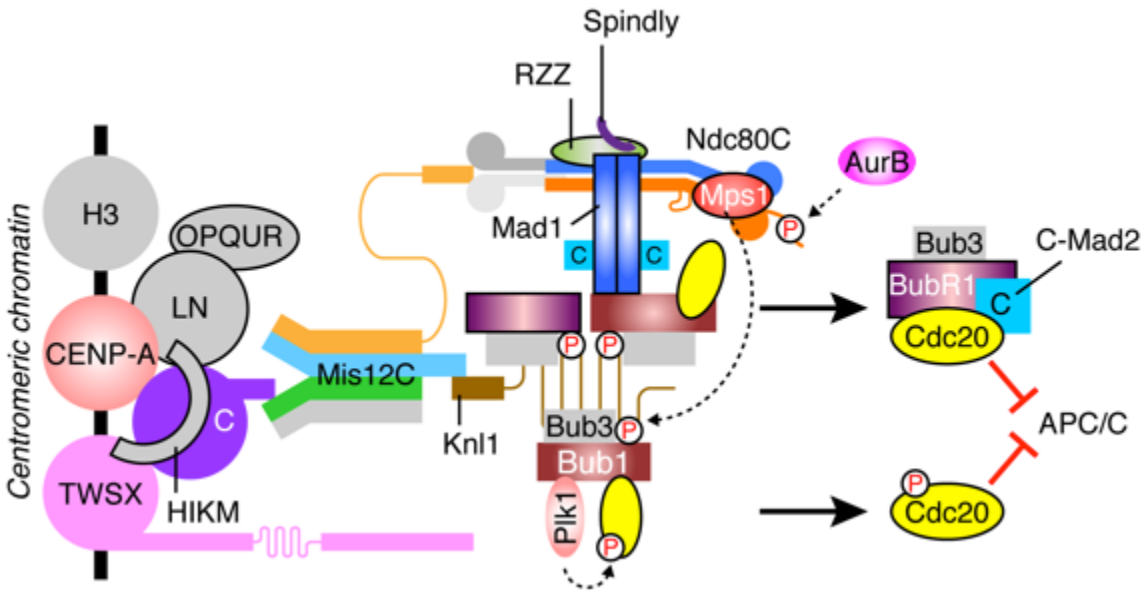

Figure 1-3. Activation of spindle checkpoint by unattached kinetochore.

In early mitosis, the Hec1 tail is highly phosphorylated by the Aurora B kinase (AurB) to weaken the microtubule attachment. Mps1 is recruited to the kinetochore depending on Ndc80C. Bub1–Bub3 and BubR1–Bub3 are recruited by Mps1-phosphorylated Knl1. Mad1–Mad is recruited through the Rod–Zwilch–ZW10 complex (RZZ) and Spindly. Cdc20 is associated with Bub1. The kinetochore association of the checkpoint proteins promotes the assembly of the mitotic checkpoint complex (MCC). In parallel, Bub1 scaffolds the Plk1-mediated phosphorylation of Cdc20. Both the assembled MCC and the phosphorylated Cdc20 contribute to the inhibition of the anaphase-promoting complex or cyclosome (APC/C).

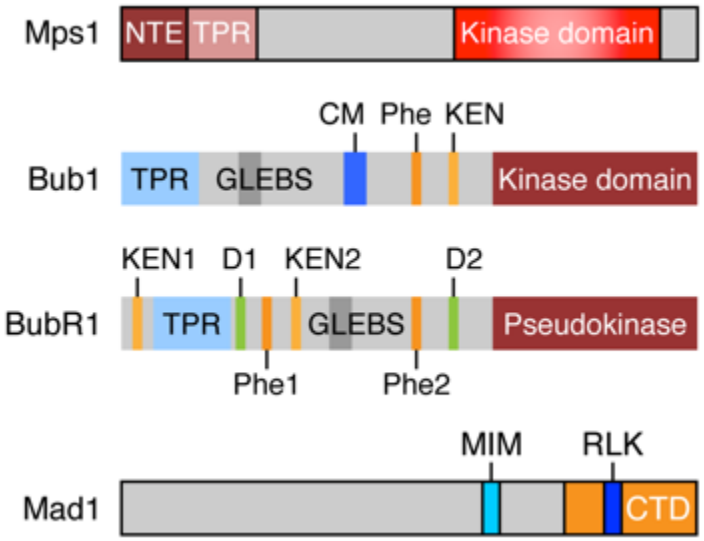

Figure 1-4. Domains and motifs of checkpoint proteins.

Mps1 contains an N-terminal extension (NTE) and a tetratricopeptide repeat (TPR) domain, and a C-terminal kinase domain. The kinetochore localization of Mps1 is mediated by NTE. Bub1 and BubR1 both contain an N-terminal TPR domain and a Gle2-binding sequence (GLEBS) for Bub3 binding. In addition, Bub1 contains a conserved motif (CM), a phenylalanine-containing box (Phe), a lysine-glutamate-asparagine box (KEN), and a C-terminal kinase domain. BubR1 has two KENs (KEN1 and KEN2), two destruction boxes (D1 and D2), two Phe boxes (Phe1 and Phe2), and a C-terminal pseudokinase domain. KEN1 is located N-terminal to BubR1 TPR, which is required for Cdc20 binding in MCC. D1, Phe1 and KEN2 are C-terminal to TPR. Phe2 and D2 are located at the middle region of BubR1. Mad1 contains an evolutionarily conserved C-terminal domain (CTD). A Mad2-interacting motif (MIN) is located N-terminal to CTD, which constitutively binds with Mad2. The arginine-leucine-lysine (RLK) motif within CTD is critical for Bub1–Mad1 interaction in yeast.

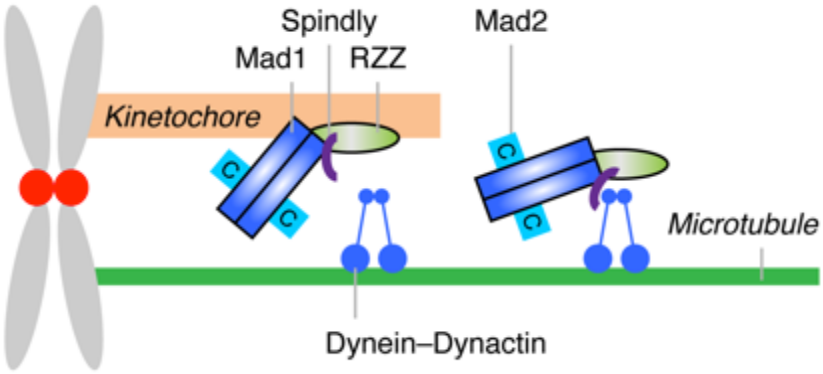

Figure 1-5. The Dynein-dependent release of Mad1–Mad2 from attached kinetochores.

Mad1–Mad2 complex is recruited to the kinetochores by Spindly and the Rod–Zwilch–ZW10 complex (RZZ). Upon microtubule attachment, Dynein–Dynactin interacts with Spindly and strips Mad1–Mad2 off the kinetochores.

CHAPTER II: MATERIALS AND METHODS

Cell culture and transfection

HeLa Tet-On cells (Clontech) were cultured in Dulbecco's Modified Eagle Medium (DMEM, Invitrogen) supplemented with 10% fetal bovine serum and 2 mM L-glutamine. For G1/S synchronization, cells were treated with 2 mM thymidine (Sigma) for 14-16 h. For mitotic arrest, cells were treated with nocodazole (Sigma) or taxol (Sigma) for 12-14 h. Other chemicals used in this study were: ZM447439 (Tocris) at 4 μM, MG132 (Selleckchem) at 10 μM, reversine (Cayman Chemical) at 1 μM, RO3306 (Sigma) at 20 μM, BI 2536 (Selleck Chemicals) at 1 μM, and okadaic acid (LC lab) at 500 nM.

For RNAi experiments, cells were transfected with siRNA oligonucleotides (Dharmacon) using Lipofectamine RNAiMAX (Invitrogen) and harvested at 24–72 h after transfection. The sequences of the siRNAs were (from 5' to 3'): siMps1, GCACGUGACUACUUUCAAA; siCdc20, CGAAAUGACUAUUACCUGA; siNuf2, AAGCAUGCCGUGAAACGUAUA (DeLuca et al., 2002); siSpindly, GAAAGGGUCUCAAACUGAA (Gassmann et al., 2010); siBub1-c, CCCAUUUGCCAGCUCAAGC (Jia et al., 2016); siBub1-d, GAGUGAUCACGAUUUCUAA (Jia et al., 2016); siBubR1, GGACACAUUUAGAUGCACU (Choi et al., 2016); siMad2, GCUUGUAACUACUGAUCUU (Choi et al., 2016).

Internal deletion mutants were constructed with overlapping extension polymerase chain reaction (PCR). Point mutations were introduced with QuickChange

Lightening Site-Directed Mutagenesis kit (Agilent Technologies). For the construction of GFP-4MD, four copies of the Mps1 MR motif (residues 261-300) containing the S281D mutation were fused to GFP. The MR motifs were separated by flexible linkers with the amino acid sequence of GGGSGGASGGGS. All plasmids were verified by sequencing. Plasmid transfections were performed with the Effectene reagent (Qiagen) according to the manufacturer's instructions.

For stable cell line generation, HeLa Tet-On cells were transfected with pTRE2 vectors containing siRNA-resistant wild-type or mutant GFP-Mps1, Nuf2-Myc, mCherry-Bub1$^{\Delta K}$ or Myc-Bub1$^{\Delta K}$ transgenes. Cells were treated with 200-300 μg/ml hygromycin (Clontech). Surviving clones were screened for expression of the desired proteins in the presence of 1 μg/ml doxycycline (Sigma). Clones that expressed Mps1, Nuf2 or Bub1$^{\Delta K}$ levels similar to those of the endogenous proteins were chosen for further analysis. Stable cell line clones were maintained with 100 μg/ml hygromycin.

Antibodies

The following commercial antibodies were used for immunoblotting and immunofluorescence: CREST (ImmunoVision, HCT-0100), anti-tubulin (Sigma, T9026), anti-Nuf2 (Abcam, ab122962), anti-BubR1 [BD Biosciences Clone 9/BUBR1 (RUO)], anti-Bub3 [mouse, BD Biosciences Clone 31/Bub3 (RUO)], anti-Bub3 (rabbit, Sigma, B7811), anti-GAPDH (Cell Signaling, 14C10), anti-GFP (Roche), anti-Myc (Roche), anti-Cdc20 (goat, Santa Cruz Biotechnology). Fluorescent secondary antibodies were purchased from Life Technologies.

Antibodies against Apc2, Hec1, Mad2, APC3, Mad1, Cdc20 (pS153), and Bub1 were previously described (Fang et al., 1998a; Kim et al., 2012; Lin et al., 2014; Tang et al., 2001a). The anti-Knl1 pT875 (pKnl1), Bub1 pS459, and Bub1 pSpT antibodies were generated at an on-campus facility. A Knl1 phospho-peptide, with the sequence of CNDMDI[pT]KSYTI, and two Bub1 phospho-peptides, CKVQP[pS]PTVH and CKVQP[pS]P[pT]VHTK, were used to immunize rabbits. The antibodies were affinity-purified using peptide-conjugated SulfoLink resins (Thermo Scientific). For the generation of anti-Knl1, anti-Mps1, anti-GFP, and anti-Spc24 and Spc25 antibodies, His_6- or GST-tagged $Knl1_{1531-1808}$, $Mps1_{1-400}$, eGFP, and $Spc24_{92-197}$–$Spc25_{70-224}$ proteins were expressed in bacteria and purified. After removal of the tags, these proteins were used to immunize rabbits at YenZym Antibodies, LLC. The antibodies were affinity-purified with AminoLink resins (Thermo Scientific) coupled to the corresponding antigens.

Live cell imaging

Cells stably expressing Bub1 transgenes were passaged onto four-well chambered coverglass (Lab-Tek). After being transfected with the Bub1 siRNA, cells were treated with thymidine for 16 h, and then released into fresh medium for 9 h before being imaged. In the case of taxol treatment, taxol was added 3 h prior to imaging. Live-cell imaging was performed with a DeltaVision microscope (Applied Precision) equipped with an environmental chamber (37°C and 5% CO_2) and a CoolSNAP HQ2 camera (Roper Scientific). Differential interference contrast images were taken with a 40x

objective (Olympus) at 4-min intervals. Images were processed with ImageJ, and the graphs were generated with Prism software (GraphPad).

Immunofluorescence

For chromosome spread, mitotic cells were harvested by shake-off. Cells were incubated with the hypotonic solution (55 mM KCl) at 37℃ for 10 min and spun onto slides with a Shandon Cytospin 4 centrifuge (Thermo Fisher). After being pre-extracted with the PHEM buffer (60 mM PIPES, 25 mM HEPES, pH 6.9, 10 mM EGTA, 2 mM $MgCl_2$) containing 0.2% Triton X-100 for 2 min, cells were fixed by 4% paraformaldehyde in PBS (PBSP) for 4 min, washed with PBS containing 0.1% Triton X-100 (PBST), and blocked for 30 min with PBST containing 3% BSA (PBSB). Chromosome spreads were then incubated with primary antibodies in PBSB at room temperature for 1 h or at 4°C overnight. Spreads were washed three times with PBST and incubated with fluorescent secondary antibodies in PBSB for 1 h at room temperature. Chromosome spreads were again washed three times with PBST and stained with PBS containing 1 μg/ml 4',6-diamidino-2-phenylindole (DAPI) for 3 min. Slides were washed with PBS, mounted with Aqua-Poly/Mount (Polysciences, Inc.), and sealed with nail polish.

For whole-cell staining, cells were grown and transfected in 12-well plates, and then transferred to 4-well chamber slides (Nunc™ Lab-Tek™ II, Thermo Scientific). (For Mps1 staining, cells were treated with reversine and MG132 to enhance the kinetochore localization of Mps1. Although we could observe weak kinetochore staining of the endogenous Mps1 in the absence of reversine, we could not reliably observe the kinetochore staining of the ectopically expressed tagged Mps1 proteins without reversine.

We cannot rule out the remote possibility that reversine might affect the kinetochore localization of different Mps1 mutants in different ways.) After the medium was removed, cells were pre-extracted with the PEM buffer (100 mM PIPES, pH 7.5, 5 mM EGTA, 1 mM $MgCl_2$) containing 0.2% Triton X-100 for 2 min, and fixed with PBSP for 4 min. Subsequent staining with antibodies and DAPI was performed as described above. For chromosome alignment assays, HeLa cells were arrested in 500 nM nocodazole, released into MG132 for 2 h, and fixed and stained with CREST, tubulin, and DAPI.

Images for chromosome alignment were acquired on a DeltaVision system (Applied Precision) with a 60X objective (Olympus) in a Z-stack series of 0.5-μm intervals. All other images were acquired on the same system with a 100X NA1.4 UPLS APO objective (Olympus) in a Z-stack series of 0.2-μm intervals. Images were deconvolved and projected as average intensity or sum intensity, and further processed and analyzed with ImageJ.

For quantification of chromosome-spread images, elliptical areas around kinetochore pairs were selected manually. The mean staining intensity at kinetochores was calculated as the integrated intensity divided by the area. In each image, an ellipse with a similar size was selected in non-kinetochore regions for background determination. The relative kinetochore intensity of a given protein was calculated as its background-subtracted, mean kinetochore intensity divided by the background-subtracted, mean kinetochore intensity of CREST. For each spread, 20 kinetochore pairs were quantified. In all plots, each dot represents one kinetochore pair.

Whole-cell staining images were quantified as described (Nijenhuis et al., 2013). Briefly, an ImageJ macro was used to threshold the images. Chromatin and kinetochore

regions were selected based on DAPI and CREST signals, respectively. The non-kinetochore region was defined as the chromatin region with the kinetochore region subtracted. The mean intensity of a given protein in each of the three regions was calculated as the integrated intensity divided by the area. The kinetochore enrichment of a given protein was calculated as the $\log_2$ ratio of its mean kinetochore and non-kinetochore intensities. In all plots, each dot represents one cell.

All p-values were calculated using the Student's t-test with the Prism software (GraphPad).

Flow cytometry

Cells were synchronized at G1/S with thymidine and released into fresh medium containing nocodazole for 13 h before being harvested. For Aurora B or Plk1 inhibition, ZM447439 or BI 2536 was added 1 h prior to harvest. Collected cells were washed with PBS and fixed with pre-chilled 70% ethanol at -20℃ overnight. After being washed with PBS, the fixed cells were permeabilized with 0.2% Triton X-100 in PBS for 20 min. Cells were then incubated with the anti-MPM2 antibody (1:100, Millipore) in PBS containing 1% BSA for 2 h. After being washed with PBS, cells were incubated with fluorescent secondary antibodies (Invitrogen) in PBS containing 1% BSA for 30 min. After being washed with PBS, cells were stained with 20 μg/ml propidium iodide (Sigma) in PBS containing 200 μg/ml RNase (Qiagen). All staining steps were performed at room temperature. Samples were analyzed on a FACSCalibur flow cytometer (BD Biosciences). Data were processed with the FlowJo software. The mitotic index was defined as the percentage of cells that had 4N DNA content and were also positive for

MPM2 staining. The graphs and statistic analysis were generated with Prism software (GraphPad).

Immunoprecipitation

Mitotic cells were harvest by shake-off and washed with PBS once. Cell pellets were lysed with the wash buffer I (50 mM Tris-HCl, pH 8.0, 150 mM KCl, 0.1% NP-40, 2 mM $MgCl_2$, 5 mM NaF, 10 mM β-glycerophosphate, 1 mM DTT) supplemented with the cOmplete EDTA-free protease inhibitor cocktail (Roche), 500 nM okadaic acid, and 10 units/ml TurboNuclease (Accelagen). Cell lysates were cleared by centrifugation. Supernatants were incubated with the antibody-coupled Protein A beads (Bio-Rad) at 4℃ for 2 h. Proteins bound on beads were released using SDS loading buffer, and analyzed by Western blotting. For quantitative Western blotting, immunoglobulin G (IgG) (H+L) conjugated with Dylight 680 or Dylight 800 (Cell Signaling) was used as secondary antibody. The membrane strips were scanned with the Odyssey Infrared Imaging System (LI-COR, Lincoln, NE).

Protein purification

Expression of GST tagged Mps1 fragments, $Hec1^{CH}$ (residues 80-202), and $Ndc80C^{bonsai}$ (wild type or mutants), $BubR1^{N}$ (residues 1–370), Mad2, scBub1 fragments, Mad1 and scMad1 fragments in BL21(DE3) were induced by 0.1mM isopropyl β-D-1-thiogalactopyranoside (IPTG) in 16°C overnight after the OD_{600} reached 0.8. Mad1 and scMad1 fragments ($Mad1^{E}$) containing Mad2-interacting motif (MIM) were co-expressed with Mad2 and scMad2, respectively. Fragments of scBub1 were co-expressed with His_6-

scMps1 (the kinase domain; residues 440–720) as appropriate. Harvested pellets were lysed in the wash buffer II [50 mM Tris-HCl, pH 8.0, 150 mM KCl, 0.1% (v/v) Triton X-100, 5% glycerol, 5 mM β-mercaptoethanol] supplemented with a protease inhibitor cocktail. After sonication, lysates were cleared by centrifugation at 4°C. Supernatants were filtered by 0.45-μm filter and incubated with pre-equilibrated Glutathione Sepharase 4B beads (GE Healthcare). Protein-bound beads were washed with 40 volume of the wash buffer I. The proteins were then eluted with reduced glutathione (Sigma) or cleaved with the PreScission protease. Eluates were dialyzed to the QA buffer (25 mM Tris-HCl, pH 8.0, 20 mM NaCl, 3 mM DTT), loaded onto Resource Q column (GE Healthcare), and then eluted with the QB buffer (25 mM Tris-HCl, pH 8.0, 1 M NaCl, 3 mM DTT). Peak fractions were pooled and further purified with a Superdex 200 size exclusion column (GE Healthcare). The relevant protein fractions were pooled, aliquoted, and snap-frozen for future experiments. For the Aurora B kinase assay, the Aurora B–INCENP complex was expressed in bacteria and purified as previously described (Elkins et al., 2012).

For expression of Mps1, full-length Ndc80C, Bub1–Bub3, Cdk1–Cyclin B, and Cdc20 in insect cells, baculoviruses encoding His_6-Strep-Mps1 (full-length; Nt, residues 1–517; Ct, 500–857; or the kinase domain, residues 516–794), His_6-Hec1–Nuf2, His_6-Spc24–Spc25, His_6-Strep-Bub1 (full-length or $Bub1^{\Delta K}$ containing residues 1–723), His_6-Bub3, GST-Cdk1 (containing constitutively active mutations T14A/Y15F), His_6-Cyclin B, and His_6-Cdc20 (full-length or the ΔN60 mutant lacking residues 1–60) were generated with Bac-to-Bac system (Invitrogen). Bub1 and Cdk1 were co-expressed with Bub3 and Cyclin B1, respectively. Insect cells were infected with the appropriate viruses

for 50 h before being harvested. Cell pellets were suspended with the wash buffer II supplemented with a protease inhibitor cocktail and Turbo Nuclease, and lysed with a high-pressure homogenizer. Lysates were cleared by ultracentrifugation and incubated with Glutathione Sepharase 4B, Strep-Tactin Superflow Plus (Qiagen), or Ni^{2+}-NTA resin (Qiagen) pre-equilibrated with buffer I. The protein-bound beads were washed and eluted with reduced glutathione, desthiobiotin (Sigma), or imidazole (Sigma). Eluates were dialyzed into the gel filtration buffer (50 mM Tris, pH 8.0, 150 mM KCl, 5% glycerol, 1 mM β-mercaptoethanol). Proteins were passed through a HiLoad 16/60 Superdex 200 PG size-exclusion column (GE Healthcare). The relevant fractions were pooled and snap-frozen. Cells expressing His_6-Cdc20 were lysed in the wash buffer III [50 mM HEPES, pH 6.8, 250 mM KCl, 5% glycerol, 0.1% (v/v) Triton X-100, 5 mM β-mercaptoethanol and 10 mM imidazole] supplemented with a protease inhibitor cocktail and TurboNuclease. Cdc20 proteins were purified with Ni^{2+}-NTA beads and eluted with 250 mM imidazole. The eluates were exchanged into the storage buffer (40 mM HEPES, pH 6.8, 200 mM KCl, 5% glycerol and 2 mM DTT) with PD-10 columns (GE Healthcare).

Uba1, UbcH10 and Myc-Securin were purified as described previously (Tang and Yu, 2004). Ube2S protein is a gift from Dr. Michael Rape (University of California at Berkeley).

In vitro kinase assay

1.5 μM $Ndc80C^{bonsai}$, 1 μM $Cdc20^{\Delta N60}$, 40 μM $Mad1^{E}$–Mad2, or 400 nM $Bub1^{\Delta K}$–Bub3 was incubated with 40 nM Aurora B–INCENP, 40 nM Bub1, 500 nM Mps1, and/ or 50

nM Cdk1–Cyclin B at 30˚C or room temperature for 30 min in the kinase buffer (25 mM Tris-HCl, pH 7.7, 100 mM NaCl, 10 mM $MgCl_2$, 5 mM NaF, 20 mM β-glycerophosphate, 0.1 mM Na_3VO_4 and 1 mM DTT) supplemented with 1 mM ATP. The reaction mixtures were stopped with the appropriate kinase inhibitors for further protein-binding assays, or quenched with the SDS loading buffer and analyzed by Coomassie blue staining or Western blotting.

Protein binding assay

Recombinant bait proteins or bacteria lysates containing bait proteins were incubated with the appropriate affinity beads. Bait-bound beads were then blocked with 2% fat-free milk when necessary before being mixed with 100 μl diluted prey proteins. After incubation, beads were washed and eluted with the SDS loading buffer. The bead-bound proteins were analyzed by Coomassie blue staining or Western blotting. In cases that synthesized peptides were used as bait, peptides were immobilized on AminoLink or SulfoLink resin (Thermo Scientific) according to the manufacturer's instructions. The synthetic scBub1 peptides contained residues 449–473 of scBub1, various phospho-residues, and a cysteine at the N-terminus. All synthetic human Bub1 peptides, except the pS459 peptide, contained residue 455–477 of human Bub1, the appropriate phospho-residues, and a cysteine at the N-terminus. The Bub1 pS459 peptide contained residues 439–480, pT452/pS459, and a cysteine at the C-terminus. Prey proteins were diluted and used for binding assays with the desired baits.

In binding assays involving $Ndc80^{CH}$, $Ndc80^{CH}$-bound beads were equilibrated with general tubulin buffers (GTB; 80 mM PIPES, pH 6.9, 2 mM $MgCl_2$, 0.5 mM EGTA)

containing 5% glycerol, blocked with 1 mg/ml BSA, incubated with $Mps1_{1-200}$ in GTB containing 5% glycerol and 1 mg/ml BSA.

In experiments involving *in vitro* translated, ^{35}S-labeled Ndc80C as preys, the gels were dried and analyzed with a phosphorimager (Fujifilm). Intensities of the bound proteins were quantified with ImageJ (NIH). The binding intensities of Hec1, Nuf2, and Spc24–Spc25 were determined as the band intensities of proteins bound to bait-containing beads subtract with the intensities of the same proteins bound to empty beads. The relative binding intensities were defined as the binding intensities divided by the intensities of the input. The average of the relative binding intensities of Hec1, Nuf2, and Spc24–Spc25 was defined as the binding efficiency of the Ndc80C complex.

For binding assays involving microtubule competition, prey proteins were prepared with 0.25 mg/ml BSA and varying amounts of taxol-stabilized microtubules. Prey proteins and microtubules were then incubated with bait-bound beads for 30 min at room temperature. After removal of the unbound prey, beads were washed with the wash buffer containing the appropriate amount of microtubules. Finally, beads were washed with GTB containing 10 mM $CaCl_2$ and incubated on ice for 10 min. Bead-bound proteins were eluted with the SDS loading buffer and resolved with SDS-PAGE. Quantitative immunoblotting was performed as described in the previous sections.

For microscale thermophoresis (MST), purified $Ndc80C^{bonsai}$ Δtail was coupled to a fluorophore in the HEPES buffer (25 mM HEPES, pH 7.5, 1 mM TCEP) with the Blue-NHS Protein Labeling Kit (Nanotemper, Munich, Germany) according to the manufacturer's instructions. Serial dilutions of $Mps1_{1-200}$ were made by 15 successive 1:1 dilutions of the highest concentration (2 mM) sample into the HEPES buffer. Each of

these solutions was mixed 1:1 with a solution of 800 nM labeled Ndc80C^{bonsai}Δtail. The final concentration of the labeled protein is 400 nM in all samples, and the highest concentration of Mps1$_{1\text{-}200}$ was 1 mM. All 16 samples were loaded into hydrophilic capillary tubes for 30 min before the final measurements were taken in a Monolith NT.115 instrument (Nanotemper, Munich, Germany). The instrument's LED (illumination) power was set to 10%, and the MST laser power was set to 40%. Measurements were performed at 25˚C. Once the LED was turned on, fluorescence was monitored as a function of time. There was a 5-s waiting period before the MST laser was ignited. The MST laser remained on for 30 s, followed by a 5-s monitoring of the recovery period. The resulting fluorescence time traces were analyzed as previously described (Wienken et al., 2010).

Isothermal titration calorimetry (ITC) assays were performed with a MicroCal Omega VP-ITC or ITC200 titration calorimeter (GE Life Sciences) at 20°C. Recombinant Ndc80C^{bonsai}, scMad1^{CTD} or scMad1–scMad2 proteins were dialyzed into the HEPES buffer (25 mM HEPES, pH7.5, 150 mM NaCl). For each titration, 2 ml of Ndc80C^{bonsai}, scMad1^{CTD} or scMad1–scMad2 proteins (20 μM) were added to the calorimeter cell. The MR24 or pMR4 peptides, scBub1 phospho-peptides or purified scMps1-phosphorylated scBub1$_{449–530}$ proteins (300 μM) in the same buffer were injected with an injection syringe in 20 8-μl portions. Raw data were processed and fitted with the NITPIC software package (Keller et al., 2012).

Microtubule pelleting assay

Porcine tubulin and general tubulin buffers (GTB; 80 mM PIPES, pH 6.9, 2 mM $MgCl_2$, 0.5 mM EGTA) were purchased from Cytoskeleton. Taxol-stabilized microtubule was prepared according to the manufacturer's instructions. In all cases, the microtubule concentration is defined as the molar concentration of the tubulin heterodimer. For pelleting reactions, microtubules were diluted in GTB containing 10% glycerol and 20 μM taxol. Test proteins and BSA were diluted in the S buffer (50 mM sodium phosphate, pH 7.0, 1 mM EGTA, 1 mM β-mercaptoethanol). 22 μl diluted microtubules and 18 μl diluted proteins were then mixed to make up a 40 μl reaction, which contained 200 nM $Ndc80C^{bonsai}$, 0.5 mg/ml BSA, and varying concentrations of microtubules, with or without 100 μM Mps1 pMR24 peptide. After a 10-min incubation, the mixtures were applied to a 40 μl cushion (GTB containing 40% glycerol) and then spun at 312,530 g at 25˚C with a TLA 100 rotor on an Optima TL Ultracentrifuge (Beckman). After the supernatant was removed, the pellet was re-suspended with 80 μl GTB supplemented with 10 mM $CaCl_2$ and incubated on ice for 10 min. Supernatant and pellet samples were resolved on SDS-PAGE and probed with quantitative immunoblotting with the α-Spc24/Spc25 antibody and DyLight™ fluorescent dye conjugated secondary antibodies (Cell Signaling). The blots were analyzed with an Odyssey® CLx Infrared Imaging system (LICOR). Band intensities in both the supernatant and pellet samples were quantified with the Image Studio software (LICOR). Binding curve fitting and apparent K_d calculation were performed with the Prism software (GraphPad).

APC/C ubiquitination assay

APC/C was isolated from *Xenopus* egg extracts using the anti-APC3/Cdc27 antibody-coupled Protein A beads (Bio-Rad). The APC/C beads were incubated with the MCC mixture containing $BubR1^{N}$, Mad2, and Cdc20 with or without $Bub1^{\Delta K}$–Bub3 and/or $Mad1^{E}$–Mad2, and then added to ubiquitination reactions. The reaction mixture was prepared with the XB buffer (10 mM HEPES, pH 7.7, 100 mM KCl, 0.1 mM $CaCl_2$, 1 mM $MgCl_2$ and 50 mM sucrose) containing 150 μM bovine ubiquitin (Sigma), 5 μM Uba1, 750 nM UbcH10, 3 μM Ube2S and 5 μM Myc-tagged human Securin, supplemented with 1X energy mixture (7.5 mM phosphocreatine, 1 mM ATP, 100 μM EGTA, and 1 mM $MgCl_2$). After incubation at room temperature with gentle shaking for 1 h, the reactions were quenched with the SDS loading buffer and analyzed by Western blotting.

CHAPTER III: KINETOCHORE ATTACHMENT SENSED BY COMPETITIVE BINDING OF MPS1 AND MICROTUBULE BINDING TO NDC80C

INTRODUCTION

Unattached kinetochores recruit and activate spindle checkpoint proteins to produce wait-anaphase signals, thereby ensuring the fidelity of chromosome segregation. Microtubule attachment releases checkpoint proteins from kinetochores and attenuates checkpoint signaling. Whether the kinetochore signaling of any checkpoint proteins is directly inhibited by microtubules remains to be established, however. The KMN network of kinetochore proteins acts both as a critical microtubule receptor and a signaling platform for the spindle checkpoint (Foley and Kapoor, 2013; Jia et al., 2013; Kim and Yu, 2015; Sacristan and Kops, 2015). In humans, KMN consists of the Knl1–Zwint complex (Knl1C), the Mis12–Nnf1–Nsl1–Dsn1 complex (Mis12C), and the Hec1/Ndc80–Nuf2–Spc25–Spc24 complex (Ndc80C). Ndc80C directly engages microtubules through the N-terminal tail of Hec1 and the calponin homology (CH) domains of Hec1 and Nuf2 (Alushin et al., 2012). Ndc80C is also required for the kinetochore localization of key checkpoint proteins, including the kinase Mps1 and the Mad1–Mad2 core complex (Martin-Lluesma et al., 2002; Stucke et al., 2004). As expected, depletion of Hec1 weakens the spindle checkpoint in human cells. Notably, cells partially depleted of Hec1 and treated with inhibitors of the centromeric kinase Aurora B can escape from mitotic

arrest in the presence of the microtubule-depolymerizing drug nocodazole (Santaguida et al., 2011; Saurin et al., 2011), whereas partial depletion of Hec1 or Aurora B inhibition alone does not produce such effect.

Because of the dual roles of KMN in microtubule attachment and checkpoint protein recruitment, one intriguing hypothesis is that microtubule binding directly dissociates checkpoint proteins from kinetochores and antagonizes checkpoint signaling. Mad1–Mad2 specifically localizes to unattached kinetochores (Chen et al., 1998; Chen et al., 1996; Li and Benezra, 1996; Waters et al., 1998). Artificial tethering of Mad1 to kinetochores sustains checkpoint signaling even when all kinetochores reach bi-orientation, indicating that removal of Mad1–Mad2 from kinetochores is a prerequisite for microtubule-mediated checkpoint silencing (Maldonado and Kapoor, 2011). On the other hand, the kinetochore association of Mad1–Mad2 is not directly competed by microtubules, but rather is indirectly attenuated through dynein-dependent transport toward the spindle poles along microtubules (Howell et al., 2001). Mutation of Spindly, the kinetochore adaptor of dynein, prevents dynein-dependent stripping and retains Mad1–Mad2 at attached kinetochores (Gassmann et al., 2010). Thus, although dynein-dependent removal of Mad1–Mad2 from kinetochores contributes to the sensing of unattached kinetochores, it remains to be established whether the kinetochore signaling of any checkpoint proteins is directly inhibited by microtubules.

Mps1 is an evolutionarily conserved spindle checkpoint kinase whose kinase activity is required for checkpoint signaling in organisms from yeast to man (Abrieu et al., 2001; Dorer et al., 2005; Hardwick et al., 1996; Kang et al., 2007; Stucke et al., 2002). Mps1 selectively localizes to unattached kinetochores in an Ndc80C-dependent

manner (Abrieu et al., 2001; Stucke et al., 2004). At kinetochores, Mps1 phosphorylates Knl1 at multiple MELT motifs and creates docking sites for the checkpoint complex Bub1–Bub3 (London et al., 2012; Primorac et al., 2013; Shepperd et al., 2012; Yamagishi et al., 2012). Bub1–Bub3 in turn recruits BubR1–Bub3 and at least a pool of Mad1–Mad2 to kinetochores (Kim et al., 2012; London and Biggins, 2014; Rischitor et al., 2007). Kinetochore-bound Mad1–Mad2 promotes the conformational activation of additional Mad2 molecules (Luo and Yu, 2008; Mapelli and Musacchio, 2007), and enhances the formation of the mitotic checkpoint complex (MCC) that consists of BubR1–Bub3–Mad2–Cdc20 (Jia et al., 2013). MCC inhibits the anaphase-promoting complex or cyclosome that has bound with the co-activator Cdc20 (APC/C^{Cdc20}) to delay anaphase onset (Izawa and Pines, 2015). Mps1 is thus a critical upstream initiator of checkpoint signaling at kinetochores. Furthermore, similar to Mad1–Mad2, artificial tethering of Mps1 to kinetochores maintains checkpoint signaling in human cells even when all kinetochores reach bi-orientation (Jelluma et al., 2010). Therefore, Mps1 is an attractive candidate for directly sensing kinetochore-microtubule attachment.

To test whether Mps1 is a direct sensor of microtubule attachment, We first showed that human Mps1 directly binds to Ndc80C through two quasi-independent interactions, which involve the binding of the N-terminal extension (NTE) and a middle region (MR) of Mps1 to the head domains of Hec1 and Nuf2, respectively. Both Mps1–Ndc80C interactions are directly inhibited by microtubules in vitro. We next examined the kinetochore targeting of Mps1 in human cells with a deficient dynein pathway. The same Spindly mutation that prevented dynein-dependent Mad1–Mad2 removal from kinetochores did not retain Mps1 at attached kinetochores. Further analyses suggest that

microtubule binding to Ndc80C attenuates kinetochore signaling of Mps1 in two ways. First, microtubules contact the Hec1 head domain and compete with NTE-dependent kinetochore targeting of Mps1. Second, through engaging the Nuf2 head domain, microtubules disrupt a transient docking interaction between Mps1 MR and KMN, reduces the phosphorylation of Knl1 by Mps1, and weakens checkpoint signaling. Therefore, Mps1 serves as a kinetochore-attachment sensor and coordinates checkpoint signaling with microtubule attachment.

RESULTS

Mps1 Kinetochore Signaling Is Sensitive to Microtubule Attachment

The strength of the spindle checkpoint in human cells can be tuned by the type and degree of spindle damage (Collin et al., 2013; Dick and Gerlich, 2013; Heinrich et al., 2013). High concentrations (5 μM) of nocodazole render virtually all kinetochores unattached and most strongly activate the checkpoint. Low concentrations (50 nM) of nocodazole produce fewer unattached kinetochores and engage a weaker checkpoint. The microtubule-stabilizing drug taxol leaves most kinetochores attached but without proper tension and produces a checkpoint that is more reliant on the kinase activity of Aurora B (Hauf et al., 2003).

We first confirmed that Mps1 preferred to localize to unattached kinetochores. In HeLa cells treated with low concentrations (50 nM) of nocodazole, a few pairs of sister chromatids clustered around the spindle poles, often with only one sister kinetochore attached to microtubules. Both Mps1 and Mad1 specifically decorated unattached kinetochores (Figure 3-1). Moreover, compared to cells treated with 5 μM nocodazole, the kinetochore localization of Mps1 and BubR1, as well as Mps1-mediatd Knl1 phosphorylation, were greatly diminished in taxol-treated cells (Figure 3-2), suggesting that microtubule attachment attenuates Mps1 kinetochore signaling.

The specific localization of Mad1 to unattached kinetochores stems from dynein-dependent poleward transport along microtubules (Griffis et al., 2007; Howell et al., 2001), rather than direct microtubule competition. This dynein transport mechanism is blocked by the F258A mutation in the kinetochore dynein receptor Spindly (Gassmann et al., 2010). In accordance with that, Mad1 was retained on attached kinetochores at

metaphase in HeLa cells depleted of endogenous Spindly and expressing Spindly F258A (Figure 3-3). The localization of Mps1 at metaphase kinetochores was significantly weaker than that at prometaphase kinetochores, many of which were likely unattached. Expression of Spindly F258A did not, however, appreciably enhance Mps1 localization to metaphase kinetochores. Therefore, in contrast to Mad1, the decreased localization of Mps1 to attached metaphase kinetochores is mediated by a dynein-independent mechanism, raising the possibility that microtubules directly compete with Mps1 for kinetochore binding. Furthermore, unlike Mad1, there is still substantial amount of Mps1 at attached kinetochores. The relatively modest decrease of Mps1 levels at attached kinetochores is more consistent with direct microtubule competition, as not all microtubule-binding sites on each kinetochore are fully occupied.

Mps1 Directly Binds to Ndc80C through Two Distinct Conserved Motifs

We next tested whether human Mps1 directly interacted with Ndc80C. The kinetochore recruitment of Mps1 depends on Ndc80C. Mps1 directly interacts with Ndc80C in vitro (Kemmler et al., 2009; Zhu et al., 2013), but the molecular interactions between Mps1 and Ndc80C are not well characterized. Mps1 contains a conserved N-terminal extension (NTE) critical for kinetochore binding, a tetratricopeptide repeat (TPR) domain, and a C-terminal kinase domain (Nijenhuis et al., 2013) (Figure 3-4A). We found that the full length (FL) and N-terminal domain (Nt; residues 1-517) of recombinant human Mps1 interacted with purified recombinant human Ndc80C (Figure 3-4B). Further deletion mutagenesis revealed that Mps1 NTE (residues 1-62) and a middle region (MR; residues 261-300) could each independently bind to Ndc80C or Ndc80C^{bonsai} [a miniaturized

Ndc80C comprising mostly the head domains of the four subunits (Ciferri et al., 2008)] (Figure 3-4 C-F). Both the NTE and MR of Mps1 are highly conserved among vertebrate Mps1 proteins (Nijenhuis et al., 2013) (Figure 3-4A), suggesting that these molecular interactions between Mps1 and Ndc80C might also be conserved.

Mps1 MR appeared to preferentially bind to Ndc80C with the N-terminal tail of Hec1 partially degraded, whereas Mps1 NTE had no such preference (Figure 3-4 C and D). This result suggested that the Hec1 tail might inhibit MR binding to Ndc80C. Indeed, deletion of the N-terminal 40 residues of Hec1 enhanced Ndc80C binding to MR (Figure 3-5A). Because S281 within Mps1 MR is phosphorylated in mitotic human cells (Kang et al., 2007), we tested whether this phosphorylation regulated MR binding to Ndc80C. We synthesized two Mps1 peptides containing the most conserved 24-residue region in MR, with S281 unphosphorylated (MR24) or phosphorylated (pMR24), and measured their binding affinity toward $Ndc80C^{bonsai}$ with its Hec1 tail deleted (Δtail). As determined by isothermal titration calorimetry (ITC), the Mps1 MR24 and pMR24 bound to $Ndc80C^{bonsai}$ Δtail with dissociation constants (K_d) of 8.4 and 2.0 μM, respectively (Figure 3-5B). Thus, S281 phosphorylation moderately enhances Mps1 MR binding to Ndc80C. We do not know which kinase phosphorylates this site. Because S281 is followed by a proline and because the activities of cyclin-dependent kinases (Cdks) are high in mitosis, this site might be phosphorylated by mitotic Cdks.

Compared to $Ndc80C^{bonsai}$ wild type (WT), pMR24 bound much more efficiently to $Ndc80C^{bonsai}$ Δtail (Figure 3-5C). The weak binding between pMR24 and $Ndc80C^{bonsai}$ WT was undetectable by ITC (data not shown). These results confirmed an auto-inhibitory effect of the Hec1 tail on Mps1 MR binding. The Hec1 tail can be

phosphorylated by the centromeric kinase Aurora B at multiple sites (Cheeseman et al., 2006; Ciferri et al., 2008; DeLuca et al., 2006). Ndc80C^{bonsai} phosphorylated by Aurora B or with phospho-mimicking mutations in Hec1 (9D) bound to pMR24 more efficiently (Figure 3-5 C-E), suggesting that Aurora B phosphorylation could relieve this auto-inhibition. Thus, the Ndc80C–Mps1 MR interaction is regulated by mitotic phosphorylation of both partners.

We next examined the relationship between the two Ndc80C-binding motifs of Mps1. Because Mps1 MR does not bind well to Ndc80C with the Hec1 tail and because the Hec1 tail does not appear to regulate Mps1 NTE binding (Figure 3-6A), we used Ndc80C Δtail in these experiments. Mps1 NTE bound to Ndc80C Δtail more weakly than Mps1 MR did (Figure 3-6B). As determined by microscale thermophoresis (MST), the K_d of the NTE–Ndc80C^{bonsai} interaction was 9.6 μM (Figure 3-6C). The Mps1$_{1–300}$ fragment containing both NTE and MR motifs did not bind to Ndc80C^{bonsai} Δtail more tightly, as compared to Mps1$_{200–300}$ (which only contained MR) (Figure 3-6B). Based on ITC, Mps1$_{1–300}$ bound to Ndc80C^{bonsai} Δtail with a stoichiometry of 1:1 and a K_d of 8.7 μM (data not shown), which was virtually identical to that of MR24 binding. Therefore, we could not detect obvious cooperativity between the two Ndc80C-binding motifs of Mps1. Our results suggest that they bind independently to Ndc80C *in vitro*.

Mps1 NTE and MR Bind to the Head Domains of Hec1 and Nuf2

We next mapped the binding sites of the two Mps1 motifs on Ndc80C. Mps1$_{1-200}$ directly bound to the calponin homology domain (CH; residues 80-202) of Hec1 (Figure 3-7A). This interaction was diminished by the K89E and K166E mutations of Hec1 CH, which

were known to compromise Ndc80C binding to microtubules (Ciferri et al., 2008). This result strongly suggests that Mps1 NTE binds to the microtubule-binding surface on Hec1.

To determine the binding site of Mps1 MR on Ndc80C, we created Ndc80C mutants with either the Hec1 or Nuf2 head domain deleted, and tested their binding with pMR24. Deletion of the Nuf2 CH domain, but not the Hec1 CH domain, abolished pMR24 binding to Ndc80C (Figure 3-7B), implicating the Nuf2 head domain in MR binding. We then made 20 mutants systematically targeting the conserved, surface-exposed residues in the Nuf2 CH domain. Six such mutants exhibited greatly reduced binding to pMR24, with N126A being the most deficient (Figure 3-7 C and Figure 3-8). These mutated residues are clustered around the microtubule-binding surface of Nuf2 (Figure 3-7D). In particular, K115 has previously been shown to be critical for microtubule binding (Ciferri et al., 2008). Thus, the Mps1-binding site on Nuf2 likely overlaps its microtubule-binding site. The unphosphorylated Hec1 tail might also bind to a similar site on Nuf2 and inhibit Mps1 binding.

Mps1 and Microtubules Compete for Ndc80C Binding

Through its NTE and MR motifs, Mps1 binds to the head domains of Hec1 and Nuf2, which are also critical for microtubule binding. We thus tested whether NTE and MR competed with microtubule for Ndc80C binding. Binding between $Mps1_{1–200}$ (containing the NTE) and $Ndc80C^{bonsai}$ was gradually reduced by the addition of increasing doses of taxol-stabilized microtubules (Figure 3-9 A-B). As a control, $Mps1_{1–200}$ binding to $Ndc80C^{bonsai}$ 9D or Δtail, which were deficient in microtubule binding, was less affected

by microtubule. Likewise, addition of increasing concentrations of microtubules reduced the binding between pMR24 and Ndc80C^{bonsai} (Figure 3-9 C-D). Expectedly, unpolymerized tubulin also did not block the two Mps1–Ndc80C interactions (Figure 3-9E). Conversely, high concentrations (100 μM) of pMR24 reduced the microtubule-binding affinity of Ndc80C^{bonsai} from 0.56 μM to 5.87 μM (Figure 3-10). Interestingly, Ndc80C^{bonsai} with the Nuf2 N126A mutation (Ndc80C^{bonsai} N126A) that was deficient in Mps1 MR binding bound to microtubules with an affinity comparable to that of Ndc80C^{bonsai} WT. Importantly, microtubule binding of Ndc80C^{bonsai} N126A was not competed by pMR24. These results indicate that both Ndc80C-binding motifs of Mps1 compete with microtubules for binding to Ndc80C. Microtubules bind Ndc80C with higher affinity and can block Mps1 binding, but at unnaturally high concentrations, Mps1 MR weakens microtubule binding to Ndc80C, indicating that these binding events are mutually exclusive.

Mps1 MR is dispensable for Mps1 localization at kinetochores

We next examined the contributions of the two Ndc80C-binding motifs to Mps1 kinetochore localization. In agreement with previous studies (Nijenhuis et al., 2013), Mps1 ΔNTE failed to localize to unattached kinetochores (Figure 3-11 A-C). In contrast, the kinetochore localization of Mps1 ΔMR appeared to be normal. The Mps1 ΔMR localization also required the kinase activity of Aurora B, similar to Mps1 WT (Figure 3-11 D-E). Therefore, the kinetochore localization of Mps1 largely depends on the NTE–Ndc80C interaction. The direct competition of this interaction with microtubules likely underlies the preference of Mps1 for unattached kinetochores.

Because the Ndc80C–Mps1 interaction is too transient to be detected by immunoprecipitation-Western methods, we tested whether MR could target Mps1 to kinetochores to some extent. As expected, GFP fused to a single MR with the phospho-mimicking S281D mutation did not localize to unattached kinetochores (data not shown). GFP fused to four tandem repeats of MR containing S281D mutations (4MD) was capable of localizing to kinetochores (Figure 3-12 A-C). This localization was abolished by the Nuf2 N126A mutation, indicating that the MR–Nuf2 interaction could occur in human cells, and could target Mps1 to kinetochores to some extent. Interestingly, GFP-4MD still localized to attached metaphase kinetochores and interfered with chromosome alignment (Figure 3-12 D-E). The artificially strengthened interaction between GFP-4MD and Ndc80C might not be competed by microtubules or might displace the endogenous Mps1 bound to Nuf2.

The Mps1 MR–Nuf2 Interaction Is Critical for Knl1 Phosphorylation and Checkpoint Signaling

Consistent with previous reports and as expected from the role of NTE in Mps1 kinetochore targeting (Nijenhuis et al., 2013), Mps1 ΔNTE was deficient in supporting nocodazole-induced mitotic arrest of HeLa cells depleted of endogenous Mps1, indicative of a requirement for the NTE in spindle checkpoint signaling (Figure 3-13A). By inference, this result suggests that microtubule binding to the head domain of Hec1 weakens the checkpoint by antagonizing the function of NTE. While Mps1 ΔMR was only mildly deficient in supporting nocodazole-induced mitotic arrest, it was largely inactive when Aurora B was inhibited by ZM447439 (ZM). Furthermore, partial

depletion of Nuf2 together with ZM addition abolished nocodazole-mediated mitotic arrest (Figure 3-13B). Expression of Myc tagged Nuf2 WT, but not N126A (which is deficient in Mps1 MR binding), rescued this mitotic arrest deficiency. Expression of Nuf2 N126A produced moderate checkpoint defects, even in the absence of ZM. Notably, Myc tagged Nuf2 N126A was expressed at levels comparable to those of WT (Figure 3-13C), and localized normally to kinetochores (Figure 3-14C). Thus, the Mps1 MR–Nuf2 interaction contributes to checkpoint signaling. Disruption of this interaction in nocodazole-treated cells renders the spindle checkpoint dependent on the Aurora B kinase activity, similar to the checkpoint in taxol-treated cells that have attached kinetochores.

We then examined the Mps1-dependent downstream events in cells with the Mps1 MR–Nuf2 interaction disrupted. The kinetochore localization of Bub1 was compromised in Mps1 ΔMR cells, even without Aurora B inhibition (Figure 3-14 A-B). Likewise, Knl1 phosphorylation at a MELT motif and the kinetochore localization of BubR1 were reduced in Nuf2 N126A cells treated with nocodazole (Figure 3-14 C-F and 3-15). Again, these phenotypes were similar to those of taxol-treated cells (Figure 3-2 C-F). Taken together, loss of the Mps1 MR–Nuf2 interaction in cells with unattached kinetochores produces checkpoint properties that are similar to those of cells with most of their kinetochores attached. These results strongly suggest that the Mps1 MR–Nuf2 interaction senses the status of kinetochore attachment in human cells.

DISCUSSION

How cells sense kinetochore-microtubule attachment is a critical unresolved question in the spindle checkpoint. We have shown herein that microtubules directly compete with Mps1 for Ndc80C binding and that the Mps1–Ndc80C interactions are critical for checkpoint signaling. Our results thus establish a straightforward cellular mechanism for kinetochore-attachment sensing.

Human Mps1 interacts Ndc80C through two binding motifs: the N-terminal extension (NTE) and the middle region (MR). Surprisingly, these two motifs do not appear to engage in highly cooperative, bipartite interactions with Ndc80C. Instead, the NTE and MR can bind independently to the head domains of Hec1 and Nuf2, respectively. Thus, our results suggest that there might be two pools of Mps1–Ndc80C complexes at kinetochores: one involving the NTE–Hec1 interface and the other involving the MR–Nuf2 interface (Figure 3-16). Alternatively, even though there is no apparent cooperativity, our results do not rule out the possibility that the NTE and MR of the same Mps1 molecule can engage the Hec1 and Nuf2 head domains of the same Ndc80C.

The MR–Ndc80C interaction is enhanced by phosphorylation of both partners. Phosphorylation of S281 of MR directly contributes to binding, whereas phosphorylation of the Hec1 tail by Aurora B relieves auto-inhibition. Even with the activating phosphorylation events, MR only binds to Ndc80C with a modest affinity of 2 μM. GFP-MR S281D does not localize to kinetochores, indicating that this low-affinity interaction is insufficient to target a detectable amount of Mps1 to kinetochores. This MR–Ndc80C

interaction is also not required for the Mps1 kinetochore targeting in human cells. Instead, the NTE–Ndc80C interaction is more critical for targeting Mps1 to kinetochores. This interaction in fact has an affinity comparable to that of the MR–Ndc80C in vitro, but might be strengthened by posttranslational modifications or binding of yet unidentified cofactors in human cells. Depending on whether the two motifs of the same Mps1 molecule engage the same or different Ndc80C molecules, MR could either recruit a minor pool of Mps1 to kinetochores, or help to anchor Mps1 on Nuf2 and position Mps1 optimally for target phosphorylation.

Regardless of the binding mode, both Mps1-Ndc80C binding events can be inhibited by microtubules in vitro. The NTE- or MR-binding surface of Hec1 or Nuf2 overlaps the microtubule-binding surface, revealing direct competition. The weak, multisite interactions between Mps1 and Ndc80C are consistent with the transient nature of Mps1 kinetochore localization and the inability to detect these interactions through conventional binding assays in human cell lysates. We propose that this type of Mps1–Ndc80C interaction might have been evolved to balance the efficiency of Mps1 recruitment to unattached kinetochores and the need to remove Mps1 from attached ones. While a high-affinity interaction can certainly increase the efficiency of Mps1 recruitment to unattached kinetochores, it might impede Mps1 removal upon microtubule binding. Indeed, GFP-4MD containing four tandem repeats of MR localizes to both unattached and attached kinetochores, and interferes with chromosome alignment. Thus, artificially increasing the affinity between Mps1 and Ndc80C can alter the delicate balance and render this interaction resistant to microtubule competition.

Despite being dispensable for the kinetochore localization of Mps1, the MR–Ndc80C interaction is required for proper spindle checkpoint signaling. Disruption of this interaction (through MR deletion or mutation of a MR-binding residue in Nuf2) attenuates the strength of the checkpoint in nocodazole-treated cells to a degree comparable to that in cells with attached kinetochores. Cells deficient for this interaction cannot undergo mitotic arrest in nocodazole when Aurora B is inhibited, similar to taxol-treated cells. In particular, the Mps1-dependent phosphorylation of Knl1 is much reduced, and events downstream of this phosphorylation are compromised. Because Knl1 and Ndc80C are components of the same constitutive protein network, the weak MR–Ndc80C interaction is reminiscent of docking interactions commonly observed in kinase–substrate interactions. For example, the polo-box domain of Plk1 binds to phospho-peptide motifs on substrates, enabling their efficient phosphorylation by Plk1 (Elia et al., 2003). Phosphorylation of Cdc20 by Bub1 is also promoted by a docking interaction between the WD40 repeat domain of Cdc20 and a central Bub1 region outside its kinase domain (Kang et al., 2007). In the case of Knl1 phosphorylation of Mps1, the docking interaction occurs between Mps1 MR and the Knl1-associated Ndc80C, not Knl1 itself. As Knl1C indirectly binds to Ndc80C through Mis12C, the two degrees of separation ensure that Mps1 preferably phosphorylates Knl1 in the intact KMN. Our results further suggest that kinetochore signaling of checkpoint proteins requires not only their kinetochore localization, but also the establishment of specific molecular interactions at kinetochores.

Our study further points to an intricate crosstalk among the mitotic kinases Mps1, Bub1, and Aurora B in sensing kinetochore attachment. Increasing phosphorylation of the

Hec1 tail by Aurora B progressively weakens microtubule binding by Ndc80C (Zaytsev et al., 2014). By contrast, Aurora B-dependent phosphorylation of the same Hec1 tail enhances Mps1 MR binding to Nuf2, which promotes Knl1 phosphorylation and Bub1 kinetochore targeting. In a feed-forward mechanism, Bub1 can then phosphorylate histone H2A and further enrich Aurora B at centromeres (Kawashima et al., 2010; Yamagishi et al., 2010). In the future, it will be interesting to test whether Aurora B acts as a rheostat to fine tune the competing microtubule- and Mps1-binding activities of Ndc80C in opposite directions.

In conclusion, sensing unattached kinetochores is an initiating event in spindle checkpoint signaling. Microtubule- and dynein-dependent stripping of Mad1–Mad2 from attached kinetochores indirectly contributes to kinetochore-attachment sensing. Moreover, the dynein-dependent mechanism only exists in metazoans, and is not conserved in yeast (Karess, 2005). Our study now establishes the competition between Mps1 and microtubules for binding to Ndc80C as a direct mechanism for monitoring kinetochore attachment. Because yeast Mps1 has been shown to interact with yeast Ndc80C (Kemmler et al., 2009), Mps1 is likely the primordial sensor of kinetochore attachment.

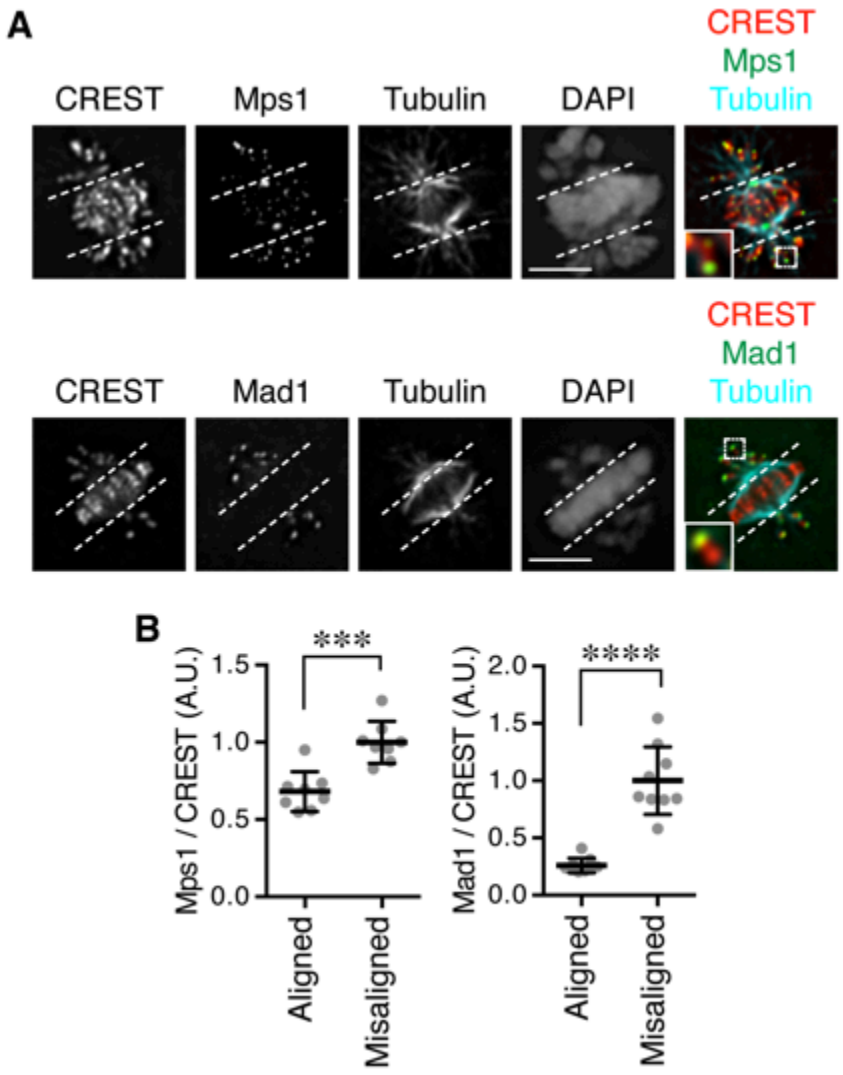

Figure 3-1. Mps1 and Mad1 preferentially localize to unattached kinetochores.

(**A**) Representative images of mitotic HeLa cells treated with 50 nM nocodazole and stained with DAPI and the indicated antibodies. For Mps1 staining (top panel), cells were also treated with reversine and MG132. Dash lines separate the few misaligned chromosomes from the aligned ones. The boxes regions were magnified and shown in insets. Scale bars, 5 μm. (**B**) Quantification of the relative intensities of Mps1 and Mad1 at kinetochores of aligned or misaligned chromosomes. Each dot represents one cell. Error bars, s.d. (n = 8 cells for Mps1 staining and n = 9 cells for Mad1 staining). ***, $p<0.001$; ****, $p<0.0001$.

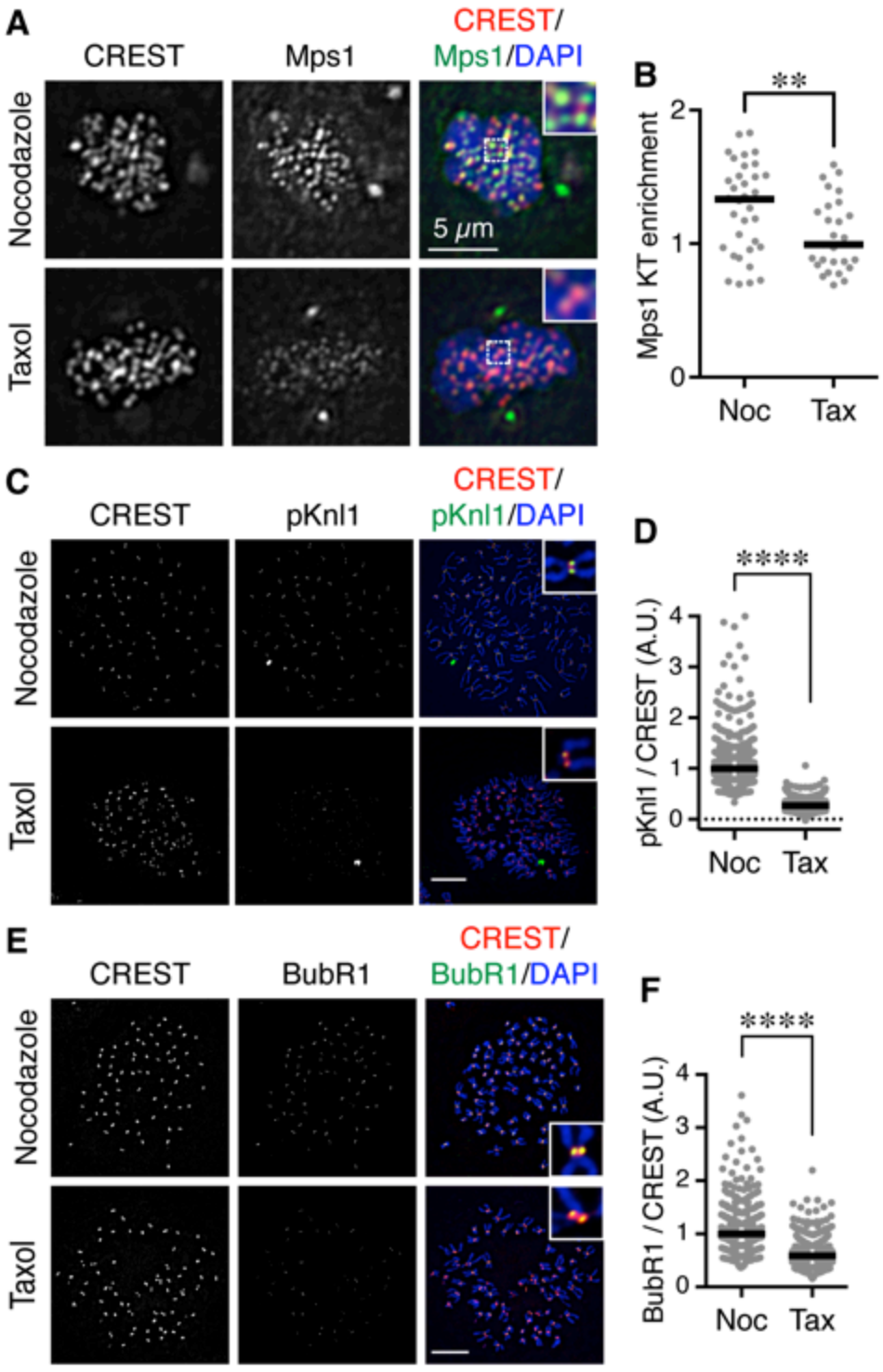

Figure 3-2. Mps1 localization and downstream signaling events are reduced at attached kinetochores.

(**A**) Immunofluorescence images of HeLa cells treated with nocodazole or taxol and with reversine and MG132. (**B**) Quantification of the kinetochore (KT) enrichment of Mps1 in

(A). Each dot represents one cell ($n_{Nocodazole}$ = 35; n_{Tax} = 27). Bar indicates the median of population. **, $p<0.01$; Student's t-test. (**C, E**) Chromosome spreads of mitotic HeLa cells arrested by nocodazole (Noc) or taxol (Tax) were stained with DAPI and the indicated antibodies. Scale bar, 10 μm. (**D, F**) Quantification of the relative kinetochore intensities of phospho-Knl1 (pKnl1) and BubR1 staining in (C, E), respectively. Each dot represents one kinetochore pair. Note that some data points in (D) fall below zero due to background subtraction. Bar indicates the median of population [n = 480 for each sample in (D); n_{Noc} = 280 and n_{Tax} = 240 in (F)]. ****, $p<0.0001$.

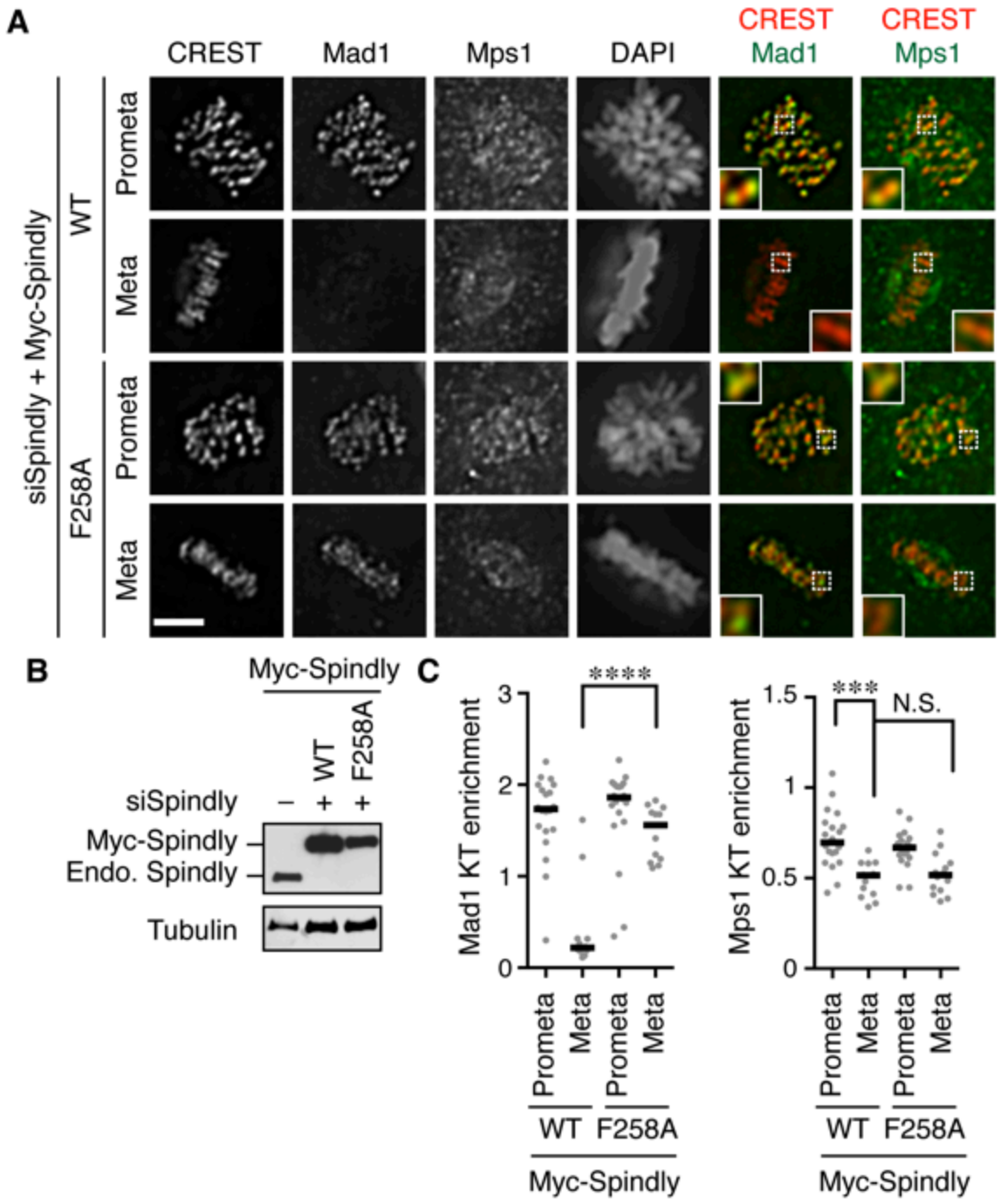

Figure 3-3. Mps1 is released from kinetochores in a dynein-independent mechanism. (**A**) Immunofluorescence images of prometaphase (Prometa) and metaphase (Meta) HeLa cells transfected with plasmids encoding Myc-Spindly wild type (WT) or the F258A mutant, and depleted of endogenous Spindly. Scale bar, 5 μm. (**B**) Immunoblots of cell lysates in (A). (**C**) Quantification of the kinetochore (KT) enrichment of Mad1 and Mps1 in (A). Each dot represents one cell. For WT, $n_{Prometa} = 19$; $n_{Meta} = 14$. For F258A, $n_{Prometa}$

= 18; n_{Meta} = 14. Bar indicates the median. ***, $p<0.001$; ****, $p<0.0001$; N.S., not significant; Student's t-test.

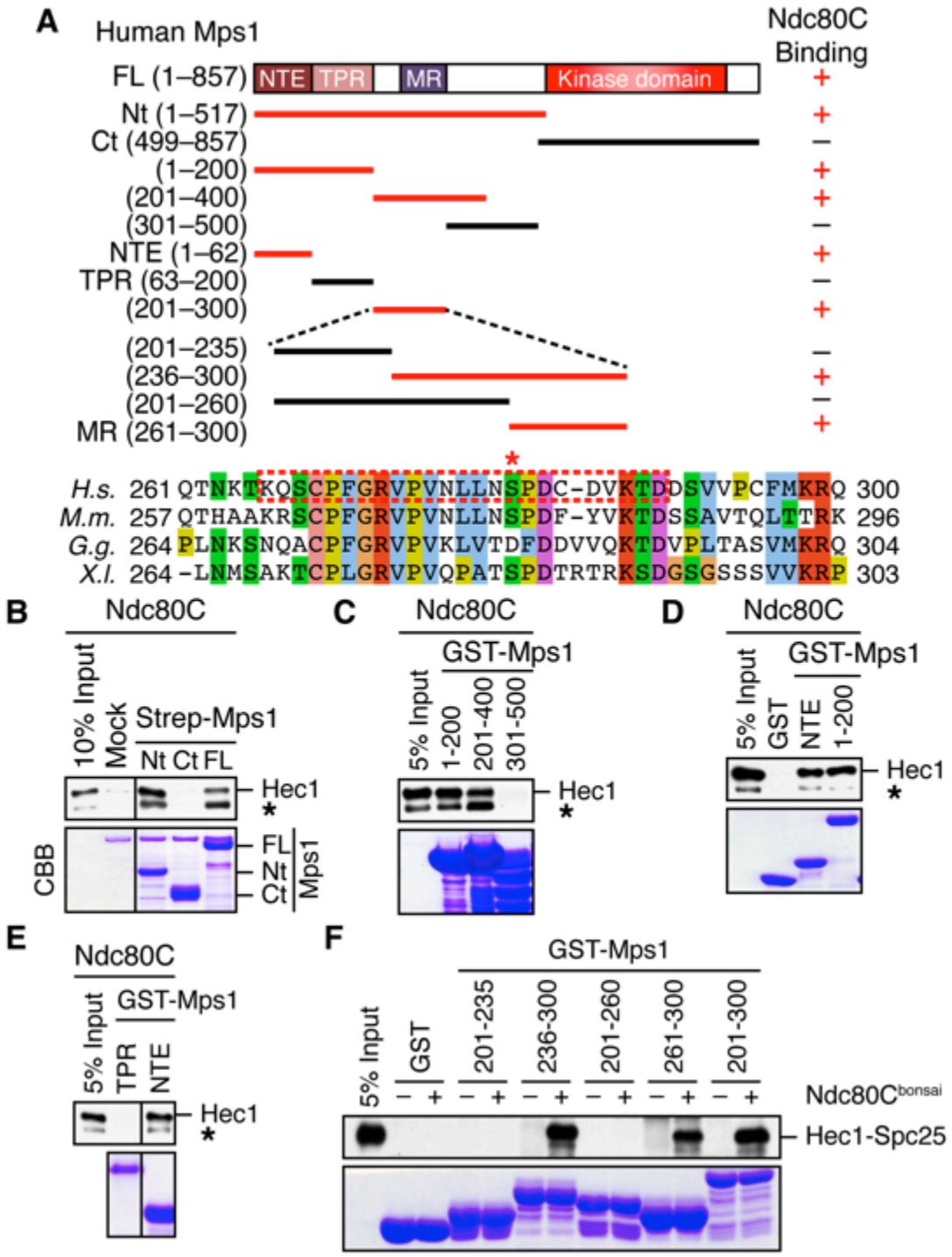

Figure 3-4. Mps1 directly interacts with Ndc80C through two distinct motifs.

(**A**) Domains and motifs of Mps1 and sequence alignment of the middle region (MR). Mps1 fragments that can or cannot bind to Ndc80C are depicted in red or black, respectively. *H.s.*, *Homo sapiens*; *M.m.*, *Mus musculus*; *G.g.*, *Gallus gallus*; *X.l.*, *Xenopus laevis*. The sequence of MR24 is boxed. Asterisk marks S281 phosphorylated in human

Mps1. (**B-F**) *In vitro* binding assays with the indicated GST-Mps1 fragments as baits and recombinant Ndc80C or Ndc80C^{bonsai} as preys. Ndc80C proteins bound to beads were blotted with the antibody to Hec1 (top panel). Bait proteins were stained with Coomassie Brilliant Blue (CBB) (bottom panel). Asterisk indicates a proteolytic fragment of Hec1 lacking part of its N-terminal tail.

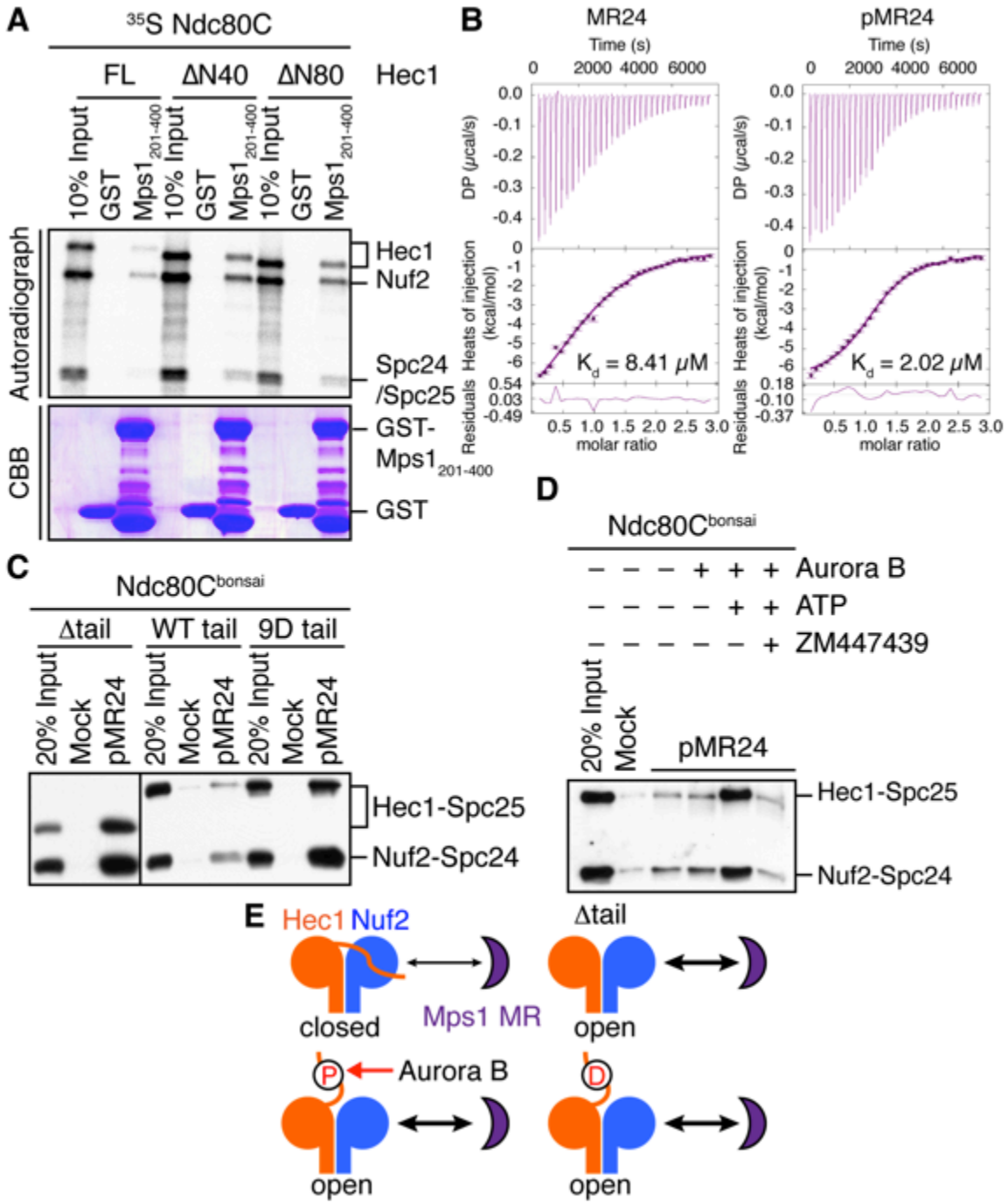

Figure 3-5. The binding between Mps1 MR and Ndc80C and the auto-inhibition of Hec1 tail.

(**A**) Full-length or N-terminal truncated Hec1 was *in-vitro* translated with Nuf2, Spc24 and Spc25 in the presence of ^{35}S-methionine. The ^{35}S-labeled Ndc80C complexes were then pulled down with GST or GST-Mps1$_{201-400}$ bound to beads. Ndc80C bound to beads was imaged with a phosphorimager (top panel). The bait proteins were stained with CBB

(bottom panel). (**B**) Isothermal titration calorimetry (ITC) assays of binding between Ndc80C^{bonsai} Δtail and unphosphorylated (MR24) or phosphorylated (pMR24) Mps1 peptides. (**C**) Binding of Ndc80C^{bonsai} containing Hec1 wild type (WT), Δtail, or 9D (Spc24 and Spc25 blot) to pMR24-coupled beads. (**D**) Ndc80C^{bonsai} WT was incubated with Aurora B–INCENP, in presence or absence of ATP or ZM447439 and then bound to pMR24-coupled beads. Bound proteins were resolved by SDS-PAGE and blotted with the antibody to Spc24 and Spc25. (**E**) Model explaining how Aurora B phosphorylation of the Hec1 tail stimulates MR binding to Ndc80C. Experiments in (B-D) were performed by Haishan Gao.

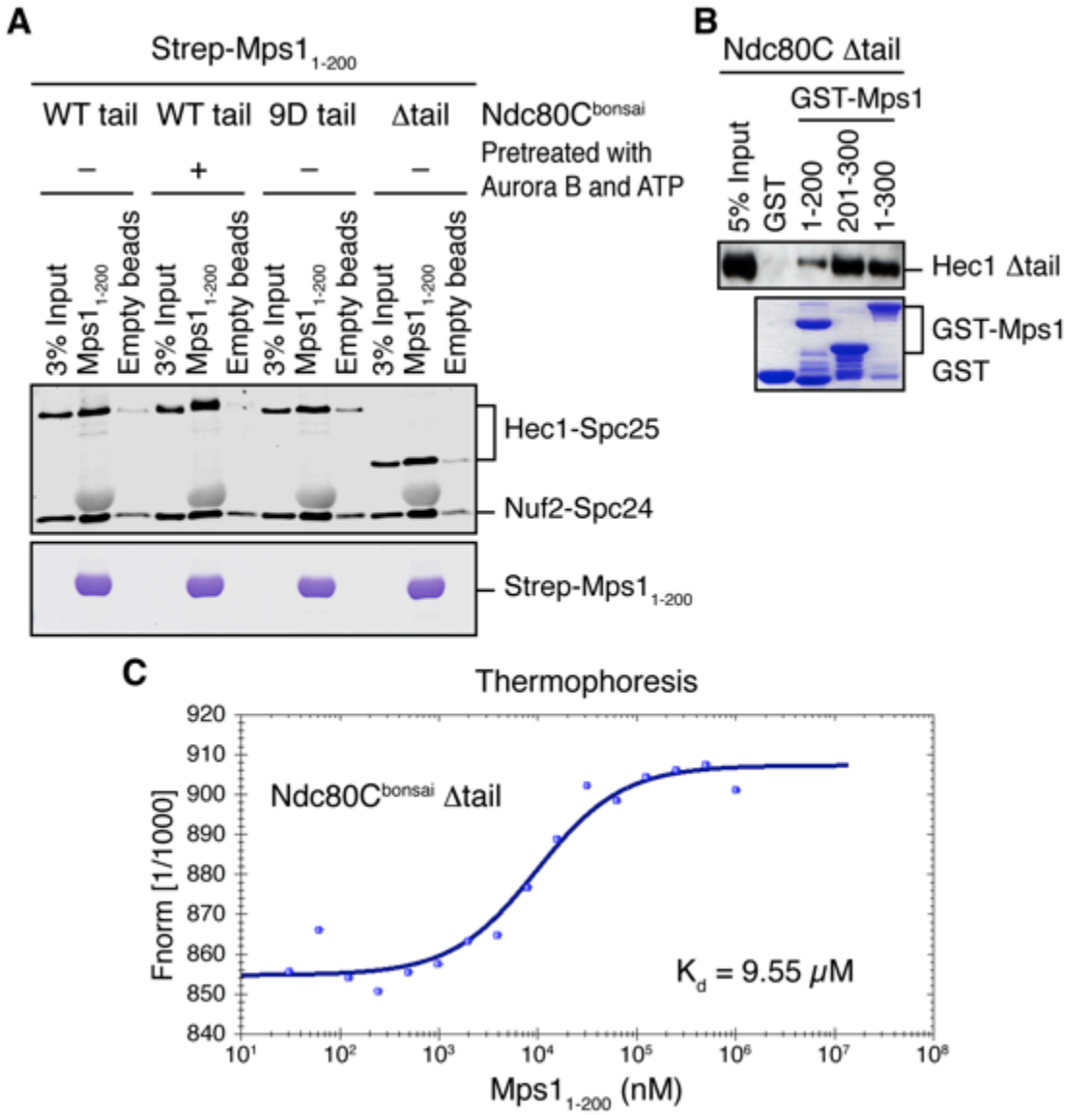

Figure 3-6. The Mps1 NTE–Ndc80C binding is not regulated by Hec1 tail and is non-cooperative with Mps1 MR–Ndc80C interaction.

(**A**) *In vitro* binding assays with Strep-Mps1$_{1\text{-}200}$ as bait and the indicated recombinant Ndc80C^{bonsai} proteins (pretreated with or without Aurora B and ATP) as preys. Ndc80C bound to beads was blotted with the antibody to Spc24 and Spc25 (top panel). Bait proteins were stained with Coomassie blue (bottom panel). (**B**) *In vitro* binding assays with the indicated GST-Mps1 fragments as baits and recombinant Ndc80C Δtail as the prey. Ndc80C bound to beads was blotted with the antibody to Hec1 (top panel). Bait proteins were stained with Coomassie blue (bottom panel). (**C**) Microscale

thermophoresis analysis of binding between Ndc80C^{bonsai} Δtail and Mps1$_{1-200}$. Experiments in (B) and (C) were performed by Haishan Gao.

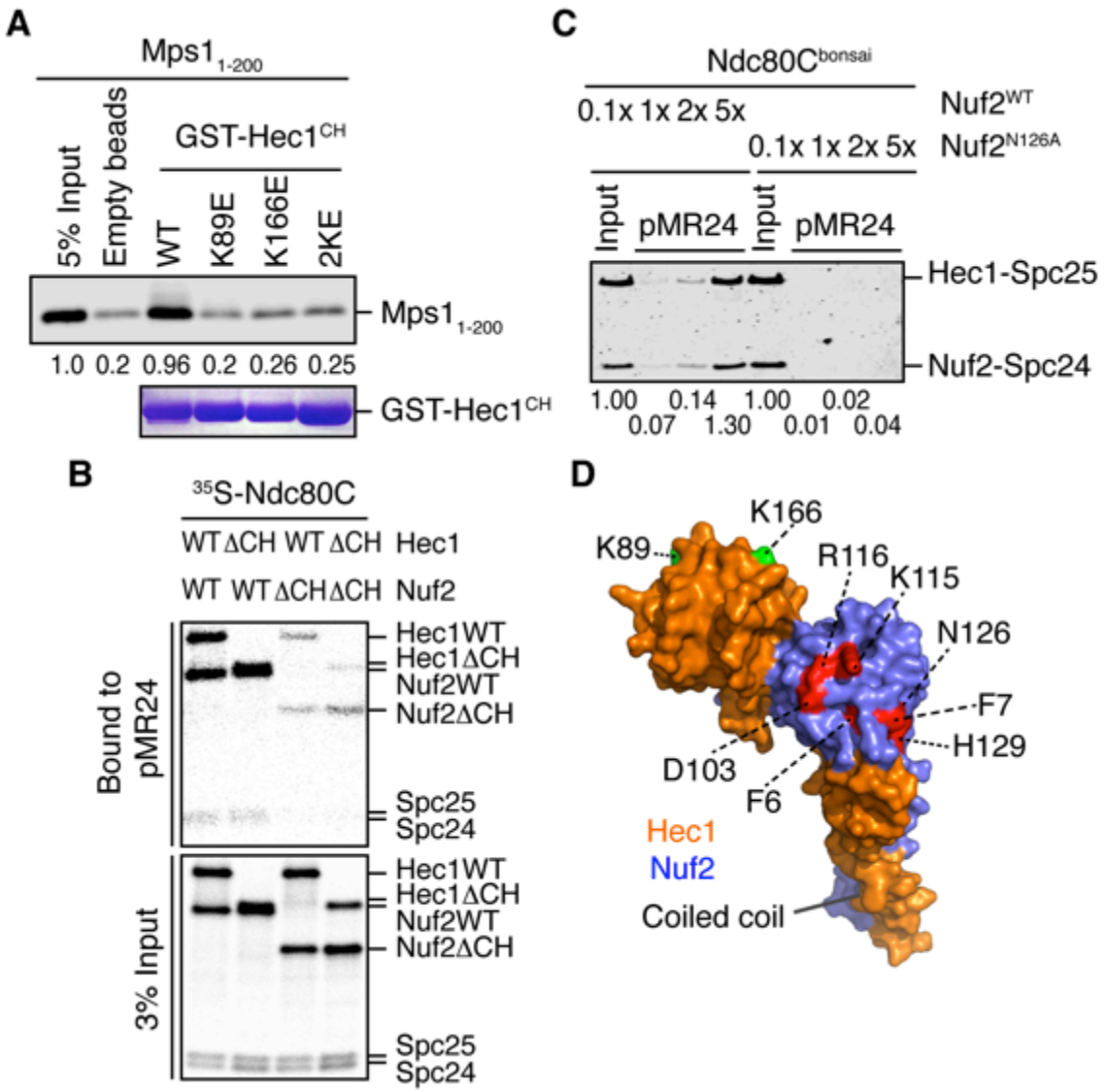

Figure 3-7. Mps1 NTE and MR bind to the head domains of Hec1 and Nuf2.

(**A**) Binding of $Mps1_{1\text{-}200}$ (blotted with antibody to Mps1; top panel) to beads bound to GST-$Hec1^{CH}$ WT or the indicated mutants (Coomassie staining; bottom panel). The relative band intensities (as ratios to that of WT) were indicated below. (**B**) The ^{35}S-labeled Ndc80C complexes containing Hec1/Nuf2 wild type (WT) or mutants with Hec1/Nuf2 CH deleted were bound to pMR24 beads. The input (3%) and bound proteins were resolved by SDS-PAGE and analyzed with a phosphorimager. (**C**) Binding of $Ndc80C^{bonsai}$ containing Nuf2 WT or N126A (Spc24 and Spc25 blot) to pMR24 beads. Relative band intensities were indicated below. (**D**) Surface drawing of the CH domains of Hec1 and Nuf2. Hec1 and Nuf2 residues critical for Mps1 NTE and MR binding were labeled.

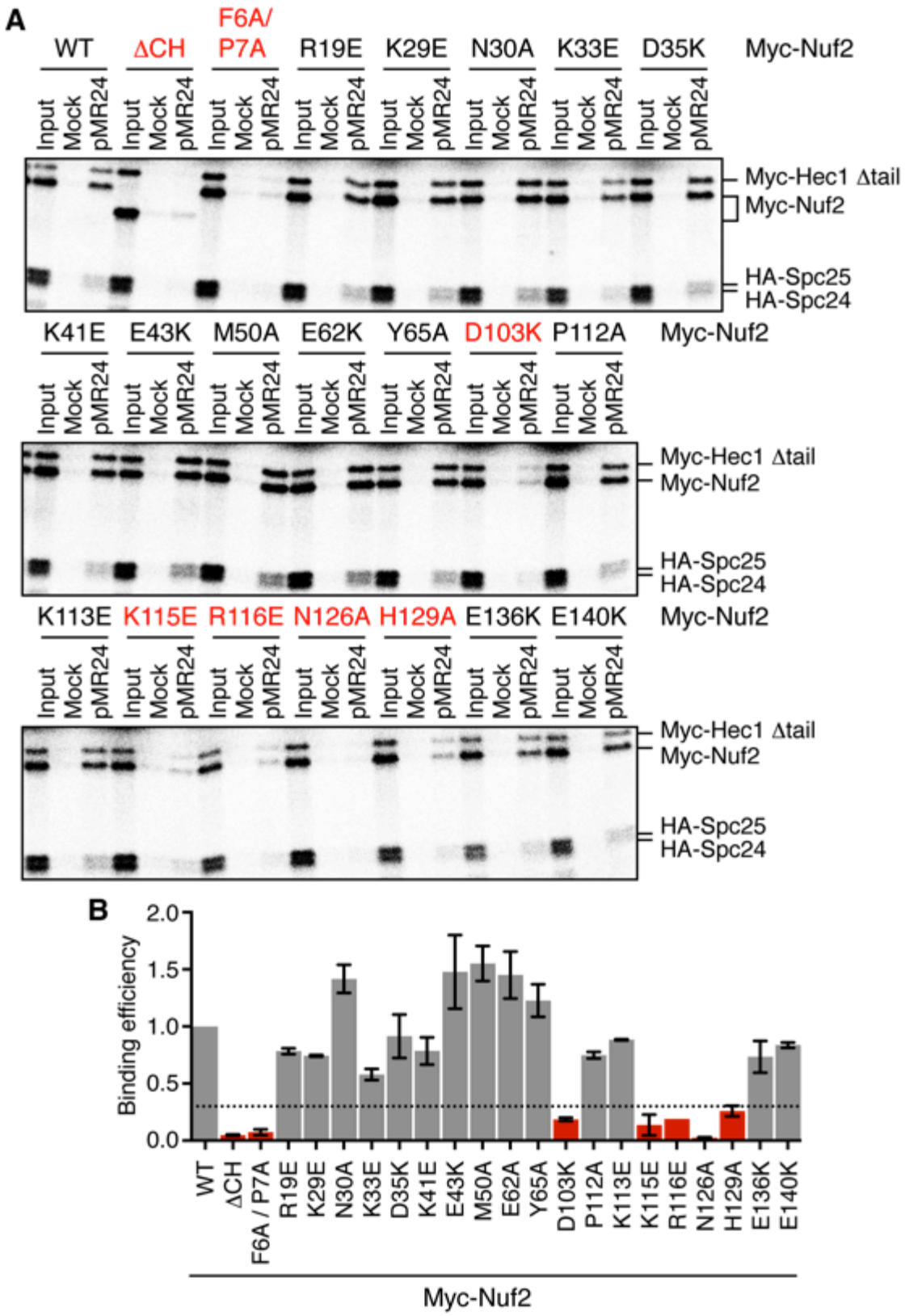

Figure 3-8. Identification of residues in the Nuf2 calponin homology domain (CH) critical for Mps1 MR binding.

(**A**) The ^{35}S-labeled Ndc80C Δtail complexes containing Nuf2 wild type (WT) or the indicated mutants were bound to empty (Mock) or pMR24 beads. The input (3%) and bound proteins were resolved by SDS-PAGE and analyzed with a phosphorimager. Nuf2 mutants deficient for MR binding are labeled in red. (**B**) Quantification of the normalized binding efficiency of binding reactions in (A). Error bars, range (n = 2 independent experiments). All mutants with binding efficiency below the cut-off of 0.3 (indicated by the dashed line) were depicted in red.

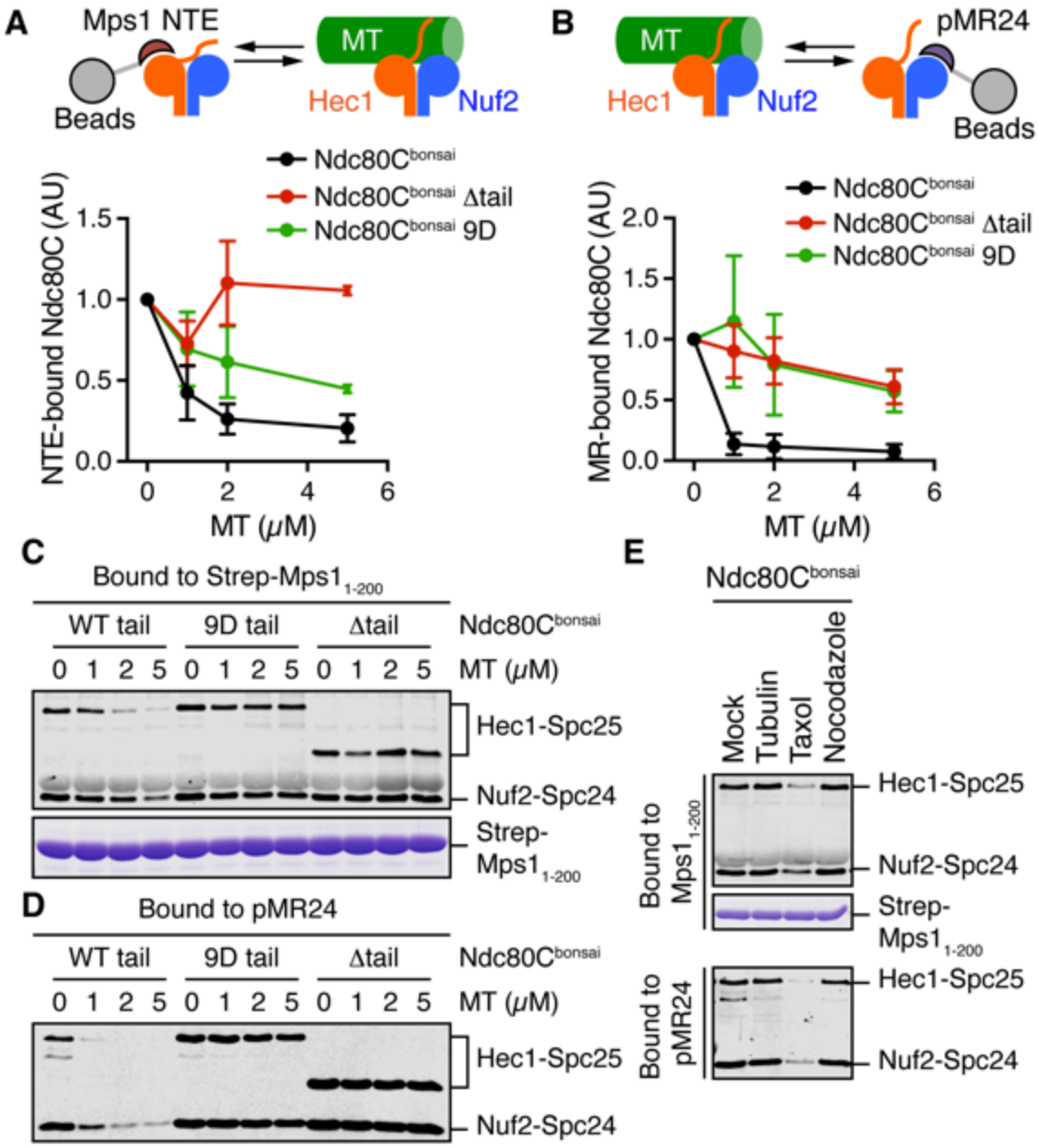

Figure 3-9. Mps1–Ndc80C interactions are inhibited by microtubule.

(**A, B**) Release of Ndc80C^{bonsai} proteins bound to beads containing GST-Mps1$_{1-200}$ (A) or pMR24 (B) by taxol-stabilized microtubules (MTs). Relative intensities of Ndc80C bound to beads were plotted against MT concentrations. AU, arbitrary unit. Error bars, s.d. (n = 3 independent experiments). (**C**) Ndc80C^{bonsai} containing Hec1 wild-type (WT) tail, 9D tail, or Δtail was bound to Strep-Mps1$_{1-200}$ beads, in the absence or presence of increasing amounts of taxol-stabilized microtubules (MT). Proteins bound to beads were examined by quantitative immunoblotting with the antibody to Spc24 and Spc25 (top

panel) and Coomassie staining (bottom panel). Band intensities were quantified and shown in (A). (**D**) The indicated Ndc80C^{bonsai} proteins were bound to pMR24-coupled beads, in the absence or presence of taxol-stabilized microtubules (MT). Proteins bound to beads were analyzed by quantitative immunoblotting with the antibody to Spc24 and Spc25 (top panel). Quantification of the assays was shown in (B). (**E**) Ndc80C^{bonsai} was bound to either Strep-Mps1$_{1-200}$ (top panel) or pMR24 (bottom panel) beads, in the absence or presence of 5 μM free tubulin dimer (Tubulin), taxol-stabilized microtubule (Taxol), or nocodazole-treated tubulin dimer (Nocodazole). Proteins bound to beads were examined by quantitative immunoblotting with the antibody to Spc24 and Spc25 (top and bottom panels) and Coomassie staining (middle panel).

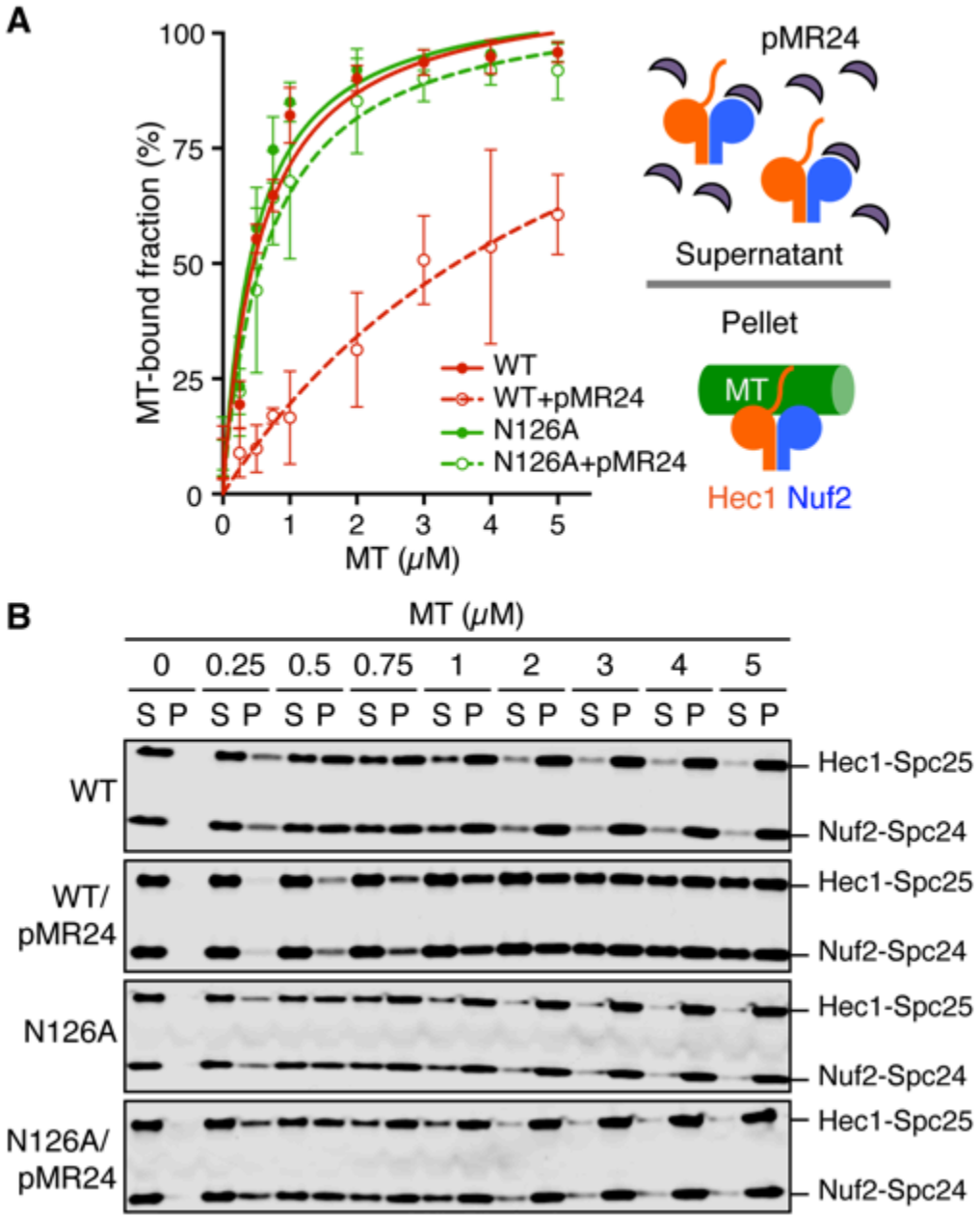

Figure 3-10. Excess amount of Mps1 MR suppresses Ndc80C binding with microtubules.

(**A**) Inhibition of Ndc80C^{bonsai} (Nuf2 WT or N126A) binding to taxol-stabilized microtubules (MTs) by pMR24, as revealed by microtubule pelleting assay. Fractions of microtubule-associated Ndc80C^{bonsai} proteins were plotted against microtubule concentrations. Data were fitted with one-site binding curves. Error bars, s.d. (n = 3 independent experiments). (**B**) Wild type (WT) or Nuf2 N126A (NA) Ndc80C^{bonsai} were precipitated with increasing amounts of taxol-stabilized microtubules, with or without

100 μM pMR24. The supernatant (S) and pellet (P) fractions of Ndc80C^{bonsai} were blotted with the antibody to Spc24 and Spc25. Quantification of the assay was shown in (A).

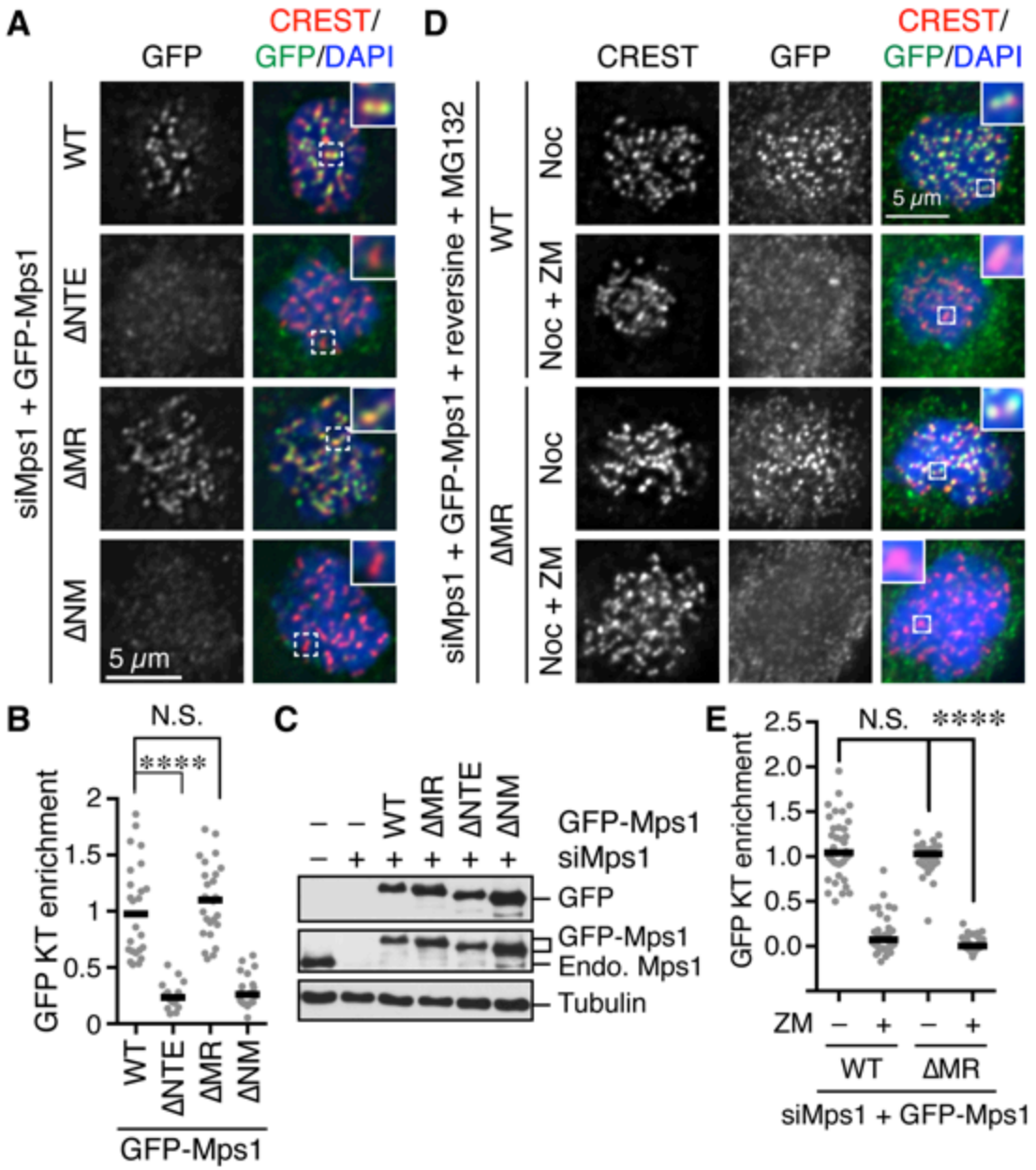

Figure 3-11. The kinetochore localization of Mps1 depends on Aurora B activity and NTE, but not MR.

(**A**) Localization of stably expressed GFP-Mps1 proteins in HeLa cells depleted of endogenous Mps1. Cells were treated with MG132, reversine, and 5 μM nocodazole for 1 h. ΔNTE, mutant lacking NTE; ΔMR, mutant lacking MR; ΔNM, mutant lacking NTE and MR. CREST, calcinosis, Raynaud's phenomenon, esophageal dysmotility, sclerodactyly, telangiectasia. DAPI, 4',6-diamidino-2-phenylindole. Boxed regions were magnified and shown in insets. (**B**) Quantification of the kinetochore (KT) enrichment of

GFP signals in (A). Each dot represents one cell. Bars indicate the median. ****, $p<0.0001$; N.S., not significant; Student's t-test. (**C**) Immunoblots of lysates of HeLa cells in (A). (**D**) Immunofluorescence images of HeLa cells stably expressing GFP-Mps1 WT or ΔMR and depleted of endogenous Mps1. Cells were treated for 1 h with MG132, reversine and 5 μM nocodazole, in absence or presence of ZM447439, before being fixed and stained. (**E**) Quantification of the kinetochore (KT) enrichment of GFP signals in (D). Each dot represents one cell. Bar indicates the median of population ($n_{WT,–ZM}$ = 39; $n_{WT,+ZM}$ = 34; $n_{\Delta MR,–ZM}$ = 32; $n_{\Delta MR,+ZM}$ = 32). ****, $p<0.0001$; N.S., not significant; Student's t-test.

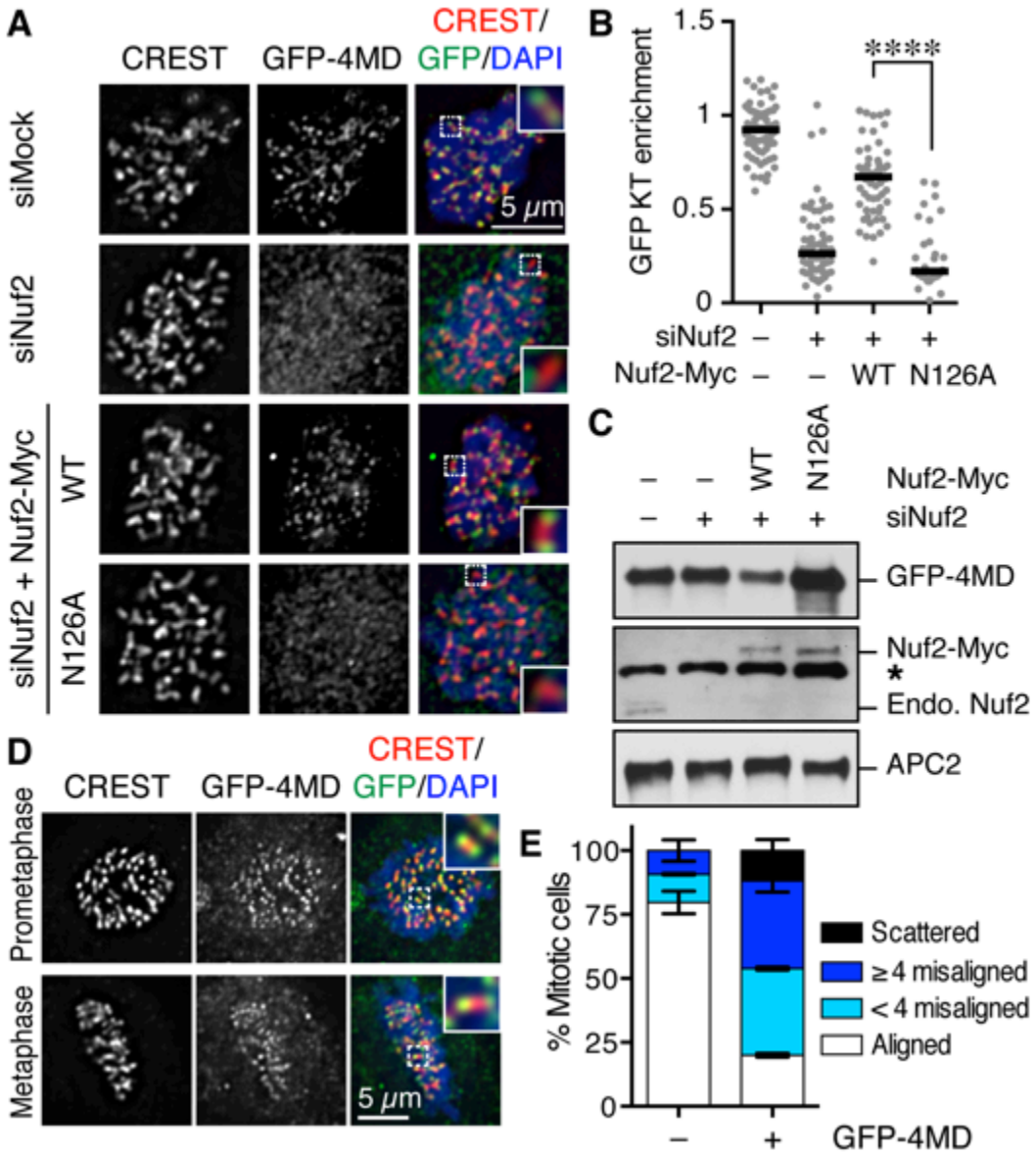

Figure 3-12. Mps1 4MD localizes to kinetochores and compromises the alignment of mitotic chromosomes.

(**A**) Immunofluorescence images of parental HeLa cells or HeLa cells stably expressing Nuf2-Myc wild type (WT) or N126A and transfected with GFP-4MD and siNuf2. (**B**) Quantification of GFP staining intensities at kinetochores (KT) of cells in (A). Each dot represents one cell. Bar indicates the median of population (n_{siMock} = 66; n_{siNuf2} = 74; n_{WT} = 58; n_{NA} = 32). ****, $p<0.0001$; Student's t-test. (**C**) Blots of cell lysates in (A). Asterisk indicates a cross-reacting band. (**D**) Immunofluorescence images of GFP-4MD-expressing HeLa cells. (**E**) Quantification of the percentages of mitotic cells with or without GFP-4MD expression that exhibited the indicated chromosome alignment

phenotypes. Mean and range of two independent experiments (n>100 cells each) are shown.

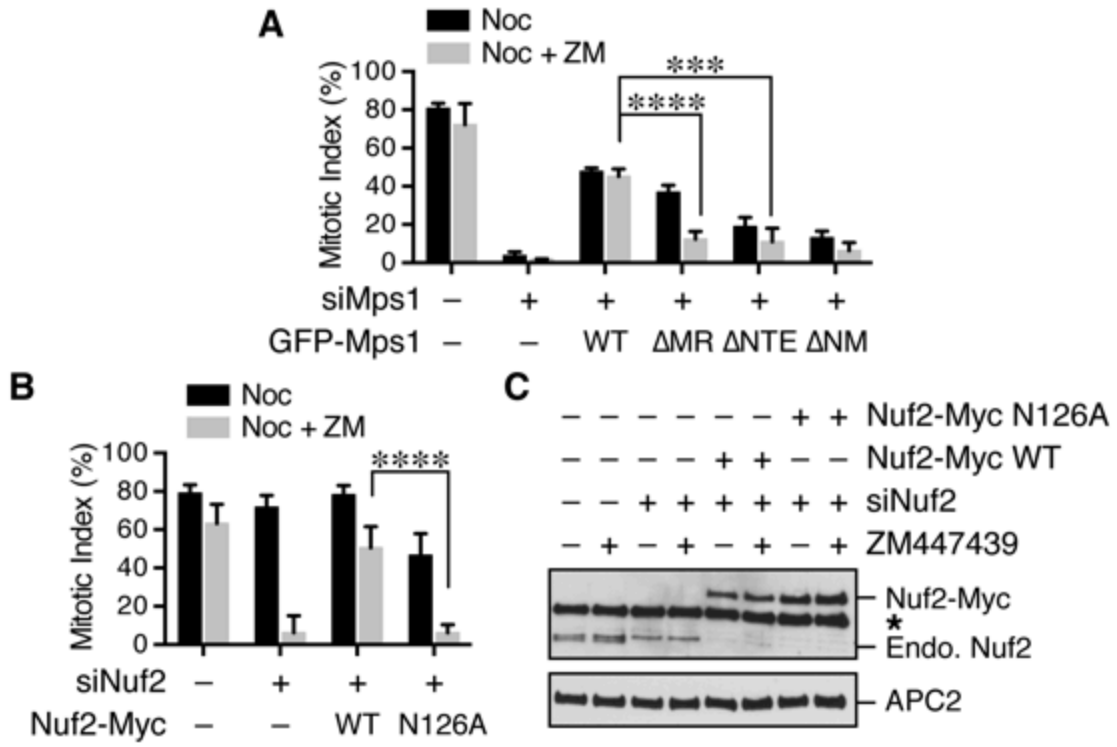

Figure 3-13. Mps1 MR contributes to Mps1 downstream signaling and the spindle checkpoint strength.

(**A**) Mitotic indices of HeLa cells stably expressing the indicated GFP-Mps1 proteins that were transfected with siMps1 and treated with nocodazole (Noc) with or without ZM447439 (ZM). WT, wild type. Error bars, s.d. (n = 4 independent experiments). ***, $p<0.001$; ****, $p<0.0001$; Student's t-test. (**B**) Mitotic indices of HeLa cells stably expressing the indicated Nuf2-Myc proteins transfected with siNuf2 and treated with nocodazole (Noc) with or without ZM447439 (ZM). WT, wild type. Error bars, s.d. (n = 4 independent experiments). ***, $p<0.001$; ****, $p<0.0001$; Student's t-test. (**C**) Lysates of HeLa cells in (B) were blotted with indicated antibodies. Asterisk indicates a cross-reacting band.

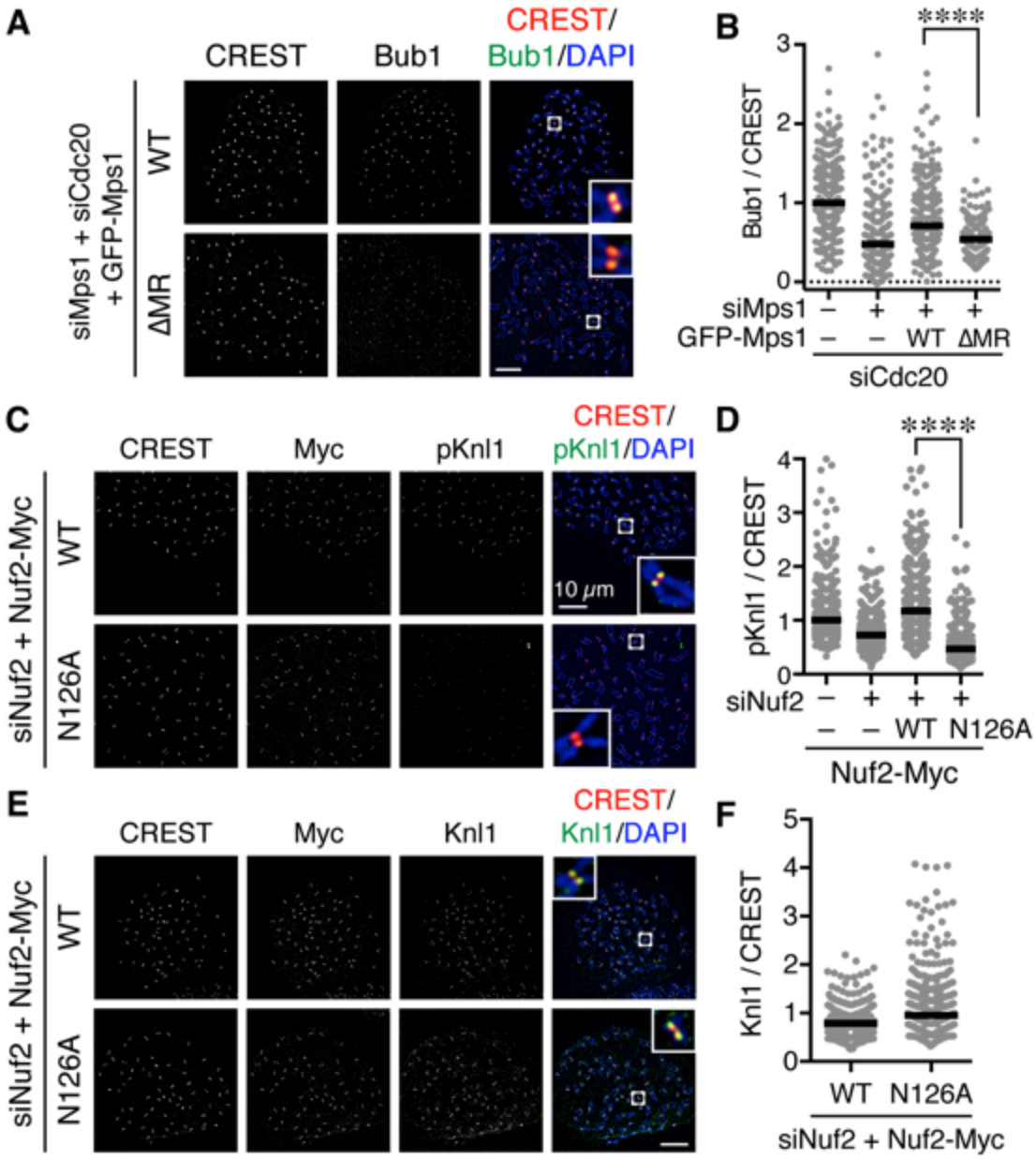

Figure 3-14. Nuf2 binding with Mps1 is required for checkpoint strength and signaling downstream of Mps1.

(**A**) Chromosome spreads of HeLa cells expressing GFP-Mps1 wild type (WT) or ΔMR transfected with siMps1 and siCdc20, and treated with nocodazole (5 μM) and MG132. Boxed regions were magnified and shown in insets. Scale bar, 10 μm. (**B**) Quantification of the relative kinetochore intensity of Bub1 staining in (A). Each dot represents one kinetochore pair. Bar indicates the median (n > 200 pairs of kinetochores per sample). Note that some data points fall below zero due to background subtraction. ****, p<0.0001; Student's t-test. (**C, E**) Chromosome spreads of cells that were stably

expressing the indicated Nuf2-Myc proteins, transfected with siNuf2, and treated with nocodazole and MG132 were stained with DAPI and indicated antibodies. Boxed regions were magnified and shown in insets. (**D, F**) Quantification of the relative kinetochore (KT) intensity of phospho-T875 Knl1 staining in (C) and (E). Each dot represents one KT pair. Bar indicates the median [n = 460 pairs of KTs in (C); n_{WT} = 440; n_{N126A} = 380 in (E)]. ****, $p<0.0001$; Student's t-test.

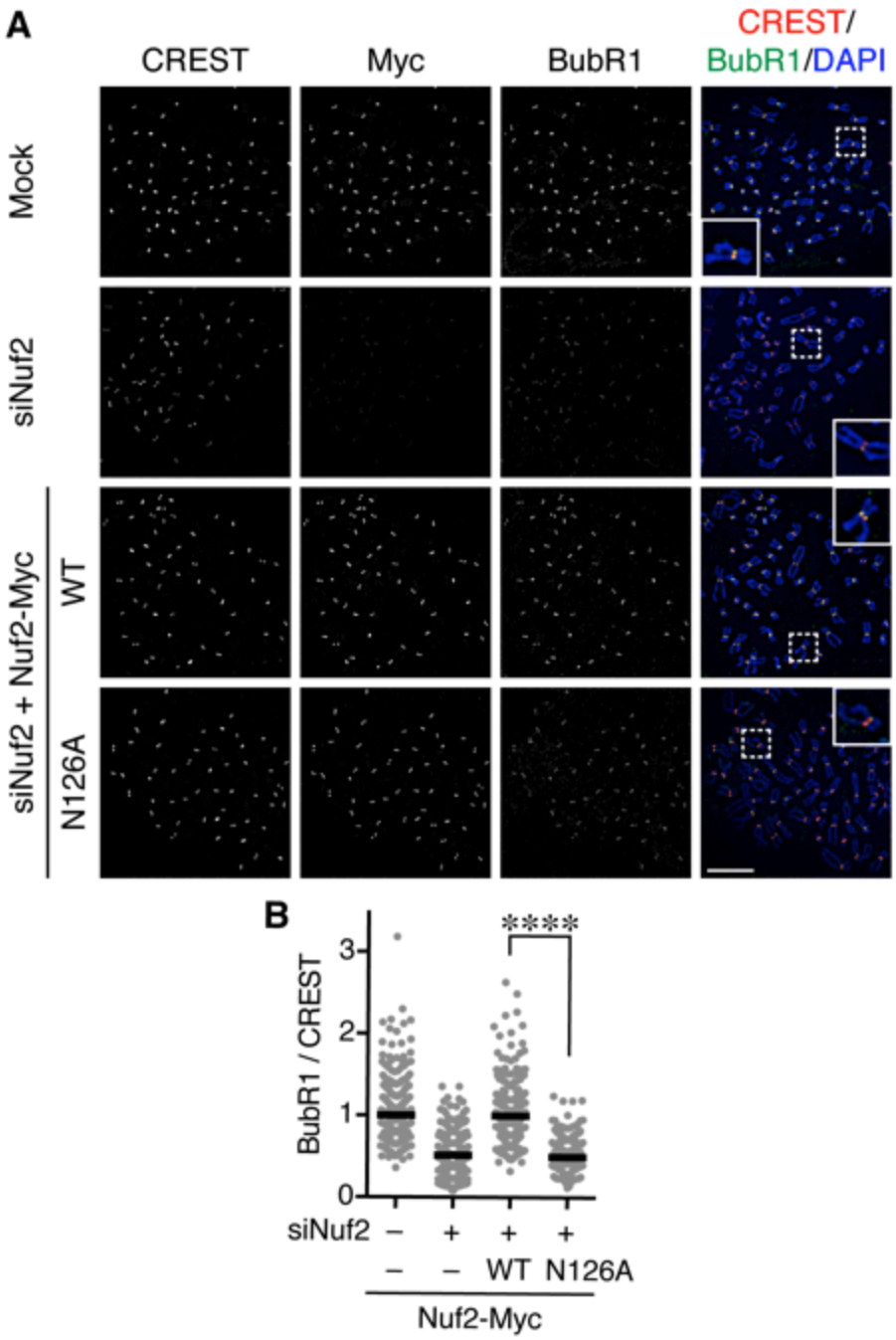

Figure 3-15. The Mps1–Ndc80C interaction enhances the kinetochore localization of BubR1.

(**A**) Chromosome spreads of HeLa cells expressing the indicated Nuf2-Myc proteins mock transfected or transfected with siNuf2, and treated with nocodazole (5 μM) and MG132. Boxed regions were magnified and shown in insets. Scale bar, 10 μm. (**B**) Quantification of the relative kinetochore intensity of BubR1 staining in (A). Each dot

represents one kinetochore pair. Bar indicates the median of the population (n_{siMock} = 280, n_{siNuf2} = 260, n_{WT} = 220, n_{NA} = 240). ****, $p<0.0001$; Student's t-test.

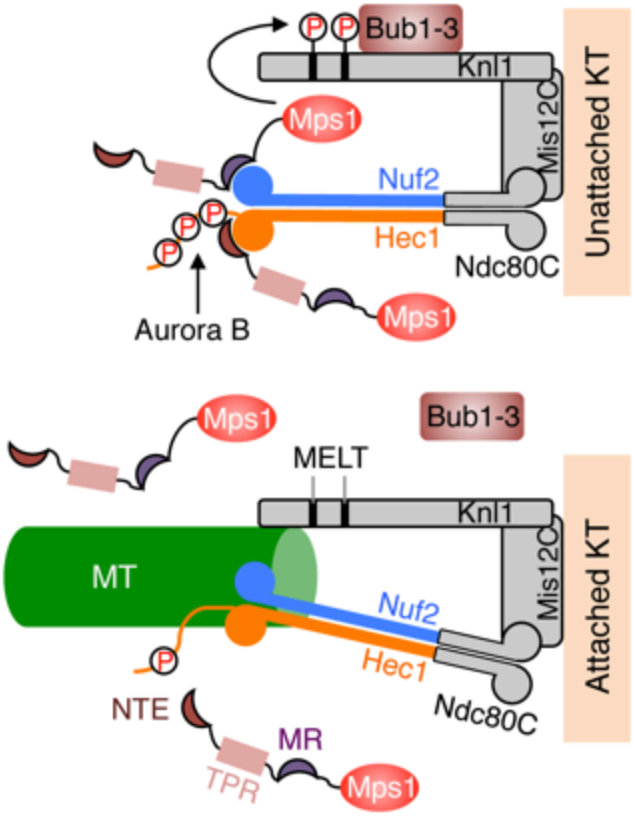

Figure 3-16. Kinetochore attachment sensed by competitive binding of Mps1 and microtubule to Ndc80C.

Model of microtubule (MT)-mediated inhibition of Mps1 signaling at kinetochores (KTs). Molecules and structures are not drawn to scale. Knl1 and Ndc80C are drawn as straight rods for simplicity.

CHAPTER VI: A SEQUENTIAL MULTI-TARGET MPS1 PHOSPHORYLATION CASCADE PROMOTES SPINDLE CHECKPOINT SIGNALING

INTRODUCTION

In the previous chapter, I have shown that the kinetochore-microtubule attachment is closely monitored by the evolutionarily conserved checkpoint kinase Mps1, which has been confirmed by several other studies (Aravamudhan et al., 2015; Hiruma et al., 2015). Mps1 recognizes unattached kinetochores through binding to the critical microtubule receptor, the Ndc80 complex (Ndc80C), when it is not bound by microtubules. Ndc80C-bound Mps1 initiates checkpoint signaling by phosphorylating multiple MELT motifs of the kinetochore scaffold Knl1 (London et al., 2012; Shepperd et al., 2012; Yamagishi et al., 2012). Phosphorylated MELT motifs recruit checkpoint complexes Bub1–Bub3 and BubR1–Bub3 to the kinetochores (Krenn et al., 2014; Primorac et al., 2013; Vleugel et al., 2013; Zhang et al., 2014). Bub1 and BubR1 in turn recruit Cdc20 (Di Fiore et al., 2015; Diaz-Martinez et al., 2015; Han et al., 2014; Jia et al., 2016; Lischetti et al., 2014). Mad1–Mad2 is also targeted to kinetochores through multiple mechanisms (Caldas et al., 2015; Kim et al., 2012; London and Biggins, 2014; Matson and Stukenberg, 2014; Silio et al., 2015), and promotes the conformational activation of open Mad2 (O-Mad2) to intermediate Mad2 (I-Mad2) (Hara et al., 2015; Luo et al., 2002; Luo et al., 2004; Luo and Yu, 2008; Mapelli et al., 2007; Mapelli and Musacchio, 2007; Sironi et al., 2002). I-

Mad2 is passed on to Cdc20 to form the Cdc20–C-Mad2 complex, which subsequently associates with BubR1–Bub3 to form MCC (Kulukian et al., 2009). MCC diffuses from kinetochores to inhibit APC/C^{Cdc20} throughout the cell.

Artificial tethering of Mad1–Mad2 to attached kinetochores causes prolonged activation of the spindle checkpoint and delays anaphase onset in the absence of spindle poisons (Maldonado and Kapoor, 2011). This artificial activation of the checkpoint still requires the kinase activity of Mps1, indicating that, aside from Knl1 phosphorylation, Mps1 has downstream functions in the checkpoint. Studies in the budding and fission yeast suggest that one such function of Mps1 is to phosphorylate Bub1 and establish a phosphorylation-dependent interaction between Bub1 and Mad1 (London and Biggins, 2014; Mora-Santos et al., 2016). Although the RLK motif in the Mad1 C-terminal domain (CTD) responsible for pBub1 binding is conserved from yeast to man (Brady and Hardwick, 2000; Kim et al., 2012), this Mps1-stimulated Bub1–Mad1 interaction has not been formally demonstrated in humans. Whether Mps1 has additional roles in regulating Mad1 also remains to be established.

Here, we report a direct phosphorylation-dependent interaction between human Bub1 and Mad1 in vitro. This interaction requires phosphorylation of Bub1 by both Cdk1 and Mps1, and is critical for spindle checkpoint activation in human cells. We have in vitro reconstituted checkpoint-dependent APC/C^{Cdc20} inhibition by MCC components, which requires a functional pBub1–Mad1 scaffold. Furthermore, we have found that Mps1 directly phosphorylates Mad1 in its CTD. Phosphorylated Mad1 CTD directly binds to the N-terminal region of Cdc20 and contributes to APC/C^{Cdc20} inhibition presumably through stimulating MCC assembly. Therefore, Mps1 activates the spindle

checkpoint through a three-step phosphorylation cascade. Phosphorylation of Knl1 by Mps1 enables Bub1 recruitment. Phosphorylation of Bub1 by Mps1 establishes the Bub1–Mad1 interaction. Phosphorylation of Mad1 by Mps1 positions Cdc20 for MCC assembly. We propose that this sequential multi-target phosphorylation cascade makes the checkpoint highly responsive to Mps1 whose function is directly regulated by kinetochore-microtubule attachment.

RESULTS

Phosphorylation of Bub1 by Cdk1 Is Required for the Spindle Checkpoint

Bub1 is a spindle checkpoint kinase conserved from yeast to man. Aside from its C-terminal kinase domain, the N-terminal non-kinase region of Bub1 contains multiple functional domains or motifs, including the tetratricopeptide repeat (TPR) domain for Knl1 binding, the Gle2-binding sequence (GLEBS) for Bub3 binding, the conserved middle region (CM; residues 458–476), and the Cdc20-binding phenylalanine box (Phe box; also known as ABBA motif) and the lysine-glutamate-asparagine (KEN) box (Di Fiore et al., 2015; Diaz-Martinez et al., 2015; Kang et al., 2008) (Figure 4-1A). Human Bub1 is highly phosphorylated in mitosis (Chen, 2004; Tang et al., 2004). A former postdoc in the lab, Jungseog Kang, has immunoprecipitated the endogenous Bub1 protein from mitotic HeLa cell lysates, and analyzed its mitotic phosphorylation sites with mass spectrometry. He has identified 30 phosphorylated residues that were scattered in the non-kinase domain of Bub1 (Figure 4-1B). One such site, S459, is located in the Bub1 CM.

A former graduate student, Luying Jia, has generated a phospho-specific antibody against Bub1 phospho-S459 (pS459). Recombinant Bub1$^{\Delta K}$–Bub3 was strongly phosphorylated at S459 by recombinant Cdk1, but not Mps1, in vitro (Figure 4-2A). This finding is consistent with the fact that Bub1 S459 is followed by a proline, and matches the minimal Cdk1 substrate consensus of [S/T]P. I next confirmed that Myc-Bub1 was indeed phosphorylated in mitotic HeLa cells (Figure 4-2B). Interestingly, Bub1 S459 phosphorylation in mitosis was reduced upon treatment of the Mps1 inhibitor, reversine.

Because recombinant Bub1 protein was not phosphorylated at S459 by Mps1 in vitro, the effect of Mps1 inhibition on S459 phosphorylation may be indirectly through checkpoint inactivation. This result further suggests that Bub1 S459 phosphorylation is regulated by the spindle checkpoint, possibly through the actions of phosphatases.

We then tested whether this phosphorylation site was required for the spindle checkpoint. HeLa cells depleted of endogenous Bub1 with a small interfering RNA (siRNA) had reduced mitotic index in the presence of taxol, indicative of checkpoint defects (Figure 4-3A). This mitotic arrest deficiency was rescued by ectopic expression of siRNA-resistant Bub1 full-length (FL), but not the S459A mutant (Figure 4-3A), suggesting a requirement for Bub1 S459 phosphorylation in the spindle checkpoint.

Bub1 is known to have a scaffolding role in the spindle checkpoint (Jia et al., 2016; Klebig et al., 2009). Indeed, expression of the Bub1 mutant lacking the kinase domain ($Bub1^{\Delta K}$) restored the taxol-induced mitotic arrest of Bub1-depleted cells. $Bub1^{\Delta K}$ S459A failed to rescue the mitotic arrest deficiency caused by Bub1 depletion (Figure 4-3A). This result suggests that the scaffolding function of the non-kinase region of Bub1 requires S459 phosphorylation.

To further confirm a role of Bub1 S459 phosphorylation in checkpoint-dependent mitotic arrest, we performed live-cell imaging of HeLa cells stably expressing mCherry tagged $Bub1^{FL}$, $Bub1^{\Delta K}$, or $Bub1^{\Delta K}$ S459A that were depleted of endogenous Bub1. In the presence of taxol, cells expressing $Bub1^{FL}$ or $Bub1^{\Delta K}$ stayed in mitosis for about 5 h before undergoing mitotic cell death or slippage. Cells expressing $Bub1^{\Delta K}$ S459A, however, escaped from mitosis after only about 2.2 h (Figure 4-3B). Furthermore, in an unperturbed cell cycle, cells expressing $Bub1^{\Delta K}$ S459A had a much shorter mitotic

duration (28 min), as compared to cells expressing Bub1$^{\Delta K}$ (58 min) (Figure 4-3C). Collectively, these lines of evidence suggest the non-kinase region of Bub1 has an important role in supporting the spindle checkpoint, and this role requires phosphorylation of S459 by Cdk1.

Phosphorylation of Yeast Bub1 by Mps1 Enables its Binding to Mad1

It has been reported previously that the middle region of *Saccharomyces cerevisiae* Bub1 (scBub1), when phosphorylated by Mps1, binds to Mad1–Mad2 and that this phosphorylation-dependent Bub1–Mad1 interaction is critical for the spindle checkpoint (London and Biggins, 2014). An attractive hypothesis is that phosphorylation of S459 in human Bub1 by Cdk1 similarly enables its binding to Mad1. However, despite repeated attempts, we could not detect binding between Mad1 and recombinant Bub1$^{\Delta K}$–Bub3 phosphorylated by Cdk1 in vitro. We decided to first examine whether phosphorylation of T453 of scBub1 (which corresponds to S459 in human Bub1) was required for binding to scMad1. Because the full-length Mad1 was difficult to express, we used a C-terminal fragment of Mad1 (Mad1^{E}) that contains both the Mad2-interacting motif (MIM) and the C-terminal domain (CTD) (Figure 4-4A). Co-expression of scBub1$_{369–608}$ with the kinase domain of scMps1 in bacteria led to phosphorylation of the scBub1 fragment. Consistent with the previous report (London and Biggins, 2014), only the phosphorylated scBub1 bound to the scMad1^{E}–scMad2 complex (Figure 4-4B). Internal deletion of the CM rendered scBub1$_{369–608}$ unable to bind to scMad1–scMad2, indicating a requirement of this motif in this interaction. Isothermal titration calorimetry (ITC) analysis showed that the smaller phosphorylated scBub1$_{449–530}$ fragment containing the CM bound to scMad1–

scMad2 with a moderate affinity of 2.2 μM (Figure 4-4C). Interestingly, this phospho-scBub1 fragment bound to the CTD of scMad1 with a similar affinity, indicating that Mad1 CTD is sufficient for the scBub1–scMad1 interaction, and Mad2 and the MIM of Mad1 are not required for this interaction.

There are three conserved serine/threonine residues in the CM of scBub1: T453, T455 and S458. Our mass spectrometry analysis revealed that all three residues were phosphorylated in scBub1$_{449–530}$ co-expressed with scMps1. We next synthesized scBub1 CM phospho-peptides containing pT453 or pT455 or both. We could not test the contribution of scBub1 pS458 to scMad1 binding, because the synthesis of pS458-containing peptides failed for unknown reasons. Both the singly phosphorylated pT455 peptide and the doubly phosphorylated pT453-pT455 peptide, but not the singly phosphorylated pT453 peptide, bound efficiently to scMad1 CTD (Figure 4-5A). Mutating the conserved RLK motif in Mad1 CTD abolished scMad1 binding to both scBub1 phospho-CM peptides. Furthermore, ITC analysis showed that the pT455 and pT453-pT455 peptides bound to scMad1 CTD with the same affinity (Figure 4-5B). Thus, Mps1-dependent phosphorylation of scBub1 at T455 alone is sufficient to establish scBub1–scMad1 binding. The scBub1–scMad1 interaction is mainly mediated by phospho-T455 of scBub1 and the RLK motif of scMad1. I note that phosphorylation of the T455 site in scBub1 has been previously reported (London and Biggins, 2014), and mutation of this residue disrupts scBub1–scMad1 binding and causes benomyl sensitivity in yeast cells, establishing the functional relevance of this phosphorylation event.

Sequential Phosphorylation of Human Bub1 by Cdk1 and Mps1 Enhances Mad1 Binding

Because phospho-T455 of scBub1 (which corresponds to T461 in human Bub1) was more critical for scMad1 binding than phospho-T453 (which corresponds to S459 in human Bub1), we wondered if phosphorylation of T461 in human Bub1 was similarly required for human Mad1 binding. We synthesized several phospho-peptides of human Bub1 CM and tested their binding to human Mad1. The pT461 peptide exhibited weak binding to human Mad1 CTD, and the doubly phosphorylated pS459-pT461 peptide had stronger binding (Figure 4-6A). As a specificity control, binding of both peptides was reduced by mutating the RLK motif in Mad1 CTD. Interestingly, the triply phosphorylated pS459-pT461-pT464 peptide bound more weakly to Mad1 than the pS459-pT461 peptide, indicating that phosphorylation of T464 had an inhibitory effect. Unfortunately, the binding between these human Bub1 phospho-peptides and Mad1 was undetectable by ITC, prohibiting us from quantitatively measuring their binding affinities. Our results suggest that phosphorylation of both S459 and T461 of human Bub1 is required for its interaction with Mad1.

We generated a phospho-specific antibody that recognized both pS459 and pT461 (pSpT) in Bub1. Incubation of recombinant Bub1$^{\Delta K}$–Bub3 with both Cdk1 and Mps1 led to efficient phosphorylation of both residues, whereas incubation with either kinase did not (Figure 4-6B). The pSpT antibody did not recognize the Bub1$^{\Delta K}$ S459A/T461A (SATA) mutant treated with both Cdk1 and Mps1, demonstrating the specificity of the antibody. The weak signal seen with Cdk1 alone was likely due to cross-reactivity of the pSpT antibody with Bub1 singly phosphorylated at S459. I then tested the order of these

two Cdk1- and Mps1-mediated phosphorylation events. When I first incubated Bub1$^{\Delta K}$ with Cdk1 to phosphorylate S459 and then inhibited Cdk1 with RO3306, subsequent addition of Mps1 led to efficient phosphorylation at T461, as detected by the pSpT antibody (Figure 4-6C). In contrast, when I first incubated Bub1$^{\Delta K}$ with Mps1, inhibited Mps1 with reversine, and then added Cdk1, Bub1$^{\Delta K}$ was still efficiently phosphorylated at S459, but was only weakly phosphorylated at T461, as revealed by a weak pSpT signal. This result suggests that phosphorylation of Bub1 at S459 and T461 by Cdk1 and Mps1 occurs sequentially (Figure 4-6D). Cdk1 phosphorylation at S459 primes Mps1 phosphorylation at T461. This notion is consistent with the fact that Mps1 prefers to phosphorylate sites with an acidic residue at the -2 position (Dou et al., 2011).

With both Cdk1- and Mps1-mediated phosphorylation, I observed a direct interaction between human Bub1$^{\Delta K}$–Bub3 and GST-Mad1^{E}–Mad2 in vitro (Figure 4-6E). As important controls, mutations of both phosphorylation sites on Bub1 or the RLK motif on Mad1 greatly reduced this interaction. Thus, the phosphorylation-dependent interaction between Bub1 CM and Mad1 CTD is conserved from yeast to man.

Bub1–Mad1 Binding is Critical for Spindle Checkpoint Activation in Human Cells

Although Jungseog's mass spectrometry analysis did not identify T461 as a phosphorylation site on endogenous human Bub1 isolated from mitotic HeLa cells, Bub1 T461 had been identified as a phospho-residue in a phospho-proteomics study (Daub et al., 2008). Using the pSpT phospho-specific antibody, I confirmed that both S459 and T461 sites were phosphorylated in checkpoint-active cells (Figure 4-7A). Interestingly, the T461A mutation also greatly reduced the pS459 signal. I do not know whether this

loss of pS459 signal was due to the dephosphorylation of this site or a direct effect of this mutation on antibody recognition.

I next tested whether phosphorylation of Bub1 T461 was required for the spindle checkpoint in human cells. As being shown previously (Jia et al., 2016), partial depletion of Bub1 and inhibition of Plk1 by BI 2536 synergistically inactivated the spindle checkpoint and hampered nocodazole-triggered mitotic arrest (Figure 4-7B and 4-7C). This mitotic arrest deficiency was rescued by the expression of siRNA-resistant Bub1 WT, but not S459A, T461A, or SATA, indicating that phosphorylation of both sites on Bub1 are critical for checkpoint signaling.

I further tested whether the RLK motif in Mad1 (which was likely the binding element of the Bub1 phospho-residues) was similarly required for the spindle checkpoint. Because I could not deplete Mad1 to sufficiently low levels to reveal a defect in nocodazole-dependent mitotic arrest, I adopted a previously reported strategy that involved the artificial targeting of Mad1 to kinetochores through a fusion to Mis12, a subunit of the outer kinetochore Mis12 complex (Figure 4-8A) (Maldonado and Kapoor, 2011). Expression of the Mis12–Mad1 fusion protein caused spontaneous mitotic arrest, which was dependent on Mps1, BubR1, and Mad2, indicating that this arrest required an active spindle checkpoint (Figure 4-8B and 4-8C). Importantly, the Mis12–Mad1 fusion proteins with the MIM or RLK motifs mutated failed to induce the mitotic arrest. Thus, both the Mad2-binding and Bub1-binding activities are critical for the checkpoint function of Mad1. Taken together, these results establish the functional importance of the phosphorylation-dependent Bub1–Mad1 interaction in the spindle checkpoint in human cells.

Bub1–Mad1 Acts as A Scaffold to Promote APC/C Inhibition by MCC Components

Next, we investigated the mechanism by which the Bub1–Mad1 interaction contributed to checkpoint activation. Although neither Bub1 nor Mad1 is a component of MCC, they both directly interact with MCC components. The constitutive Mad1–C-Mad2 complex interacts with O-Mad2 and converts it to I-Mad2, which can bind to Cdc20 to form the Cdc20–C-Mad2 complex. Furthermore, several previous studies have characterized the direct, checkpoint-relevant binding of Bub1 to Cdc20 (Di Fiore et al., 2015; Diaz-Martinez et al., 2015; Kang et al., 2008). These results raise the intriguing possibility that the Bub1–Mad1 complex functions as a scaffold to recruit MCC components (particularly I-Mad2 and Cdc20) into close proximity, thus promoting MCC assembly.

To test this hypothesis, we decided to reconstitute the process of MCC assembly and subsequent APC/C^{Cdc20} inhibition using a pre-assembled phospho-Bub1–Mad1 complex (Figure 4-9). For this purpose, recombinant full-length (FL), functional domains, or the relevant binary complexes of Bub1, Bub3, Mad1, Cdk1, Mps1, BubR1, Mad2, and Cdc20 were expressed in bacteria or insect cells and purified (Figure 4-10A). The N-terminal fragment of BubR1 (residues 1-370, $BubR1^{N}$) has been shown previously to support the formation of functional MCC (Jia et al., 2016; Lara-Gonzalez et al., 2011). We separated monomeric and dimeric forms of Mad2 with ion exchange chromatography (Figure 4-10B) (Luo et al., 2004). The monomeric Mad2 ($Mad2^{Mono}$) is mostly the inactive O-Mad2, while the dimeric Mad2 ($Mad2^{Di}$) contains a mixture of dimers of active C-Mad2 and asymmetric dimers between C-Mad2 and I-Mad2 (Hara et al., 2015; Yang et al., 2008).

We first compared the activities of $Mad2^{Mono}$ and $Mad2^{Di}$ to assemble functional MCC that was capable of inhibiting APC/C^{Cdc20}, in the absence of $Bub1^{\Delta K}$–Bub3, $Mad1^{E}$–Mad2, Cdk1, and Mps1 (Figure 4-11A). Incubation of $BubR1^{N}$ and $Cdc20^{\Delta N60}$ with $Mad2^{Di}$ allowed the spontaneous formation of functional MCC that inhibited Securin ubiquitination by APC/C^{Cdc20}. $Mad2^{Mono}$ was much less efficient in forming functional MCC and only showed weak APC/C^{Cdc20} inhibition at very high doses. This result suggests that the conformational change of Mad2 is a rate-limiting step in MCC assembly. Thus, the APC/C inhibition assay involving the use of $Mad2^{Mono}$ can be employed to test the conformational activation of Mad2 in the presence of the pre-assembled Bub1–Mad1 complex.

$Bub1^{\Delta K}$–Bub3 was first phosphorylated extensively by Cdk1 and Mps1 kinases and then mixed with the $Mad1^{E}$–Mad2 complex to form the Bub1–Mad1 complex. Subsequently, the mixture of $Bub1^{\Delta K}$–Bub3, $Mad1^{E}$–Mad2, Cdk1, and Mps1 (hereafter referred to as the Bub1–Mad1 mixture) were mixed with $BubR1^{N}$, $Cdc20^{\Delta N60}$, and $Mad2^{Mono}$ (referred to as the MCC mixture) to allow MCC formation (Figure 4-9). (The reason for using $Cdc20^{\Delta N60}$ as opposed to $Cdc20^{FL}$ will become apparent later.) The entire reaction mixture was then assayed for its ability to inhibit APC/C^{Cdc20}. Strikingly, Securin ubiquitination by APC/C^{Cdc20} was strongly inhibited when the MCC mixture containing $Mad2^{Mono}$ was pre-incubated with the WT Bub1–Mad1 mixture (Figure 4-11B). Omitting $Mad2^{Mono}$ abolished APC/C inhibition, indicating that MCC was formed by the activated $Mad2^{Mono}$, and not by the C-Mad2 bound to Mad1. This finding is consistent with the in vivo observation that Mad1 overexpression abrogates the spindle checkpoint, presumably by titrating free Mad2 (Chung and Chen, 2002). Remarkably,

Mps1 inhibition by reversine, mutations of S459 and T461 in Bub1 (SATA), or mutation of the Mad1 RLK motif (RLK/AAA) all greatly weakened APC/C^{Cdc20} inhibition by the MCC mixture. These results indicate that the intact phosphorylation-dependent Bub1–Mad1 interaction promotes APC/C^{Cdc20} inhibition by the MCC mixture, presumably through facilitating MCC assembly.

Phosphorylation of Mad1 by Mps1 Facilitates MCC Assembly and Checkpoint Activation

When testing different conditions for the in vitro reconstitution of Mps1-dependent APC/C^{Cdc20} inhibition by MCC, we noticed that, in the presence of only $Mad1^{E}$–Mad2 (without Bub1), Mps1 stimulated APC/C^{Cdc20} inhibition by the MCC mixture containing $Cdc20^{FL}$ (Figure 4-12A and 4-12B). Interestingly, this Bub1-independent stimulatory effect of Mps1 was not observed with the MCC mixture containing $Cdc20^{\Delta N60}$. This was the reason for the use of $Cdc20^{\Delta N60}$ in the APC/C assays described in the previous section, as $Cdc20^{\Delta N60}$ allowed us to eliminate the complications from this Bub1-independent function of Mps1.

It has been reported previously that overexpression of scMps1 in the budding yeast causes constitutive activation of the spindle checkpoint and hyper-phosphorylation of scMad1 (Hardwick et al., 1996), although the functional relevance of this Mps1-dependent Mad1 phosphorylation has not been further explored. Incubation of the human $Mad1^{E}$–Mad2 complex with human Mps1 and ATP slightly reduced the gel mobility of $Mad1^{E}$ (Figure 4-12C), suggestive of Mad1 phosphorylation by Mps1. Mass spectrometry analysis identified 15 phosphorylation sites in $Mad1^{E}$, with 13 sites located

in the flexible region N-terminal to the CTD (Figure 4-13A). Only two sites, T644 and T716, were located in Mad1 CTD, a domain known to be important for the spindle checkpoint (Heinrich et al., 2014; Kruse et al., 2014). Consistent with the initial discovery of Mps1 as a dual-specificity kinase (Mills et al., 1992), a tyrosine residue in Mad1, Y535, was phosphorylated by Mps1.

Then I used the Mis12–Mad1 fusion protein to test the potential relevance of these phosphorylation sites in human cells (Figure 4-13B and 4-13C). Mutating all identified phosphorylation sites in Mis12–Mad1 (YF-14A) abolished the mitotic arrest exerted by this fusion protein. Strikingly, mutating the two sites in the CTD individually (T644A and T716A) abrogated the function of Mis12–Mad1 more strongly than simultaneously mutating the 13 sites outside of the CTD. Thus, phosphorylation of Mad1 by Mps1 is required for Mad1 function in human cells, with the two sites in the CTD being the most critical ones.

We tested whether phosphorylation of these Mad1 sites was involved in MCC assembly and APC/C inhibition. Mad1^{E}–Mad2 WT, but not the phosphorylation-deficient YF-14A mutant, supported Mps1-dependent MCC formation and APC/C inhibition (Figure 4-13D). Strikingly, mutation of a single phosphorylation site T716 in Mad1 abolished the stimulatory effect of Mps1. Thus, phosphorylation of Mad1 T716 by Mps1 enhances the formation of APC/C-inhibitory MCC in vitro. In contrast, the Mad1 T644A mutation did not affect the ability of Mps1 to stimulate MCC formation, suggesting that phosphorylation of this residue contributes to Mad1 function in vivo through other mechanisms.

Mps1-mediated Phosphorylation of Mad1 at T716 Promotes Cdc20 Binding

As shown in Figure 4-12B, Mps1 and Mad1^{E}–Mad2 only stimulated the APC/C^{Cdc20}-inhibitory activity of the MCC mixture containing Cdc20^{FL}, but not that of the mixture containing Cdc20$^{\Delta N60}$. This suggests that Mps1-phosphorylated Mad1 might bind to the N-terminal tail of Cdc20, which contains two conserved basic motifs (BM1 and BM2) (Figure 4-14A). Indeed, the Mad1^{E}–Mad2 complex pre-treated with the kinase domain of Mps1 was efficiently pulled down by the His_6-tagged N-terminal fragment of Cdc20 (residues 1-170, Cdc20^{N}) (Figure 4-14B). Inhibition of Mps1 by reversine greatly reduced this interaction. Mutating T716, but not all other phosphorylation sites, greatly diminished this interaction. These results indicate that phosphorylation of Mad1 at T716 by Mps1 is necessary and sufficient for Cdc20^{N} binding. Further mapping revealed a requirement for residues 26-37 of Cdc20 in phospho-Mad1 binding (Figures 4-14C and 4-14D), suggesting that BM1 (^{27}RWQRK^{31}) might be the binding site for Mad1 pT716. Because I-Mad2 binds to the Mad1-bound C-Mad2, this phosphorylation-dependent binding between Mad1 CTD and Cdc20^{N} might place the MIM of Cdc20 in the vicinity of I-Mad2, promoting the formation of Cdc20–C-Mad2 complex, which can further bind BubR1 to form MCC.

DISCUSSION

Mps1 is a master kinase for spindle checkpoint activation. How Mps1 regulates checkpoint signaling is not fully understood. It is well established that Mps1 can phosphorylate Knl1 at multiple MELT motifs to recruit the Bub1–Bub3 complex to kinetochores (Krenn et al., 2014; London et al., 2012; Primorac et al., 2013; Shepperd et al., 2012; Vleugel et al., 2013; Yamagishi et al., 2012; Zhang et al., 2014). Mps1-dependent Bub1–Mad1 interaction has also been characterized in the budding and fission yeast (London and Biggins, 2014; Mora-Santos et al., 2016), but has so far not been reported in humans. In the current study, we have shown that after priming phosphorylation by Cdk1, human Mps1 can phosphorylate the conserved motif of human Bub1, which enables the binding of human Mad1. Therefore, Bub1 is another evolutionarily conserved substrate of Mps1. We have reconstituted phospho-Bub1–Mad1-dependent APC/C inhibition by MCC components in vitro and demonstrated a requirement for this interaction in the spindle checkpoint in human cells. In addition, we have identified novel phosphorylation events of Mad1 by Mps1, which are also required for checkpoint activation and APC/C inhibition. As a master kinase in the spindle checkpoint, Mps1 establishes a phosphorylation cascade by sequentially phosphorylating Knl1, Bub1, and Mad1 (Figure 4-15A). Such a multiple-target phosphorylation cascade reinforces the requirement for Mps1 during checkpoint activation, making checkpoint signaling highly responsive to the kinase activity of Mps1.

The phosphorylated region of Bub1 and the RLK motif in Mad1 involved in phospho-peptide binding are both conserved from yeast to man, indicating a conserved

binding mode. The checkpoint-dependent Bub1–Mad1 interaction is readily detectable in the budding yeast (Brady and Hardwick, 2000; London and Biggins, 2014), even though we have demonstrated a role for Bub1 and the RLK motif of Mad1 in the kinetochore targeting of Mad1 (Kim et al., 2012). The yeast Bub1–Mad1 interaction requires only a single Mps1-dependent phosphorylation event at scBub1 T455, whereas the human Bub1–Mad1 interaction needs sequential phosphorylation at both S459 and T461 of human Bub1 by Cdk1 and Mps1 in vitro. The affinity of scBub1–scMad1 binding was about 1.6 μM as measured by ITC, but the binding between human Bub1 and Mad1 was not detectable by ITC, suggesting a much weaker affinity between the human proteins. Thus, in human cells, the Bub1–Mad1 interaction is likely buttressed by other factors at mitotic kinetochores. For example, the metazoan-specific Rod-Zwilch-ZW10 (RZZ) complex is particularly important for the Mad1 kinetochore localization (Caldas et al., 2015; Silio et al., 2015). It is possible that RZZ contributes to the Bub1–Mad1 interaction when all are anchored at kinetochores. The intrinsically weak affinity between Bub1 and Mad1, along with the difficulty of preserving the doubly phosphorylated Bub1 and other auxiliary interactions only present at intact kinetochores, may underlie the difficulty in detecting the Bub1–Mad1 interaction in human cell lysates. The Bub1–Mad1 interaction is also observed in *C. elegans*, although in that case the interaction involves different domains of Bub1 and Mad1 (Moyle et al., 2014). Thus, there are species-specific differences in this functionally important interaction.

Mps1 prefers to phosphorylate serine and threonine residues with a negatively charged residue at the -2 position (Dou et al., 2011). Similar to the MELT motifs of Knl1, the T644 site of Mad1 (^{641}IDIT^{644}) identified in this study matches the substrate

consensus of Mps1. Furthermore, phosphorylation of T461 in human Bub1 by Mps1 is enhanced by prior phosphorylation at S459 by Cdk1. The negatively charged phospho-S459 can serve the same purpose as the -2 acidic residue in the substrate recognition by Mps1. This type of Cdk1-primed Mps1 phosphorylation consensus likely exists in other Mps1 substrates. To our surprise, Mad1 T716 and adjacent residues do not match the consensus of Mps1 substrates. The MELT motifs of Knl1, Bub1 T461, and Mad1 T644 are all located in loops or flexible regions. In contrast, although it is surface exposed, Mad1 T716 resides in a well-folded α helix. We speculate that Mps1 might recognize Mad1 T716 through tertiary contacts, instead of a linear peptide motif. On the other hand, we cannot completely rule out the possibility that T716 is phosphorylated by a kinase other than Mps1 in vivo.

We do not know how phosphorylation of Mad1 T644 by Mps1 contributes to the spindle checkpoint, as it is not required for the reconstituted APC/C inhibition by MCC components in vitro. This phosphorylation does not appear to enhance the binding of phospho-Bub1 CM to Mad1. One possibility is that this phosphorylation is required for Mad1 CTD to interact with other regions of Bub1.

A key downstream activity of the spindle checkpoint is to inhibit APC/C^{Cdc20}. We have reconstituted Bub1–Mad1- and Cdk1/Mps1-dependent checkpoint inhibition of APC/C^{Cdc20}. Although we did not directly monitor the kinetics of MCC formation, it is very likely that the effects of Bub1–Mad1 and Mps1 on APC/C^{Cdc20} inhibition are through promoting the assembly of MCC. We note that Bub1 has been reported to directly interact with BubR1 (Overlack et al., 2015). The Bub1–BubR1 interaction has been reported to be dispensable for the spindle checkpoint, however (Zhang et al., 2015).

$BubR1^{N}$ used in our assay does not contain the Bub1-binding region, however. Thus, our assays do not test whether the Bub1–BubR1 interaction can contribute to MCC assembly and APC/C inhibition.

How the upstream checkpoint proteins, after being recruited to kinetochores, direct the assembly of MCC is an unresolved question. Our in vitro reconstitution experiments have provided important insight into this question. Our results support a model in which Bub1–Mad1 acts as a scaffold to recruit and activate MCC components, thus promoting MCC assembly (Figure 4-15B). Two phosphorylation-dependent molecular interactions, the Bub1–Mad1 interaction and the Mad1–Cdc20 interaction, are critical for the assembly and proper function of the scaffold. We have dissected the individual contributions of these two interactions to MCC assembly and APC/C inhibition in vitro. For example, to define the function of Bub1–Mad1 in MCC assembly, we eliminated the effect of Mad1 phosphorylation by Mps1 through inhibiting Mps1 prior to the addition of Mad1, and through the use $Cdc20^{\Delta N60}$, which no longer interacts with phosphorylated Mad1. Likewise, to assay the contribution of Mad1–Cdc20 to MCC assembly, we simply omitted Bub1 to eliminate its contribution. Although either interaction suffices to promote MCC assembly in vitro, disruption of either Bub1–Mad1 or Mad1–Cdc20 interactions largely abolished checkpoint activation caused by the forced targeting of Mad1 to kinetochores. Therefore, these two interactions likely cooperate with each other to promote checkpoint signaling in vivo. The $Cdc20^{N}$-binding function of phosphorylated Mad1 CTD can explain the recent findings that Mad1 has additional checkpoint functions aside from recruiting and activating Mad2 (Heinrich et al., 2014; Kruse et al., 2014).

We propose that Bub1–Mad1 can simultaneously recruit I-Mad2, Cdc20, and BubR1 into the same large complex (Figure 4-15B). Within this complex, the WD40 domain of Cdc20 binds to the Phe and KEN boxes of Bub1, and the N-terminal tail of Cdc20 is anchored to phosphorylated Mad1 CTD. This bipartite anchorage may optimally position the MIM of Cdc20 in the vicinity of I-Mad2, allowing I-Mad2 to entrap the MIM. The resulting C-Mad2–Cdc20 complex can then bind to BubR1 to form MCC. Even though we do not have direct evidence that the Bub1–BubR1 interaction is critical for the checkpoint, the Bub1-bound BubR1 is in a good position to encounter Mad2–Cdc20 and to be incorporated into MCC.

In conclusion, combining in vitro reconstitution and cellular experiments, we have established the Bub1–Mad1 complex as an evolutionarily conserved catalytic platform for stimulating APC/C inhibition by MCC components. We have further demonstrated the importance of an Mps1-orchestrated phosphorylation cascade in forming and activating this catalytic engine. This multi-target, sequential phosphorylation cascade renders the checkpoint highly sensitive to changes in the kinase activity of Mps1. As shown in the previous chapter and similar work from other lab (Hiruma et al., 2015), the kinetochore targeting of Mps1 itself is directly controlled by kinetochore-microtubule attachment, our findings further highlight a unique signal-transducing principle of the spindle checkpoint that not only enables signal amplification but also keeps the final signaling output responsive to kinetochore attachment status.

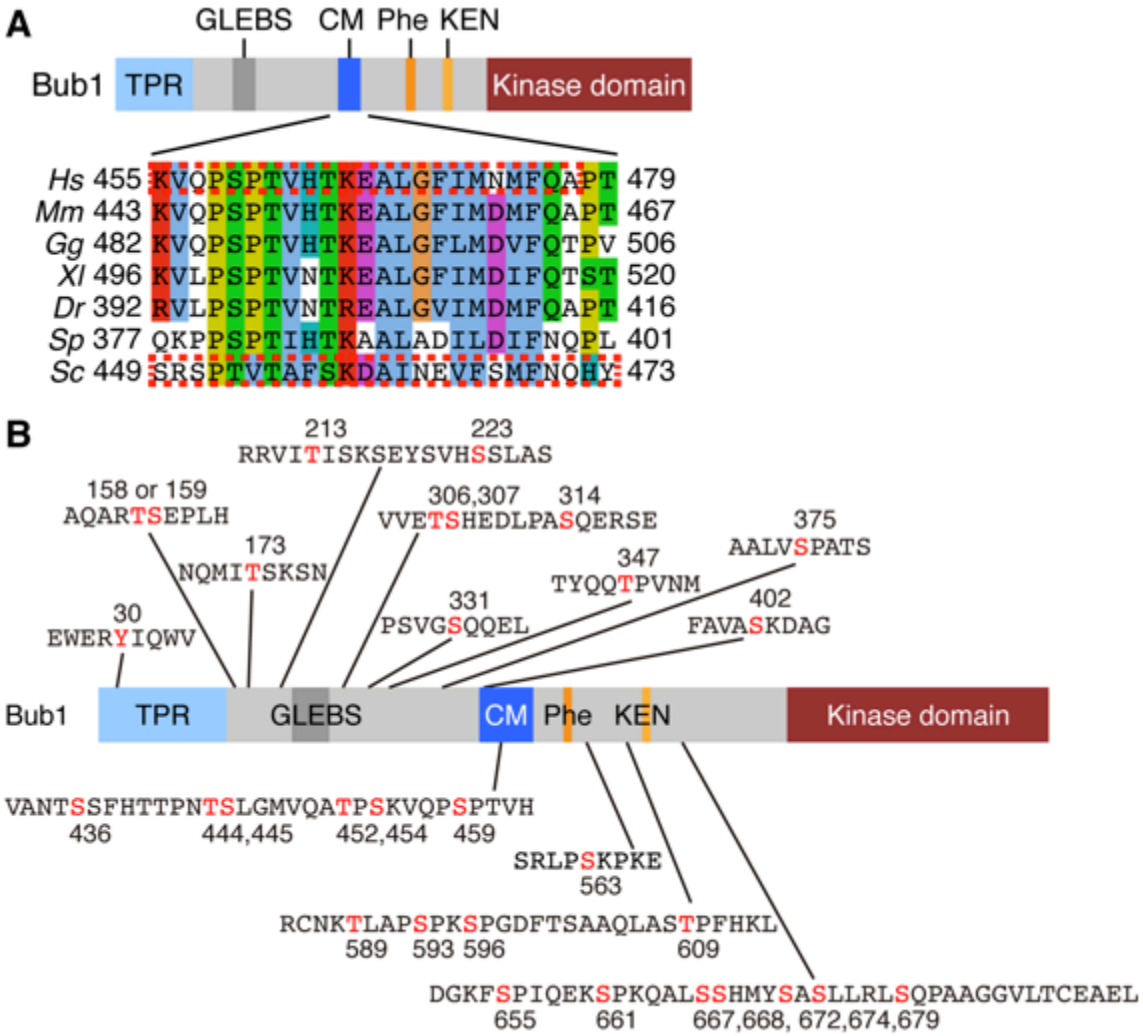

Figure 4-1. Human Bub1 is highly phosphorylated in its non-kinase region during mitosis.

(**A**) Domain and motifs of Bub1 and sequence alignment of its conserved motif (CM). TPR, tetratricopeptide repeat; GLEBS, Gle2-binding sequence; Phe, phenylalanine-containing motif, also known as "ABBA" motif; KEN, lysine-glutamate-asparagine motif. *Hs*, *Homo sapiens*; *Mm*, *Mus musculus*; *Gg*, *Gallus gallus*; *Xl*, *Xenopus laevis*; *Dr*, *Danio rerio*; *Sp*, *Schizosaccharomyces pombe*; *Sc*, *Saccharomyces cerevisiae*. The boxed regions in scBub1 and hsBub1 were synthesized as phospho-peptides and used in this study. (**B**) A summary of all 30 mitotic phosphorylation sites of Bub1 identified by mass spectrometry. Phosphorylated residues are denoted in red. Endogenous Bub1 was isolated from mitotic cells by Jungseog Kang.

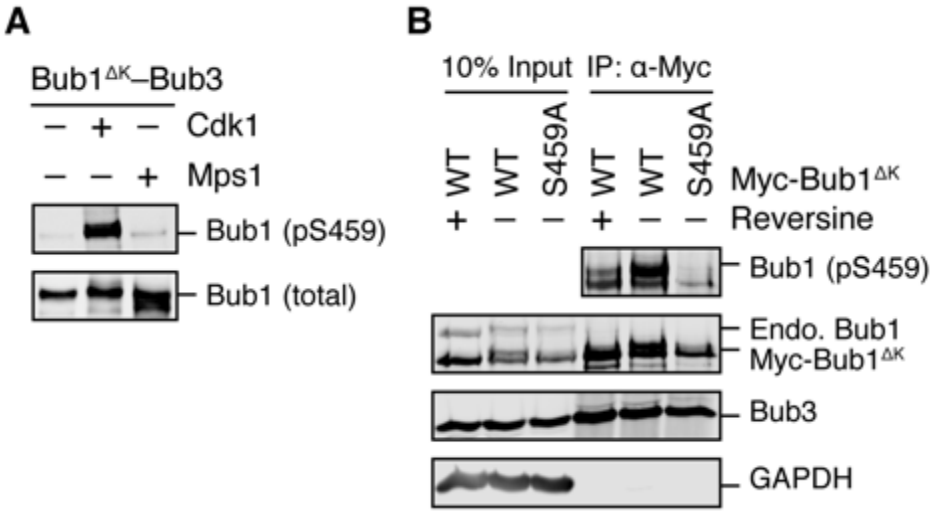

Figure 4-2. Bub1 S459 is phosphorylated by Cdk1 in checkpoint-active cells.

(**A**) Recombinant Bub1$^{\Delta K}$–Bub3 complex was incubated with Cdk1–Cyclin B1 (Cdk1) or Mps1 in the presence of ATP. The kinase reactions were blotted with indicated antibodies. The experiment was performed by Luying Jia. (**B**) HeLa cells stably expressing Myc-Bub1$^{\Delta K}$ wild-type (WT) or S459A mutant were treated with nocodazole and MG132 in the presence or absence of reversine. Myc-Bub1 was immunoprecipitated and blotted with indicated antibodies. Endo., endogenous.

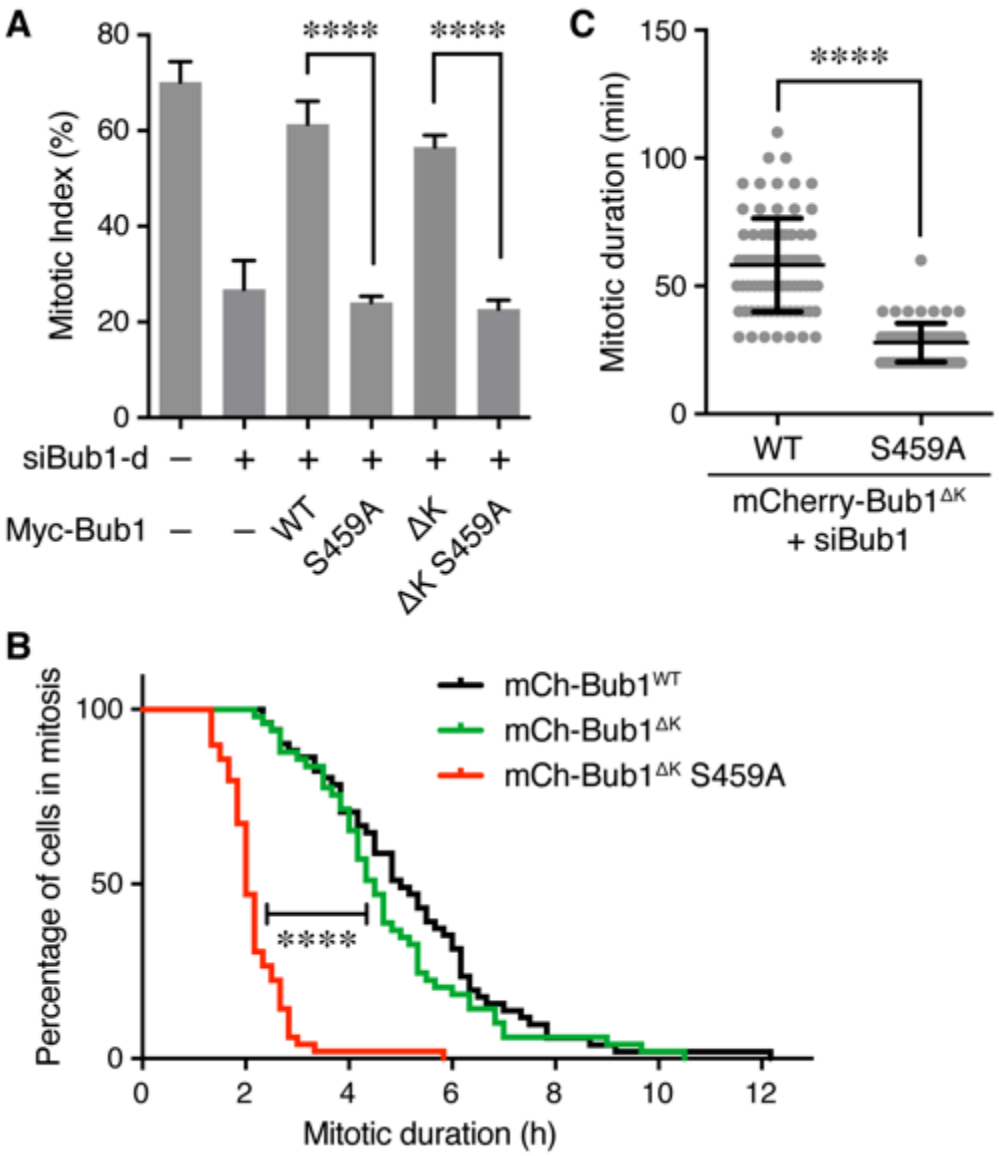

Figure 4-3. Phosphorylation of Bub1 S459 is crucial for checkpoint activation.

(**A**) Flow cytometry of HeLa Tet-On cells stably expressing indicated siRNA-resistant Myc-Bub1 transgenes that were transfected with siBub1-d and treated with taxol. Mitotic indices were calculated as percentages of $MPM2^{+}$ 4N cells in flow cytometry, and then plotted. FL, full-length. ΔK, mutant with the kinase domain truncated. Error bars, s.d. (n = 4 independent experiments). ****, $p<0.0001$; Student's t-test. (**B**) HeLa Tet-On cells stably expressing indicated Bub1 transgenes were transfected with siBub1-d, treated with taxol, and imaged with time-lapse microscopy. Cumulative percentages of cells remaining in mitosis were plotted against mitotic duration. mCh, mCherry. n (FL) = 51; n (ΔK) = 49; n (ΔK S459A) = 49. ****, $p<0.0001$; Log-rank test. (**C**) Mitotic durations of

cells stably expressing mCherry-Bub1$^{\Delta K}$ WT or S459A that were depleted of endogenous Bub1 and not treated with microtubule poisons. Each dot represents one cell. n (WT) = 79; n (S459A) = 66. ****, $p<0.0001$; Student's t-test. Experiments were performed by Luying Jia.

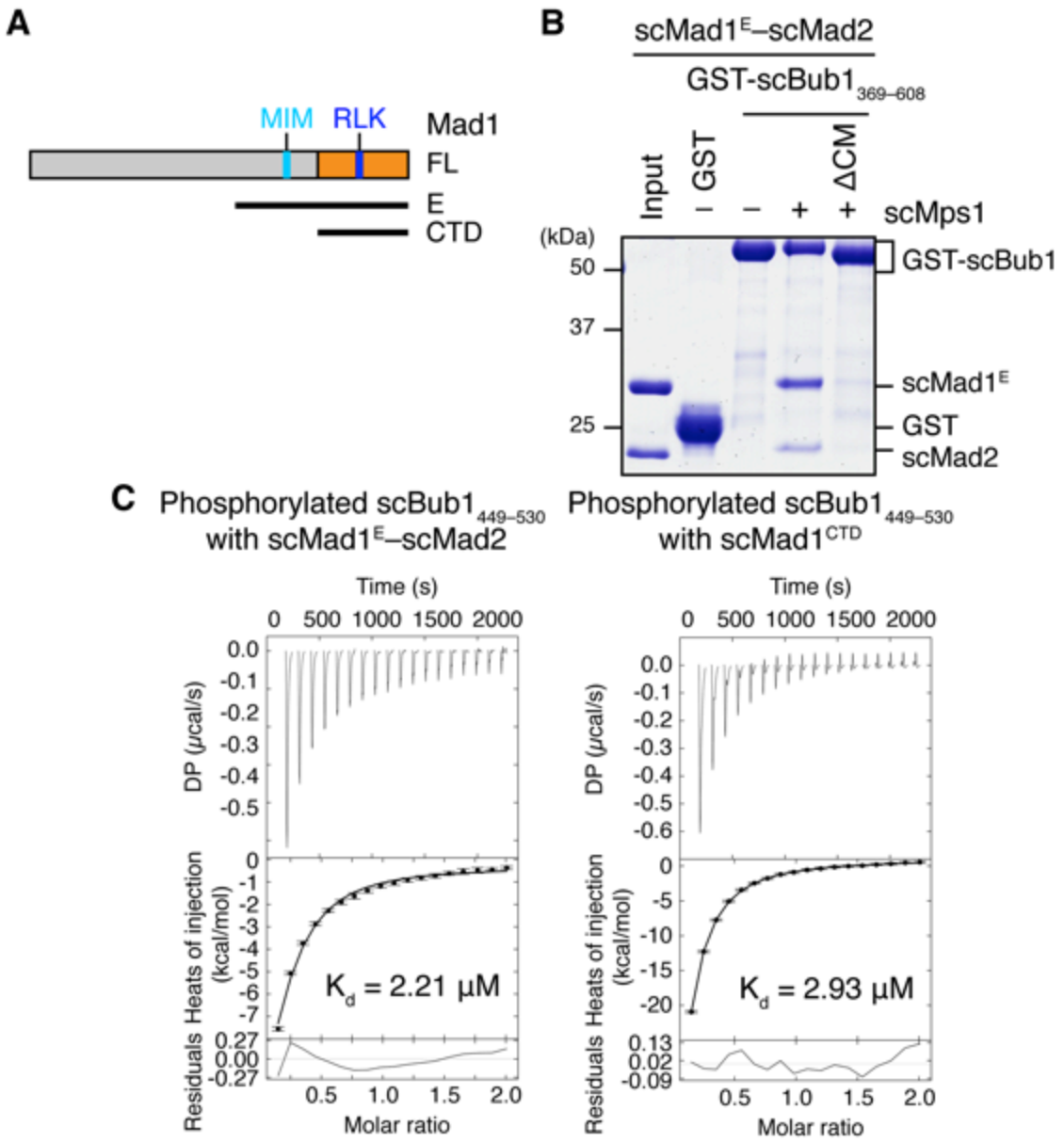

Figure 4-4. Budding yeast Bub1 binds with Mad1 in an Mps1 dependent manner.

(**A**) Domains and motifs of Mad1. Schematic domain structures and tested fragments of Mad1 protein. CTD, C-terminal domain; MIM, Mad2-interacting motif; RLK, the arginine-leucine-lysine motif. The E fragment of Mad1 contains both MIM and CTD was used to make the Mad1–Mad2 complex in this study. (**B**) In vitro pull-down of the scMad1^{E}–scMad2 complex with beads bound to GST or the indicated GST-scBub1 fragments, which were expressed alone or co-expressed with the kinase domain of scMps1. Proteins bound to the beads were analyzed with SDS-PAGE and stained with Coomassie blue. (**C**) Isothermal titration calorimetry (ITC) assay of binding between

Mps1-phosphorylated scBub1$_{449–530}$ and the scMad1^{E}–scMad2 complex or the CTD of scMad1. K_d, dissociation constant. Experiments in (B) and (C) were performed by Haishan Gao.

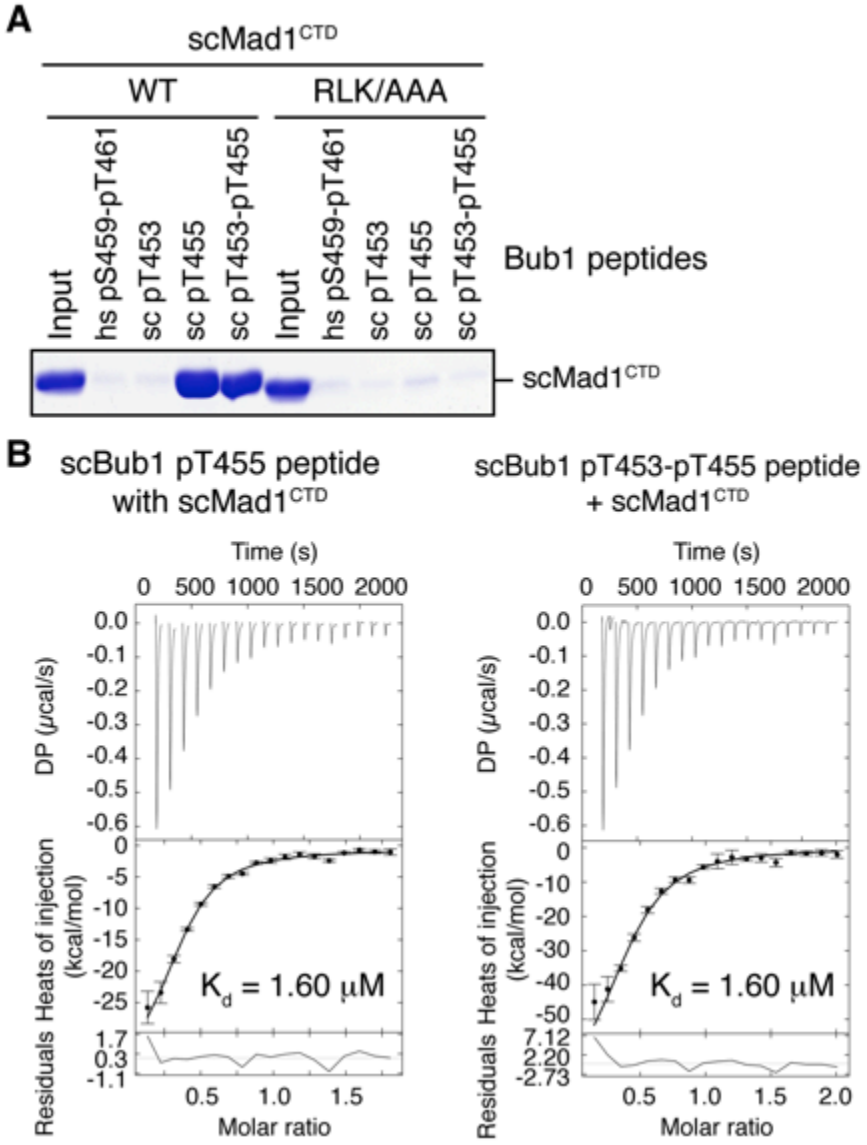

Figure 4-5. The phosphorylated conserved motif of scBub1 binds to scMad1 CTD.

(**A**) In vitro pull-down of scMad1^{CTD} WT and RLK/AAA with beads conjugated to the indicated scBub1 peptides. The phosphorylated residues of Bub1 peptides were denoted. hs, *Homo sapiens*. (**B**) ITC assay of binding between the CTD of scMad1 and the scBub1 peptide containing only phospho-T455 or both phospho-T453 and phospho-T455. K_d, dissociation constant. Experiments were performed by Haishan Gao.

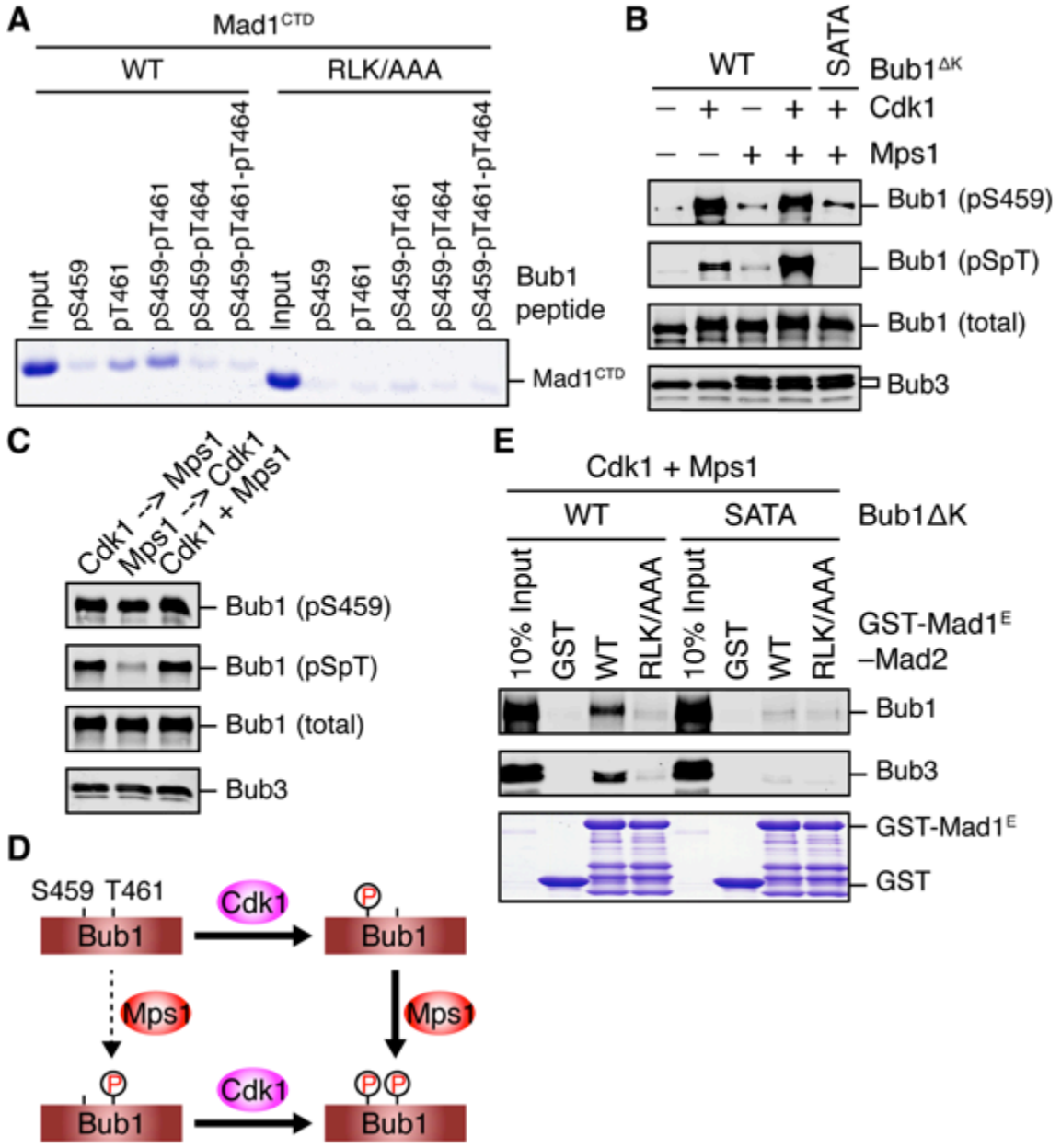

Figure 4-6. Human Bub1–Mad1 interaction requires sequential phosphorylation in the conserved motif of Bub1.

(**A**) In vitro pull-down of Mad1^{CTD} using beads conjugated to the indicated Bub1 peptides. Proteins bound on beads were separated on SDS-PAGE and visualized by Coomassie staining. The binding assay was performed by Haishan Gao. (**B**) In vitro kinase assays of recombinant Bub1$^{\Delta K}$–Bub3 WT or S459A/T461A (SATA) treated with Cdk1 or Mps1 or both. The kinase reactions were resolved on SDS-PAGE and blotted with indicated antibodies. pSpT, a phospho-specific antibody recognizing both phospho-

S459 and phospho-T461. (**C**) In vitro kinase assays similar to (B), except that the kinases were added in the indicated orders. In lanes 1 and 2, Cdk1 or Mps1 was first incubated with the substrate for 30 min before being inhibited by RO3306 or reversine, respectively. (**D**) Schematic drawing of the sequential phosphorylation of Bub1 at S459 and T461 by Cdk1 and Mps1. (**E**) Bub1$^{\Delta K}$–Bub3 WT and SATA were first phosphorylated by both Cdk1 and Mps1, and then assayed for binding to GST-Mad1^{E}–Mad2 beads. The bound proteins were blotted with the indicated antibodies.

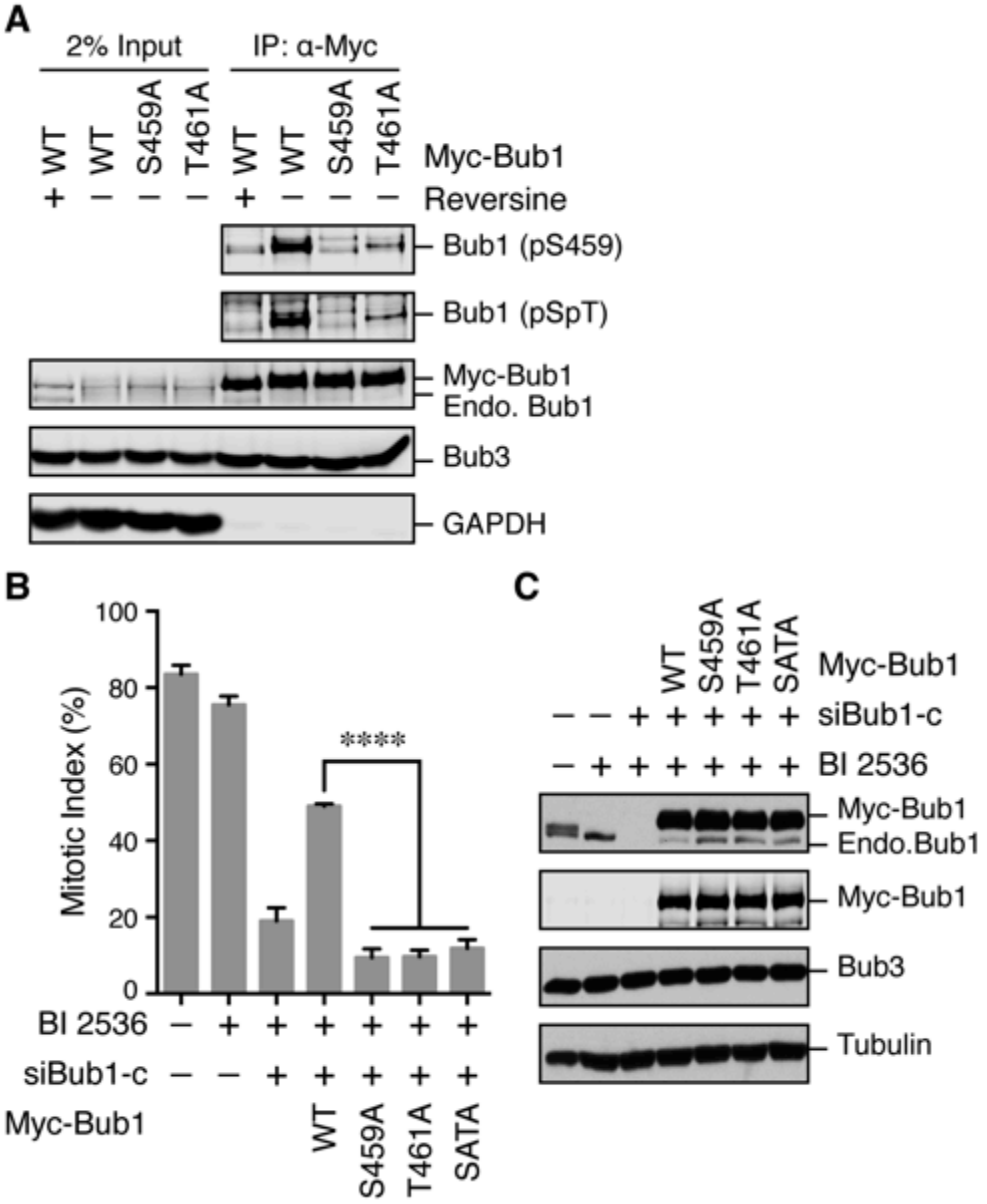

Figure 4-7. Phosphorylation of Bub1 T461 is required for checkpoint activation.

(**A**) HeLa cells expressing Myc-Bub1 transgenes were treated with nocodazole and MG132 in the presence or absence of reversine. Myc-Bub1 proteins were immunoprecipitated and blotted with the indicated antibodies. (**B**) Mitotic indices of cells expressing Bub1 transgenes that were transfected siBub1-c and treated with nocodazole in the presence or absence of the Plk1 inhibitor BI 2536. Error bars, s.d. (n = 3 independent experiments). ****, $p<0.0001$; Student's t-test. (**C**) Lysates of cells in (B) were blotted with the indicated antibodies. Endo., endogenous.

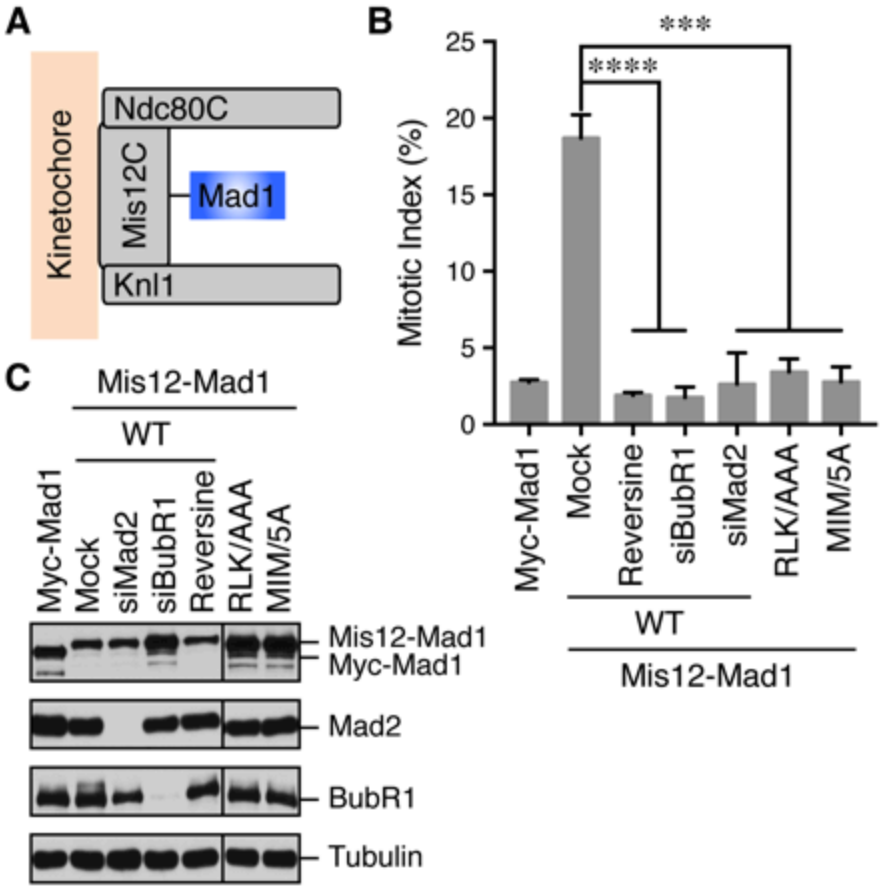

Figure 4-8. Mad1 RLK is required for its function in spindle checkpoint activation.

(**A**) Schematic view of the ectopic kinetochore targeting of Mad1. (**B**) Mitotic indices of cells expressing the indicated Mis12–Mad1 fusion proteins that were treated with reversine or siRNAs against BubR1 or Mad2. MIM/5A, Mad1 mutant with its MIM (^{541}KVLHM^{545}) changed to five alanines. Error bars, s.d. (n = 3 independent experiments). ***, $p<0.001$; ****, $p<0.0001$; Student's t-test. (**C**) Lysates of cells in (B) were blotted with the indicated antibodies.

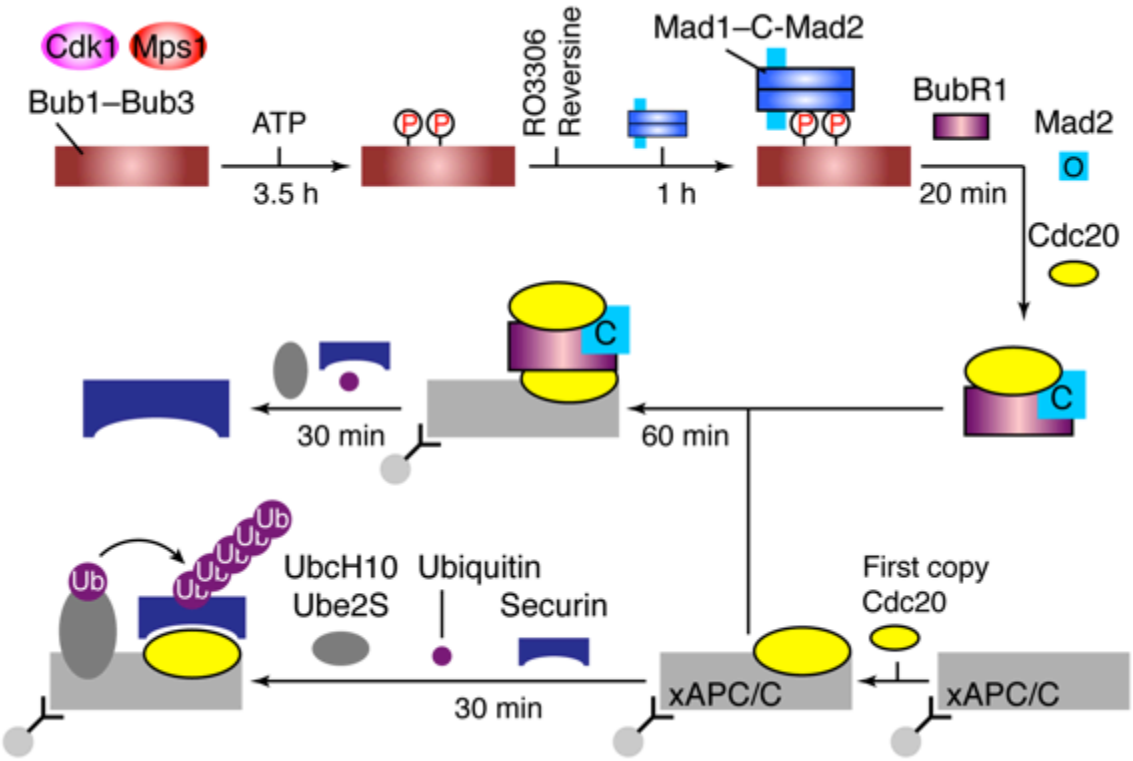

Figure 4-9. *In-vitro* reconstitution of spindle checkpoint signaling.

Flow charts of the *in-vitro* reconstitution of Mps1-stimulated APC/C inhibition by MCC components. The incubation times of each reaction step are indicated. All processes were performed at room temperature. Molecules are not drawn to scale. xAPC/C, the APC/C complex isolated from *Xenopus* egg extract by immunoprecipitation. Ub, ubiquitin.

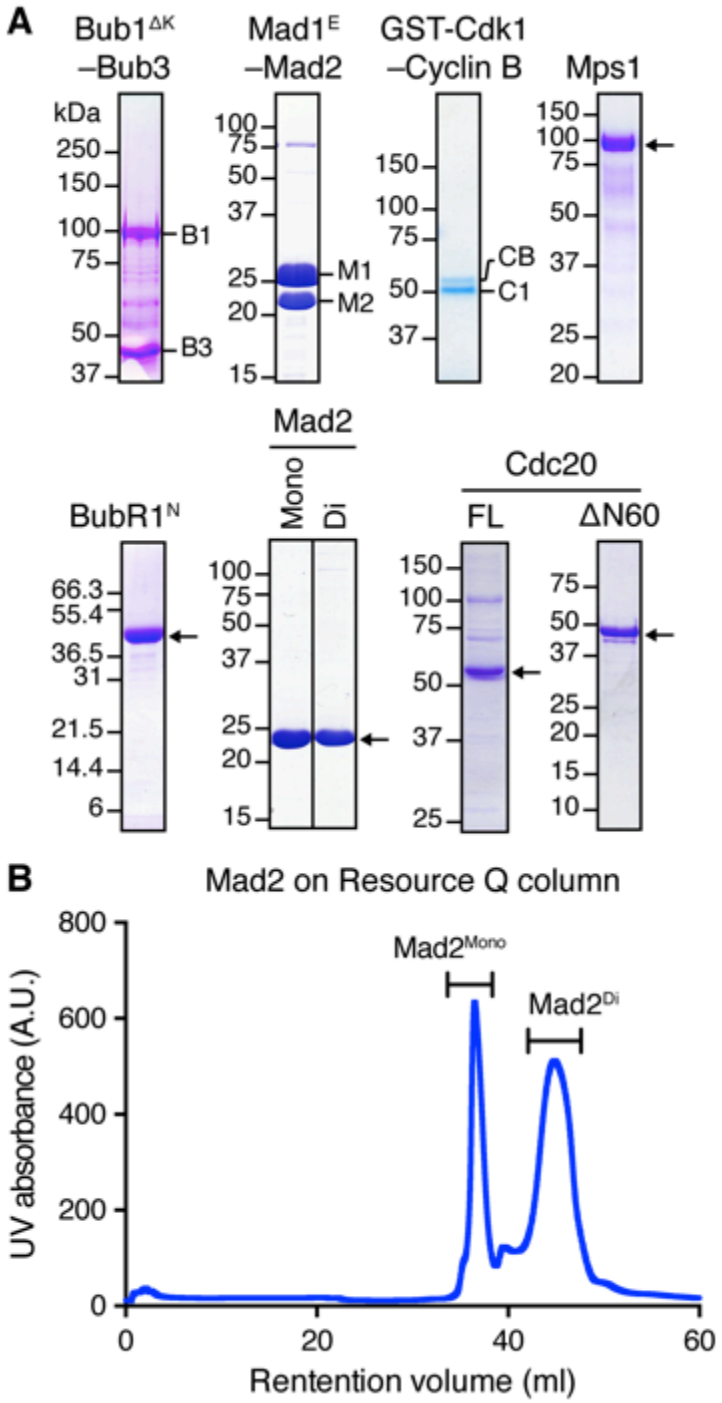

Figure 4-10. Purification of checkpoint proteins for the *in-vitro* reconstitution.

(**A**) A collection of recombinant proteins used for the *in vitro* reconstitution. Relevant protein bands were labeled or indicated by arrows. B1, Bub1$^{\Delta K}$; B3, Bub3; M1, Mad1^{E}; M2, Mad2; CB, Cyclin B1; C1, GST-Cdk1; Mono, monomeric Mad2; Di, dimeric Mad2; FL, full-length. (**B**) UV trace of recombinant purified Mad2 fractionated on a Resource Q column. The first peak belongs to the Mad2 monomer (Mad2^{Mono}), whereas the second

peak contains the Mad2 dimer ($Mad2^{Di}$). Recombinant $Bub1^{\Delta K}$–Bub3, $Mad1^{E}$–Mad2, $BubR1^{N}$, and Mad2 were purified by Haishan Gao. Recombinant Cdk1–Cyclin B1 and Cdc20 were purified by Bing Li.

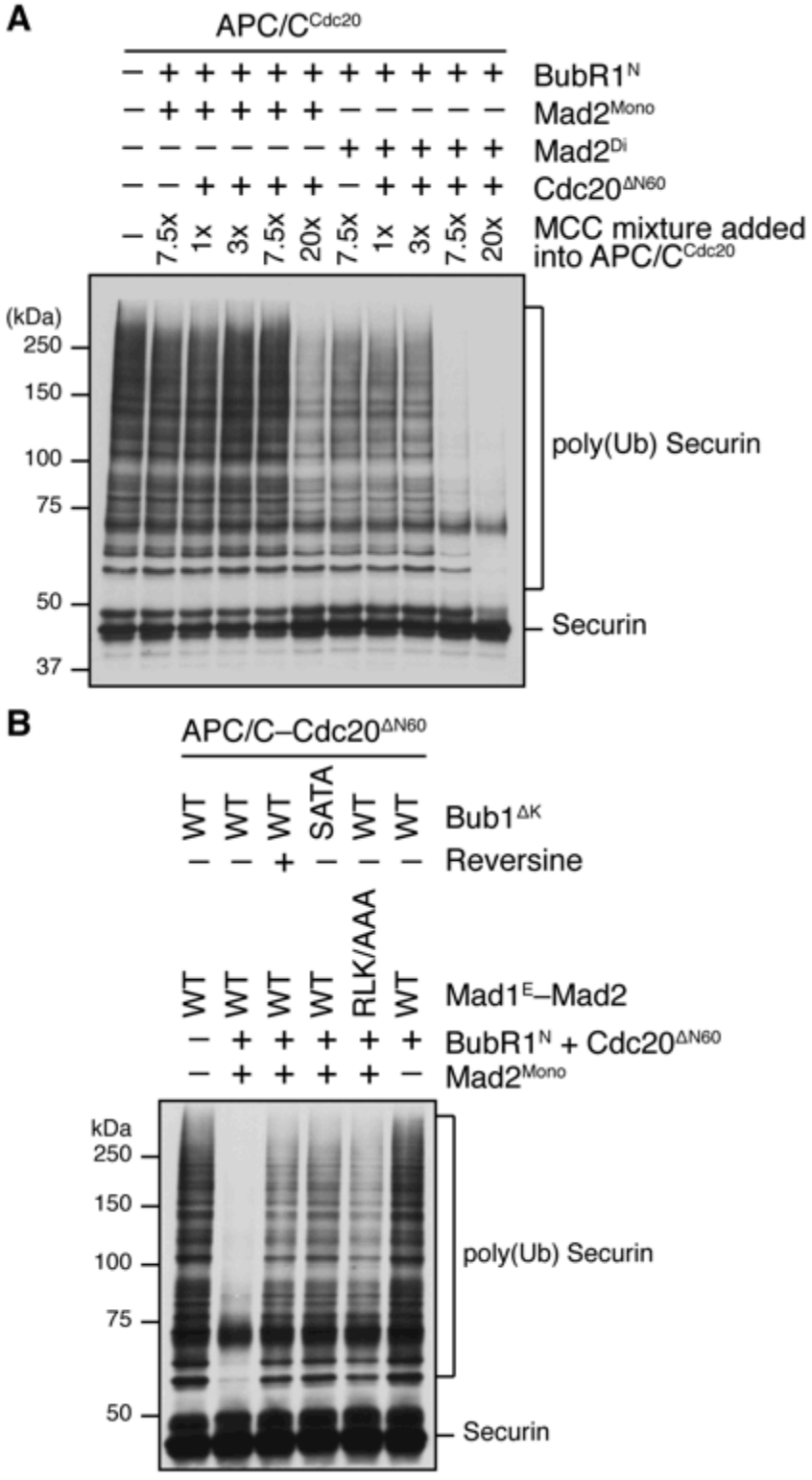

Figure 4-11. Phospho-Bub1–Mad1 complex promotes APC/C^{Cdc20} inhibition by MCC components with O-Mad2.

(**A**) Spontaneous MCC assembly with $Mad2^{Mono}$ or $Mad2^{Di}$ and the subsequent inhibition of APC/C^{Cdc20}. Experiments were performed as depicted in Figure 4-9, except that the Bub1 phosphorylation and Bub1–Mad1 binding steps were omitted. Varying amounts of the MCC mixture were added to APC/C^{Cdc20}. The ubiquitination reaction mixtures were resolved on SDS-PAGE and blotted with the anti-Myc antibody that detected Myc-Securin. The slow-migrating species represented the poly-ubiquitinated forms of Securin. (**B**) The ubiquitination reactions as depicted in Figure 4-9 were resolved on SDS-PAGE and blotted with the anti-Myc antibody that detected Myc-Securin. The slow-migrating species represented the poly-ubiquitinated forms of Securin. For the reversine sample, the inhibitor was added to the kinase reaction containing Mps1 and $Bub1^{\Delta K}$–Bub3 prior to ATP addition. Experiments were performed by Bing Li.

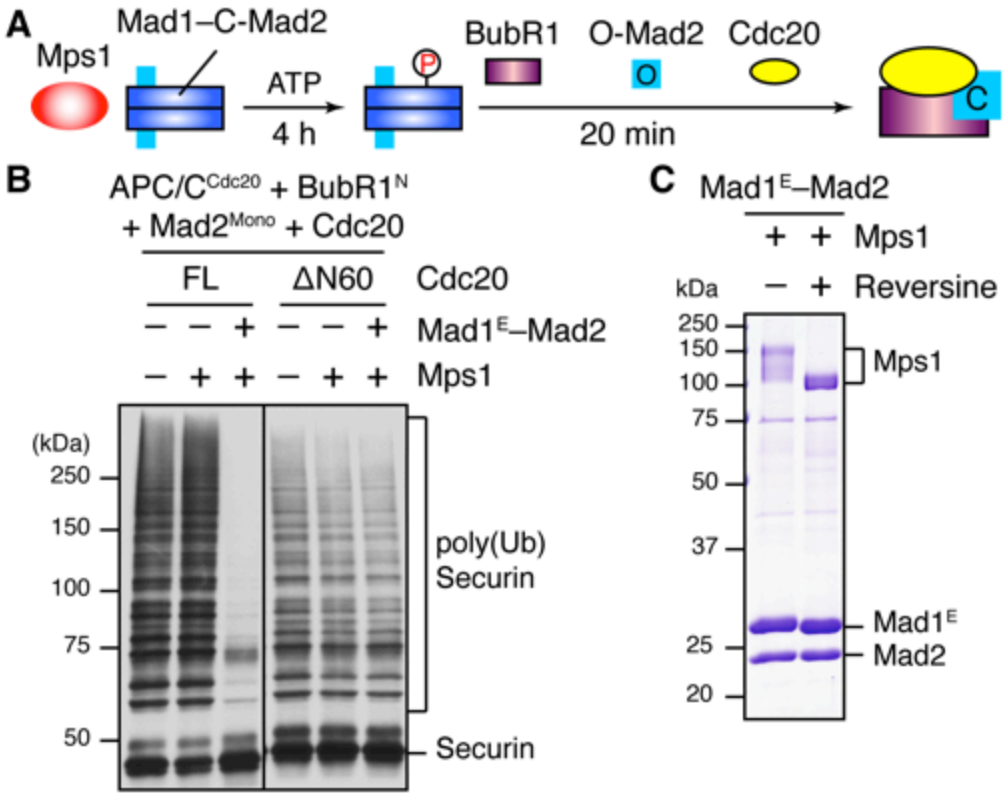

Figure 4-12. Mad1–Mad2 phosphorylated by Mps1 promotes APC/C^{Cdc20} inhibition through a Bub1-independent mechanism.

(**A**) Schematic drawing of the assay examining MCC assembly facilitated by Mps1-phosphorylated Mad1–C-Mad2. (**B**) MCC assembly and APC/C inhibition were performed as depicted in (A). The ubiquitination reaction mixtures were resolved on SDS-PAGE and blotted with the anti-Myc antibody that detected Myc-Securin. The slow-migrating species represented the poly-ubiquitinated forms of Securin. FL, full-length. Cdc20$^{\Delta N60}$ lacks residues 1–60. Experiment was performed by Bing Li. (**C**) Recombinant human Mad1^{E}–Mad2 complex was incubated with Mps1 in the presence or absence of reversine. The reactions were resolved on SDS-PAGE and stained with Coomassie. Note that Mps1 underwent autophosphorylation in the absence of reversine.

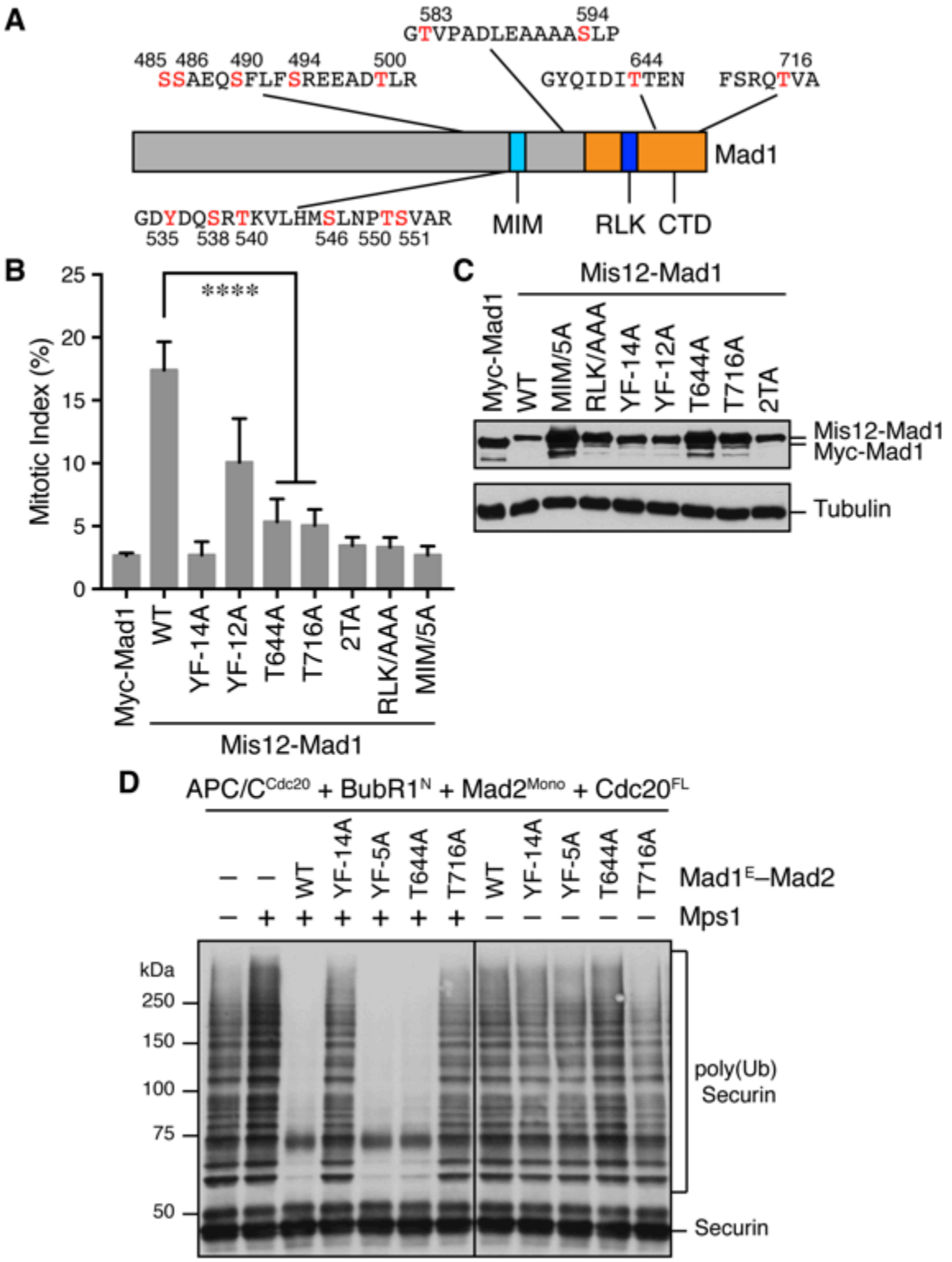

Figure 4-13. Phosphorylation of Mad1 is critical for checkpoint activation and APC/C^{Cdc20} inhibition by MCC components.

(**A**) A summary of all 15 Mps1-phosphorylation sites of $Mad1^{E}$ identified by mass spectrometry. Phosphorylated residues are depicted in red. (**B**) Mitotic indices of HeLa cells expressing the indicated Mis12–Mad1 fusion proteins. Error bars, s.d. (n = 5 independent experiments). ****, $p<0.0001$; Student's t-test. (**C**) Lysates of cells in (B) were blotted with anti-Mad1 and anti-Tubulin antibodies. (**D**) The MCC mixtures were prepared as depicted in Figure 4-12A with the indicated $Mad1^{E}$ proteins, and then applied to the APC/C-dependent ubiquitination assay. The ubiquitination reaction mixtures were resolved on SDS-PAGE and blotted with the anti-Myc antibody that detected Myc-Securin. The slow-migrating species represented the poly-ubiquitinated forms of Securin. Experiment was performed by Bing Li. YF-5A, Y535F/S538A/T540/S546A/T550A/ S551A; YF-13A-T716, mutant with 14 phosphorylation sites of Mad1 (except T716) mutated to phenylalanine or alanine.

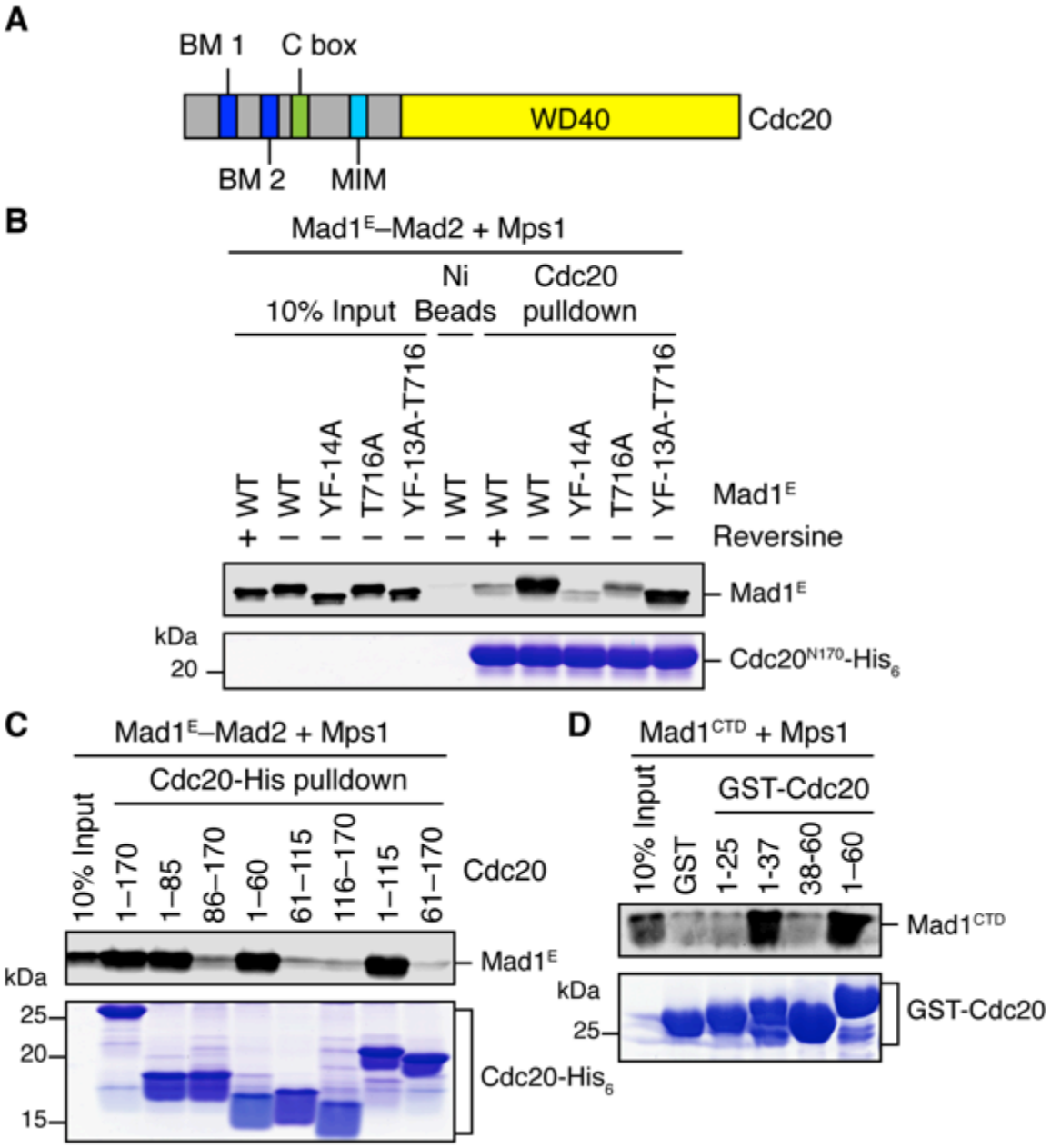

Figure 4-14. Phosphorylation of Mad1 T716 promotes its binding to Cdc20.

(**A**) Domains and motifs of Cdc20. C box, a conserved APC/C-binding motif; MIM, Mad2-interacting motif; BM1, basic motif 1 (^{27}RWQRK^{31}); BM2, basic motif 2 (^{54}RTPGRTPGK^{62}). (**B**) In vitro pull-down of the indicated Mad1^{E}–Mad2 complexes (which had been pre-treated with the kinase domain of Mps1) by Ni^{2+} beads bound to Cdc20^{N170}-His$_6$. The bait protein was stained with Coomassie, and the prey proteins bound to beads were blotted with the anti-Mad1 antibody. (**C**) In vitro pull-down of the Mad1^{E}–Mad2 complex (which had been pre-treated with the kinase domain of Mps1) by

Ni^{2+} beads bound to the indicated Cdc20-His_6 proteins. The bait proteins were stained with Coomassie, and the prey proteins bound to beads were blotted with the anti-Mad1 antibody. (**D**) In vitro pull-down of $Mad1^{CTD}$ (which had been pre-treated with the kinase domain of Mps1) by beads bound to the indicated GST-Cdc20 fragments. The bait proteins were stained with Coomassie, and the prey proteins bound to beads were blotted with the anti-Mad1 antibody. Experiments in (B) and (C) were performed by Bing Li. (D) was performed by Haishan Gao.

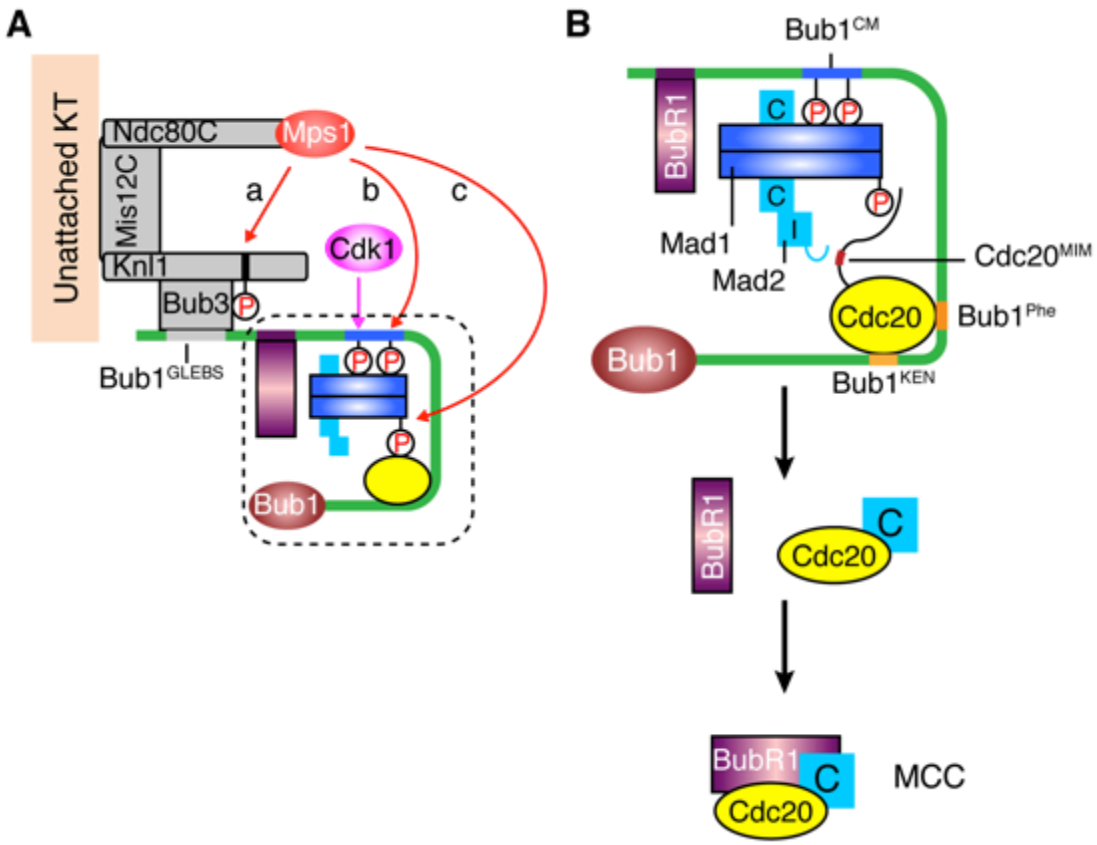

Figure 4-15. A sequential multi-target phosphorylation cascade by Mps1 promotes the assembly and activation of the Bub1–Mad1 scaffold.

(**A**) Mps1 recognizes unattached kinetochores (KT) through its direct binding to the Ndc80 complex (Ndc80C). At kinetochores, Mps1 first phosphorylates Knl1 at multiple MELT motifs to recruit the Bub1–Bub3 complex (a). After Cdk1 phosphorylates Bub1 S459, Mps1 then phosphorylates Bub1 T461 (b). The doubly phosphorylated Bub1 conserve motif (CM) binds to and recruits the Mad1–C-Mad2 core complex. Mps1 then phosphorylates Mad1 at T716, and this phosphorylation enables Mad1 binding to Cdc20 (c). (**B**) The boxed region in (A) is magnified and shown with more molecular details here. The Mad1–C-Mad2 core complex bound to phosphorylated Bub1 CM can further recruit O-Mad2 and convert it to I-Mad2. The WD40 domain of Cdc20 is anchored to the Phe and KEN boxes of Bub1, whereas the N-terminal basic tail of Cdc20 is bound by the phosphorylated Mad1 CTD. This bipartite Cdc20-binding mode positions the MIM of Cdc20 close to I-Mad2, promoting the formation of the C-Mad2–Cdc20 complex. This binary complex can further bind to BubR1 (bound to Bub1 or from cytosol) to form MCC.

CHAPTER V: PERSPECTIVES

My graduate work has further the understanding of spindle checkpoint activation in mitosis. The spindle checkpoint keeps the kinetochore-microtubule attachment under constant check. In presence of unattached or improperly attached kinetochores, the spindle checkpoint is activated in orchestra of a handful of checkpoint proteins. Like many other signaling pathways, the checkpoint-signaling pathway contains an initiation step to sense the unattached kinetochores, a signal transduction cascade to amplify and transduce upstream signals, and an execution step to ultimately inhibit APC/C activity. My work has elucidated the attachment-sensing mechanism for checkpoint initiation and lineated the signal transduction and execution steps. Both processes involve an essential checkpoint protein Mps1.

In the first story, I have discovered that Mps1 uses its non-kinase domain to directly interact with the microtubule-binding sites of Ndc80C, therefore becomes sensitive to the status of the kinetochore-microtubule attachment. In the second story, it has been illustrated that an Mps1-mediated multi-target phosphorylation cascade occurs along the checkpoint-signaling pathway, which makes the checkpoint responsive to Mps1 function. It has been further demonstrated that the phosphorylation and binding events in the initiation and transduction steps are required for checkpoint activation in human cells. Thus the Mps1-dependent phosphorylation and molecular interactions constitute a major pathway for spindle checkpoint activation.

A potential missing link in the checkpoint signaling is how the Ndc80C-bound Mps1 in the initiation step leads to its kinase function in signal transduction step. A straightforward hypothesis is the Ndc80C binding leads to the accumulation of Mps1 at kinetochores. The local enrichment of Mps1 induces the kinase auto-activation through trans-phosphorylation therefore turns on the downstream signaling. Alternatively, an equally likely possibility is that the Mps1 binding with Ndc80C positions the kinase domain towards its substrates: Knl1, Bub1, and Mad1. Future work is needed to experimentally test either hypothesis. Since all the checkpoint proteins are cytosolic components, understanding the function of Ndc80C-bound Mps1 would help to answer why the kinetochore is a necessary platform for spindle checkpoint activation.

BIBLIOGRAPHY

Abad, M.A., Medina, B., Santamaria, A., Zou, J., Plasberg-Hill, C., Madhumalar, A., Jayachandran, U., Redli, P.M., Rappsilber, J., Nigg, E.A*., et al.* (2014). Structural basis for microtubule recognition by the human kinetochore Ska complex. Nat Commun *5*, 2964.

Abrieu, A., Magnaghi-Jaulin, L., Kahana, J.A., Peter, M., Castro, A., Vigneron, S., Lorca, T., Cleveland, D.W., and Labbe, J.C. (2001). Mps1 is a kinetochore-associated kinase essential for the vertebrate mitotic checkpoint. Cell *106*, 83-93.

Alfieri, C., Chang, L., Zhang, Z., Yang, J., Maslen, S., Skehel, M., and Barford, D. (2016). Molecular basis of APC/C regulation by the spindle assembly checkpoint. Nature *536*, 431-436.

Alushin, G.M., Musinipally, V., Matson, D., Tooley, J., Stukenberg, P.T., and Nogales, E. (2012). Multimodal microtubule binding by the Ndc80 kinetochore complex. Nature structural & molecular biology *19*, 1161-1167.

Aravamudhan, P., Goldfarb, A.A., and Joglekar, A.P. (2015). The kinetochore encodes a mechanical switch to disrupt spindle assembly checkpoint signalling. Nat Cell Biol *17*, 868-879.

Basilico, F., Maffini, S., Weir, J.R., Prumbaum, D., Rojas, A.M., Zimniak, T., De Antoni, A., Jeganathan, S., Voss, B., van Gerwen, S*., et al.* (2014). The pseudo GTPase CENP-M drives human kinetochore assembly. eLife *3*, e02978.

Bock, L.J., Pagliuca, C., Kobayashi, N., Grove, R.A., Oku, Y., Shrestha, K., Alfieri, C., Golfieri, C., Oldani, A., Dal Maschio, M*., et al.* (2012). Cnn1 inhibits the interactions between the KMN complexes of the yeast kinetochore. Nat Cell Biol *14*, 614-624.

Bolanos-Garcia, V.M., Lischetti, T., Matak-Vinkovic, D., Cota, E., Simpson, P.J., Chirgadze, D.Y., Spring, D.R., Robinson, C.V., Nilsson, J., and Blundell, T.L. (2011). Structure of a Blinkin-BUBR1 complex reveals an interaction crucial for kinetochore-mitotic checkpoint regulation via an unanticipated binding Site. Structure *19*, 1691-1700.

Brady, D.M., and Hardwick, K.G. (2000). Complex formation between Mad1p, Bub1p and Bub3p is crucial for spindle checkpoint function. Curr Biol *10*, 675-678.

Caldas, G.V., Lynch, T.R., Anderson, R., Afreen, S., Varma, D., and DeLuca, J.G. (2015). The RZZ complex requires the N-terminus of KNL1 to mediate optimal Mad1 kinetochore localization in human cells. Open Biol *5*.

Carroll, C.W., Milks, K.J., and Straight, A.F. (2010). Dual recognition of CENP-A nucleosomes is required for centromere assembly. The Journal of cell biology *189*, 1143-1155.

Carroll, C.W., Silva, M.C., Godek, K.M., Jansen, L.E., and Straight, A.F. (2009). Centromere assembly requires the direct recognition of CENP-A nucleosomes by CENP-N. Nat Cell Biol *11*, 896-902.

Chang, L., Zhang, Z., Yang, J., McLaughlin, S.H., and Barford, D. (2015). Atomic structure of the APC/C and its mechanism of protein ubiquitination. Nature *522*, 450-454.

Chao, W.C., Kulkarni, K., Zhang, Z., Kong, E.H., and Barford, D. (2012). Structure of the mitotic checkpoint complex. Nature *484*, 208-213.

Cheeseman, I.M., Chappie, J.S., Wilson-Kubalek, E.M., and Desai, A. (2006). The conserved KMN network constitutes the core microtubule-binding site of the kinetochore. Cell *127*, 983-997.

Chen, R.H. (2002). BubR1 is essential for kinetochore localization of other spindle checkpoint proteins and its phosphorylation requires Mad1. The Journal of cell biology *158*, 487-496.

Chen, R.H. (2004). Phosphorylation and activation of Bub1 on unattached chromosomes facilitate the spindle checkpoint. EMBO J *23*, 3113-3121.

Chen, R.H., Shevchenko, A., Mann, M., and Murray, A.W. (1998). Spindle checkpoint protein Xmad1 recruits Xmad2 to unattached kinetochores. The Journal of cell biology *143*, 283-295.

Chen, R.H., Waters, J.C., Salmon, E.D., and Murray, A.W. (1996). Association of spindle assembly checkpoint component XMAD2 with unattached kinetochores. Science *274*, 242-246.

Choi, E., Zhang, X., Xing, C., and Yu, H. (2016). Mitotic Checkpoint Regulators Control Insulin Signaling and Metabolic Homeostasis. Cell *166*, 567-581.

Chung, E., and Chen, R.H. (2002). Spindle checkpoint requires Mad1-bound and Mad1-free Mad2. Mol Biol Cell *13*, 1501-1511.

Ciferri, C., Pasqualato, S., Screpanti, E., Varetti, G., Santaguida, S., Dos Reis, G., Maiolica, A., Polka, J., De Luca, J.G., De Wulf, P.*, et al.* (2008). Implications for kinetochore-microtubule attachment from the structure of an engineered Ndc80 complex. Cell *133*, 427-439.

Cleveland, D.W., Mao, Y., and Sullivan, K.F. (2003). Centromeres and kinetochores: from epigenetics to mitotic checkpoint signaling. Cell *112*, 407-421.

Collin, P., Nashchekina, O., Walker, R., and Pines, J. (2013). The spindle assembly checkpoint works like a rheostat rather than a toggle switch. Nat Cell Biol *15*, 1378-1385.

Daub, H., Olsen, J.V., Bairlein, M., Gnad, F., Oppermann, F.S., Korner, R., Greff, Z., Keri, G., Stemmann, O., and Mann, M. (2008). Kinase-selective enrichment enables quantitative phosphoproteomics of the kinome across the cell cycle. Mol Cell *31*, 438-448.

DeLuca, J.G., Gall, W.E., Ciferri, C., Cimini, D., Musacchio, A., and Salmon, E.D. (2006). Kinetochore microtubule dynamics and attachment stability are regulated by Hec1. Cell *127*, 969-982.

DeLuca, J.G., Moree, B., Hickey, J.M., Kilmartin, J.V., and Salmon, E.D. (2002). hNuf2 inhibition blocks stable kinetochore-microtubule attachment and induces mitotic cell death in HeLa cells. The Journal of cell biology *159*, 549-555.

DeLuca, K.F., Lens, S.M., and DeLuca, J.G. (2011). Temporal changes in Hec1 phosphorylation control kinetochore-microtubule attachment stability during mitosis. Journal of cell science *124*, 622-634.

Di Fiore, B., Davey, N.E., Hagting, A., Izawa, D., Mansfeld, J., Gibson, T.J., and Pines, J. (2015). The ABBA motif binds APC/C activators and is shared by APC/C substrates and regulators. Dev Cell *32*, 358-372.

Diaz-Martinez, L.A., Tian, W., Li, B., Warrington, R., Jia, L., Brautigam, C.A., Luo, X., and Yu, H. (2015). The Cdc20-binding Phe box of the spindle checkpoint protein

BubR1 maintains the mitotic checkpoint complex during mitosis. The Journal of biological chemistry *290*, 2431-2443.

Dick, A.E., and Gerlich, D.W. (2013). Kinetic framework of spindle assembly checkpoint signalling. Nat Cell Biol *15*, 1370-1377.

Dimitrova, Y.N., Jenni, S., Valverde, R., Khin, Y., and Harrison, S.C. (2016). Structure of the MIND Complex Defines a Regulatory Focus for Yeast Kinetochore Assembly. Cell *167*, 14.

Dorer, R.K., Zhong, S., Tallarico, J.A., Wong, W.H., Mitchison, T.J., and Murray, A.W. (2005). A small-molecule inhibitor of Mps1 blocks the spindle-checkpoint response to a lack of tension on mitotic chromosomes. Curr Biol *15*, 1070-1076.

Dou, Z., Sawagechi, A., Zhang, J., Luo, H., Brako, L., and Yao, X.B. (2003). Dynamic distribution of TTK in HeLa cells: insights from an ultrastructural study. Cell Res *13*, 443-449.

Dou, Z., von Schubert, C., Korner, R., Santamaria, A., Elowe, S., and Nigg, E.A. (2011). Quantitative mass spectrometry analysis reveals similar substrate consensus motif for human Mps1 kinase and Plk1. PLoS One *6*, e18793.

Earnshaw, W.C., and Rothfield, N. (1985). Identification of a family of human centromere proteins using autoimmune sera from patients with scleroderma. Chromosoma *91*, 313-321.

Elia, A.E., Rellos, P., Haire, L.F., Chao, J.W., Ivins, F.J., Hoepker, K., Mohammad, D., Cantley, L.C., Smerdon, S.J., and Yaffe, M.B. (2003). The molecular basis for phosphodependent substrate targeting and regulation of Plks by the Polo-box domain. Cell *115*, 83-95.

Elkins, J.M., Santaguida, S., Musacchio, A., and Knapp, S. (2012). Crystal structure of human aurora B in complex with INCENP and VX-680. Journal of medicinal chemistry *55*, 7841-7848.

Espeut, J., Cheerambathur, D.K., Krenning, L., Oegema, K., and Desai, A. (2012). Microtubule binding by KNL-1 contributes to spindle checkpoint silencing at the kinetochore. The Journal of cell biology *196*, 469-482.

Eytan, E., Wang, K., Miniowitz-Shemtov, S., Sitry-Shevah, D., Kaisari, S., Yen, T.J., Liu, S.T., and Hershko, A. (2014). Disassembly of mitotic checkpoint complexes by

the joint action of the AAA-ATPase TRIP13 and p31(comet). Proceedings of the National Academy of Sciences of the United States of America *111*, 12019-12024.

Fang, G., Yu, H., and Kirschner, M.W. (1998a). The checkpoint protein MAD2 and the mitotic regulator CDC20 form a ternary complex with the anaphase-promoting complex to control anaphase initiation. Genes & development *12*, 1871-1883.

Fang, G., Yu, H., and Kirschner, M.W. (1998b). Direct binding of CDC20 protein family members activates the anaphase-promoting complex in mitosis and G1. Mol Cell *2*, 163-171.

Foley, E.A., and Kapoor, T.M. (2013). Microtubule attachment and spindle assembly checkpoint signalling at the kinetochore. Nature reviews Molecular cell biology *14*, 25-37.

Foltz, D.R., Jansen, L.E., Black, B.E., Bailey, A.O., Yates, J.R., 3rd, and Cleveland, D.W. (2006). The human CENP-A centromeric nucleosome-associated complex. Nat Cell Biol *8*, 458-469.

Garnett, M.J., Mansfeld, J., Godwin, C., Matsusaka, T., Wu, J., Russell, P., Pines, J., and Venkitaraman, A.R. (2009). UBE2S elongates ubiquitin chains on APC/C substrates to promote mitotic exit. Nat Cell Biol *11*, 1363-1369.

Gassmann, R., Holland, A.J., Varma, D., Wan, X., Civril, F., Cleveland, D.W., Oegema, K., Salmon, E.D., and Desai, A. (2010). Removal of Spindly from microtubule-attached kinetochores controls spindle checkpoint silencing in human cells. Genes & development *24*, 957-971.

Gorbsky, G.J. (2015). The spindle checkpoint and chromosome segregation in meiosis. The FEBS journal *282*, 2471-2487.

Griffis, E.R., Stuurman, N., and Vale, R.D. (2007). Spindly, a novel protein essential for silencing the spindle assembly checkpoint, recruits dynein to the kinetochore. J Cell Biol *177*, 1005-1015.

Han, J.S., Vitre, B., Fachinetti, D., and Cleveland, D.W. (2014). Bimodal activation of BubR1 by Bub3 sustains mitotic checkpoint signaling. Proceedings of the National Academy of Sciences of the United States of America *111*, E4185-4193.

Hara, M., Ozkan, E., Sun, H., Yu, H., and Luo, X. (2015). Structure of an intermediate conformer of the spindle checkpoint protein Mad2. Proceedings of the National Academy of Sciences of the United States of America *112*, 11252-11257.

Hardwick, K.G., Weiss, E., Luca, F.C., Winey, M., and Murray, A.W. (1996). Activation of the budding yeast spindle assembly checkpoint without mitotic spindle disruption. Science *273*, 953-956.

Hauf, S., Cole, R.W., LaTerra, S., Zimmer, C., Schnapp, G., Walter, R., Heckel, A., van Meel, J., Rieder, C.L., and Peters, J.M. (2003). The small molecule Hesperadin reveals a role for Aurora B in correcting kinetochore-microtubule attachment and in maintaining the spindle assembly checkpoint. J Cell Biol *161*, 281-294.

Heinrich, S., Geissen, E.M., Kamenz, J., Trautmann, S., Widmer, C., Drewe, P., Knop, M., Radde, N., Hasenauer, J., and Hauf, S. (2013). Determinants of robustness in spindle assembly checkpoint signalling. Nat Cell Biol *15*, 1328-1339.

Heinrich, S., Sewart, K., Windecker, H., Langegger, M., Schmidt, N., Hustedt, N., and Hauf, S. (2014). Mad1 contribution to spindle assembly checkpoint signalling goes beyond presenting Mad2 at kinetochores. EMBO reports *15*, 291-298.

Heun, P., Erhardt, S., Blower, M.D., Weiss, S., Skora, A.D., and Karpen, G.H. (2006). Mislocalization of the Drosophila centromere-specific histone CID promotes formation of functional ectopic kinetochores. Dev Cell *10*, 303-315.

Hewitt, L., Tighe, A., Santaguida, S., White, A.M., Jones, C.D., Musacchio, A., Green, S., and Taylor, S.S. (2010). Sustained Mps1 activity is required in mitosis to recruit O-Mad2 to the Mad1-C-Mad2 core complex. The Journal of cell biology *190*, 25-34.

Hiruma, Y., Sacristan, C., Pachis, S.T., Adamopoulos, A., Kuijt, T., Ubbink, M., von Castelmur, E., Perrakis, A., and Kops, G.J. (2015). CELL DIVISION CYCLE. Competition between MPS1 and microtubules at kinetochores regulates spindle checkpoint signaling. Science *348*, 1264-1267.

Holland, A.J., and Cleveland, D.W. (2012). Losing balance: the origin and impact of aneuploidy in cancer. EMBO reports *13*, 501-514.

Hori, T., Amano, M., Suzuki, A., Backer, C.B., Welburn, J.P., Dong, Y., McEwen, B.F., Shang, W.H., Suzuki, E., Okawa, K.*, et al.* (2008). CCAN makes multiple contacts

with centromeric DNA to provide distinct pathways to the outer kinetochore. Cell *135*, 1039-1052.

Howell, B.J., McEwen, B.F., Canman, J.C., Hoffman, D.B., Farrar, E.M., Rieder, C.L., and Salmon, E.D. (2001). Cytoplasmic dynein/dynactin drives kinetochore protein transport to the spindle poles and has a role in mitotic spindle checkpoint inactivation. J Cell Biol *155*, 1159-1172.

Hsu, K.S., and Toda, T. (2011). Ndc80 internal loop interacts with Dis1/TOG to ensure proper kinetochore-spindle attachment in fission yeast. Curr Biol *21*, 214-220.

Izawa, D., and Pines, J. (2015). The mitotic checkpoint complex binds a second CDC20 to inhibit active APC/C. Nature *517*, 631-634.

Jelluma, N., Dansen, T.B., Sliedrecht, T., Kwiatkowski, N.P., and Kops, G.J. (2010). Release of Mps1 from kinetochores is crucial for timely anaphase onset. The Journal of cell biology *191*, 281-290.

Jeyaprakash, A.A., Santamaria, A., Jayachandran, U., Chan, Y.W., Benda, C., Nigg, E.A., and Conti, E. (2012). Structural and functional organization of the Ska complex, a key component of the kinetochore-microtubule interface. Mol Cell *46*, 274-286.

Jia, L., Kim, S., and Yu, H. (2013). Tracking spindle checkpoint signals from kinetochores to APC/C. Trends in biochemical sciences *38*, 302-311.

Jia, L., Li, B., and Yu, H. (2016). The Bub1-Plk1 kinase complex promotes spindle checkpoint signalling through Cdc20 phosphorylation. Nat Commun *7*, 10818.

Johnson, V.L., Scott, M.I., Holt, S.V., Hussein, D., and Taylor, S.S. (2004). Bub1 is required for kinetochore localization of BubR1, Cenp-E, Cenp-F and Mad2, and chromosome congression. Journal of cell science *117*, 1577-1589.

Kang, J., Chen, Y., Zhao, Y., and Yu, H. (2007). Autophosphorylation-dependent activation of human Mps1 is required for the spindle checkpoint. Proceedings of the National Academy of Sciences of the United States of America *104*, 20232-20237.

Kang, J., Yang, M., Li, B., Qi, W., Zhang, C., Shokat, K.M., Tomchick, D.R., Machius, M., and Yu, H. (2008). Structure and substrate recruitment of the human spindle checkpoint kinase Bub1. Mol Cell *32*, 394-405.

Karess, R. (2005). Rod-Zw10-Zwilch: a key player in the spindle checkpoint. Trends in cell biology *15*, 386-392.

Kawashima, S.A., Tsukahara, T., Langegger, M., Hauf, S., Kitajima, T.S., and Watanabe, Y. (2007). Shugoshin enables tension-generating attachment of kinetochores by loading Aurora to centromeres. Genes & development *21*, 420-435.

Kawashima, S.A., Yamagishi, Y., Honda, T., Ishiguro, K., and Watanabe, Y. (2010). Phosphorylation of H2A by Bub1 prevents chromosomal instability through localizing shugoshin. Science *327*, 172-177.

Keller, S., Vargas, C., Zhao, H., Piszczek, G., Brautigam, C.A., and Schuck, P. (2012). High-precision isothermal titration calorimetry with automated peak-shape analysis. Anal Chem *84*, 5066-5073.

Kelly, A.E., Ghenoiu, C., Xue, J.Z., Zierhut, C., Kimura, H., and Funabiki, H. (2010). Survivin reads phosphorylated histone H3 threonine 3 to activate the mitotic kinase Aurora B. Science *330*, 235-239.

Kemmler, S., Stach, M., Knapp, M., Ortiz, J., Pfannstiel, J., Ruppert, T., and Lechner, J. (2009). Mimicking Ndc80 phosphorylation triggers spindle assembly checkpoint signalling. The EMBO journal *28*, 1099-1110.

Kim, S., Sun, H., Tomchick, D.R., Yu, H., and Luo, X. (2012). Structure of human Mad1 C-terminal domain reveals its involvement in kinetochore targeting. Proceedings of the National Academy of Sciences of the United States of America *109*, 6549-6554.

Kim, S., and Yu, H. (2015). Multiple assembly mechanisms anchor the KMN spindle checkpoint platform at human mitotic kinetochores. J Cell Biol *208*, 181-196.

Kim, Y., Holland, A.J., Lan, W., and Cleveland, D.W. (2010). Aurora kinases and protein phosphatase 1 mediate chromosome congression through regulation of CENP-E. Cell *142*, 444-455.

Kiyomitsu, T., Murakami, H., and Yanagida, M. (2011). Protein interaction domain mapping of human kinetochore protein Blinkin reveals a consensus motif for binding of spindle assembly checkpoint proteins Bub1 and BubR1. Mol Cell Biol *31*, 998-1011.

Kiyomitsu, T., Obuse, C., and Yanagida, M. (2007). Human Blinkin/AF15q14 is required for chromosome alignment and the mitotic checkpoint through direct interaction with Bub1 and BubR1. Dev Cell *13*, 663-676.

Klare, K., Weir, J.R., Basilico, F., Zimniak, T., Massimiliano, L., Ludwigs, N., Herzog, F., and Musacchio, A. (2015). CENP-C is a blueprint for constitutive centromere-associated network assembly within human kinetochores. The Journal of cell biology *210*, 11-22.

Klebig, C., Korinth, D., and Meraldi, P. (2009). Bub1 regulates chromosome segregation in a kinetochore-independent manner. The Journal of cell biology *185*, 841-858.

Kraft, C., Herzog, F., Gieffers, C., Mechtler, K., Hagting, A., Pines, J., and Peters, J.M. (2003). Mitotic regulation of the human anaphase-promoting complex by phosphorylation. EMBO J *22*, 6598-6609.

Krenn, V., Overlack, K., Primorac, I., van Gerwen, S., and Musacchio, A. (2014). KI motifs of human Knl1 enhance assembly of comprehensive spindle checkpoint complexes around MELT repeats. Curr Biol *24*, 29-39.

Krenn, V., Wehenkel, A., Li, X., Santaguida, S., and Musacchio, A. (2012). Structural analysis reveals features of the spindle checkpoint kinase Bub1-kinetochore subunit Knl1 interaction. The Journal of cell biology *196*, 451-467.

Kruse, T., Larsen, M.S., Sedgwick, G.G., Sigurdsson, J.O., Streicher, W., Olsen, J.V., and Nilsson, J. (2014). A direct role of Mad1 in the spindle assembly checkpoint beyond Mad2 kinetochore recruitment. EMBO reports *15*, 282-290.

Kulukian, A., Han, J.S., and Cleveland, D.W. (2009). Unattached kinetochores catalyze production of an anaphase inhibitor that requires a Mad2 template to prime Cdc20 for BubR1 binding. Dev Cell *16*, 105-117.

Lampson, M.A., and Cheeseman, I.M. (2011). Sensing centromere tension: Aurora B and the regulation of kinetochore function. Trends Cell Biol *21*, 133-140.

Lara-Gonzalez, P., Scott, M.I., Diez, M., Sen, O., and Taylor, S.S. (2011). BubR1 blocks substrate recruitment to the APC/C in a KEN-box-dependent manner. Journal of cell science *124*, 4332-4345.

Li, Y., and Benezra, R. (1996). Identification of a human mitotic checkpoint gene: hsMAD2. Science *274*, 246-248.

Lin, Z., Jia, L., Tomchick, D.R., Luo, X., and Yu, H. (2014). Substrate-specific activation of the mitotic kinase Bub1 through intramolecular autophosphorylation and kinetochore targeting. Structure *22*, 1616-1627.

Lischetti, T., Zhang, G., Sedgwick, G.G., Bolanos-Garcia, V.M., and Nilsson, J. (2014). The internal Cdc20 binding site in BubR1 facilitates both spindle assembly checkpoint signalling and silencing. Nat Commun *5*, 5563.

Liu, D., Vleugel, M., Backer, C.B., Hori, T., Fukagawa, T., Cheeseman, I.M., and Lampson, M.A. (2010). Regulated targeting of protein phosphatase 1 to the outer kinetochore by KNL1 opposes Aurora B kinase. The Journal of cell biology *188*, 809-820.

Liu, H., Qu, Q., Warrington, R., Rice, A., Cheng, N., and Yu, H. (2015). Mitotic Transcription Installs Sgo1 at Centromeres to Coordinate Chromosome Segregation. Mol Cell *59*, 426-436.

Liu, X., and Winey, M. (2012). The MPS1 family of protein kinases. Annu Rev Biochem *81*, 561-585.

London, N., and Biggins, S. (2014). Mad1 kinetochore recruitment by Mps1-mediated phosphorylation of Bub1 signals the spindle checkpoint. Genes & development *28*, 140-152.

London, N., Ceto, S., Ranish, J.A., and Biggins, S. (2012). Phosphoregulation of Spc105 by Mps1 and PP1 regulates Bub1 localization to kinetochores. Curr Biol *22*, 900-906.

Luo, X., Tang, Z., Rizo, J., and Yu, H. (2002). The Mad2 spindle checkpoint protein undergoes similar major conformational changes upon binding to either Mad1 or Cdc20. Mol Cell *9*, 59-71.

Luo, X., Tang, Z., Xia, G., Wassmann, K., Matsumoto, T., Rizo, J., and Yu, H. (2004). The Mad2 spindle checkpoint protein has two distinct natively folded states. Nat Struct Mol Biol *11*, 338-345.

Luo, X., and Yu, H. (2008). Protein metamorphosis: the two-state behavior of Mad2. Structure *16*, 1616-1625.

Maldonado, M., and Kapoor, T.M. (2011). Constitutive Mad1 targeting to kinetochores uncouples checkpoint signalling from chromosome biorientation. Nat Cell Biol *13*, 475-482.

Malvezzi, F., Litos, G., Schleiffer, A., Heuck, A., Mechtler, K., Clausen, T., and Westermann, S. (2013). A structural basis for kinetochore recruitment of the Ndc80 complex via two distinct centromere receptors. EMBO J *32*, 409-423.

Mapelli, M., Massimiliano, L., Santaguida, S., and Musacchio, A. (2007). The Mad2 conformational dimer: structure and implications for the spindle assembly checkpoint. Cell *131*, 730-743.

Mapelli, M., and Musacchio, A. (2007). MAD contortions: conformational dimerization boosts spindle checkpoint signaling. Curr Opin Struct Biol *17*, 716-725.

Martin-Lluesma, S., Stucke, V.M., and Nigg, E.A. (2002). Role of Hec1 in spindle checkpoint signaling and kinetochore recruitment of Mad1/Mad2. Science *297*, 2267-2270.

Matson, D.R., and Stukenberg, P.T. (2014). CENP-I and Aurora B act as a molecular switch that ties RZZ/Mad1 recruitment to kinetochore attachment status. The Journal of cell biology *205*, 541-554.

Maure, J.F., Komoto, S., Oku, Y., Mino, A., Pasqualato, S., Natsume, K., Clayton, L., Musacchio, A., and Tanaka, T.U. (2011). The Ndc80 loop region facilitates formation of kinetochore attachment to the dynamic microtubule plus end. Curr Biol *21*, 207-213.

McKinley, K.L., Sekulic, N., Guo, L.Y., Tsinman, T., Black, B.E., and Cheeseman, I.M. (2015). The CENP-L-N Complex Forms a Critical Node in an Integrated Meshwork of Interactions at the Centromere-Kinetochore Interface. Mol Cell *60*, 886-898.

Mendiburo, M.J., Padeken, J., Fulop, S., Schepers, A., and Heun, P. (2011). Drosophila CENH3 is sufficient for centromere formation. Science *334*, 686-690.

Miller, M.P., Asbury, C.L., and Biggins, S. (2016). A TOG Protein Confers Tension Sensitivity to Kinetochore-Microtubule Attachments. Cell *165*, 1428-1439.

Mills, G.B., Schmandt, R., McGill, M., Amendola, A., Hill, M., Jacobs, K., May, C., Rodricks, A.M., Campbell, S., and Hogg, D. (1992). Expression of TTK, a novel human protein kinase, is associated with cell proliferation. The Journal of biological chemistry *267*, 16000-16006.

Mora-Santos, M.D., Hervas-Aguilar, A., Sewart, K., Lancaster, T.C., Meadows, J.C., and Millar, J.B. (2016). Bub3-Bub1 Binding to Spc7/KNL1 Toggles the Spindle Checkpoint Switch by Licensing the Interaction of Bub1 with Mad1-Mad2. Curr Biol.

Moyle, M.W., Kim, T., Hattersley, N., Espeut, J., Cheerambathur, D.K., Oegema, K., and Desai, A. (2014). A Bub1-Mad1 interaction targets the Mad1-Mad2 complex to

unattached kinetochores to initiate the spindle checkpoint. The Journal of cell biology *204*, 647-657.

Musacchio, A. (2015). The Molecular Biology of Spindle Assembly Checkpoint Signaling Dynamics. Curr Biol *25*, R1002-1018.

Nijenhuis, W., von Castelmur, E., Littler, D., De Marco, V., Tromer, E., Vleugel, M., van Osch, M.H., Snel, B., Perrakis, A., and Kops, G.J. (2013). A TPR domain-containing N-terminal module of MPS1 is required for its kinetochore localization by Aurora B. The Journal of cell biology *201*, 217-231.

Nishino, T., Rago, F., Hori, T., Tomii, K., Cheeseman, I.M., and Fukagawa, T. (2013). CENP-T provides a structural platform for outer kinetochore assembly. EMBO J *32*, 424-436.

Nishino, T., Takeuchi, K., Gascoigne, K.E., Suzuki, A., Hori, T., Oyama, T., Morikawa, K., Cheeseman, I.M., and Fukagawa, T. (2012). CENP-T-W-S-X forms a unique centromeric chromatin structure with a histone-like fold. Cell *148*, 487-501.

Okada, M., Cheeseman, I.M., Hori, T., Okawa, K., McLeod, I.X., Yates, J.R., 3rd, Desai, A., and Fukagawa, T. (2006). The CENP-H-I complex is required for the efficient incorporation of newly synthesized CENP-A into centromeres. Nat Cell Biol *8*, 446-457.

Overlack, K., Primorac, I., Vleugel, M., Krenn, V., Maffini, S., Hoffmann, I., Kops, G.J., and Musacchio, A. (2015). A molecular basis for the differential roles of Bub1 and BubR1 in the spindle assembly checkpoint. eLife *4*, e05269.

Petrovic, A., Keller, J., Liu, Y., Overlack, K., John, J., Dimitrova, Y.N., Jenni, S., van Gerwen, V., Stege, P., Wohlgemuth, S.*, et al.* (2016). Structure of the MIS12 Complex and Molecular Basis of Its Interaction with CENP-C at Human Kinetochores. Cell *167*, 13.

Petrovic, A., Mosalaganti, S., Keller, J., Mattiuzzo, M., Overlack, K., Krenn, V., De Antoni, A., Wohlgemuth, S., Cecatiello, V., Pasqualato, S.*, et al.* (2014). Modular assembly of RWD domains on the Mis12 complex underlies outer kinetochore organization. Mol Cell *53*, 591-605.

Petrovic, A., Pasqualato, S., Dube, P., Krenn, V., Santaguida, S., Cittaro, D., Monzani, S., Massimiliano, L., Keller, J., Tarricone, A.*, et al.* (2010). The MIS12 complex is a

protein interaction hub for outer kinetochore assembly. The Journal of cell biology *190*, 835-852.

Primorac, I., Weir, J.R., Chiroli, E., Gross, F., Hoffmann, I., van Gerwen, S., Ciliberto, A., and Musacchio, A. (2013). Bub3 reads phosphorylated MELT repeats to promote spindle assembly checkpoint signaling. eLife *2*, e01030.

Putkey, F.R., Cramer, T., Morphew, M.K., Silk, A.D., Johnson, R.S., McIntosh, J.R., and Cleveland, D.W. (2002). Unstable kinetochore-microtubule capture and chromosomal instability following deletion of CENP-E. Dev Cell *3*, 351-365.

Qi, W., Tang, Z., and Yu, H. (2006). Phosphorylation- and polo-box-dependent binding of Plk1 to Bub1 is required for the kinetochore localization of Plk1. Mol Biol Cell *17*, 3705-3716.

Rischitor, P.E., May, K.M., and Hardwick, K.G. (2007). Bub1 is a fission yeast kinetochore scaffold protein, and is sufficient to recruit other spindle checkpoint proteins to ectopic sites on chromosomes. PLoS ONE *2*, e1342.

Rosenberg, J.S., Cross, F.R., and Funabiki, H. (2011). KNL1/Spc105 recruits PP1 to silence the spindle assembly checkpoint. Curr Biol *21*, 942-947.

Ruchaud, S., Carmena, M., and Earnshaw, W.C. (2007). Chromosomal passengers: conducting cell division. Nat Rev Mol Cell Biol *8*, 798-812.

Sacristan, C., and Kops, G.J. (2015). Joined at the hip: kinetochores, microtubules, and spindle assembly checkpoint signaling. Trends Cell Biol *25*, 21-28.

Saffery, R., Irvine, D.V., Griffiths, B., Kalitsis, P., Wordeman, L., and Choo, K.H. (2000). Human centromeres and neocentromeres show identical distribution patterns of >20 functionally important kinetochore-associated proteins. Hum Mol Genet *9*, 175-185.

Samejima, I., Spanos, C., Alves Fde, L., Hori, T., Perpelescu, M., Zou, J., Rappsilber, J., Fukagawa, T., and Earnshaw, W.C. (2015). Whole-proteome genetic analysis of dependencies in assembly of a vertebrate kinetochore. The Journal of cell biology *211*, 1141-1156.

Santaguida, S., Tighe, A., D'Alise, A.M., Taylor, S.S., and Musacchio, A. (2010). Dissecting the role of MPS1 in chromosome biorientation and the spindle checkpoint

through the small molecule inhibitor reversine. The Journal of cell biology *190*, 73-87.

Santaguida, S., Vernieri, C., Villa, F., Ciliberto, A., and Musacchio, A. (2011). Evidence that Aurora B is implicated in spindle checkpoint signalling independently of error correction. EMBO J *30*, 1508-1519.

Saurin, A.T., van der Waal, M.S., Medema, R.H., Lens, S.M., and Kops, G.J. (2011). Aurora B potentiates Mps1 activation to ensure rapid checkpoint establishment at the onset of mitosis. Nat Commun *2*, 316.

Schleiffer, A., Maier, M., Litos, G., Lampert, F., Hornung, P., Mechtler, K., and Westermann, S. (2012). CENP-T proteins are conserved centromere receptors of the Ndc80 complex. Nat Cell Biol *14*, 604-613.

Screpanti, E., De Antoni, A., Alushin, G.M., Petrovic, A., Melis, T., Nogales, E., and Musacchio, A. (2011). Direct binding of Cenp-C to the Mis12 complex joins the inner and outer kinetochore. Curr Biol *21*, 391-398.

Sczaniecka, M., Feoktistova, A., May, K.M., Chen, J.S., Blyth, J., Gould, K.L., and Hardwick, K.G. (2008). The spindle checkpoint functions of Mad3 and Mad2 depend on a Mad3 KEN box-mediated interaction with Cdc20-anaphase-promoting complex (APC/C). The Journal of biological chemistry *283*, 23039-23047.

Shepperd, L.A., Meadows, J.C., Sochaj, A.M., Lancaster, T.C., Zou, J., Buttrick, G.J., Rappsilber, J., Hardwick, K.G., and Millar, J.B. (2012). Phosphodependent recruitment of Bub1 and Bub3 to Spc7/KNL1 by Mph1 kinase maintains the spindle checkpoint. Curr Biol *22*, 891-899.

Silio, V., McAinsh, A.D., and Millar, J.B. (2015). KNL1-Bubs and RZZ Provide Two Separable Pathways for Checkpoint Activation at Human Kinetochores. Dev Cell *35*, 600-613.

Sironi, L., Mapelli, M., Knapp, S., De Antoni, A., Jeang, K.T., and Musacchio, A. (2002). Crystal structure of the tetrameric Mad1-Mad2 core complex: implications of a 'safety belt' binding mechanism for the spindle checkpoint. EMBO J *21*, 2496-2506.

Sivakumar, S., Janczyk, P.L., Qu, Q., Brautigam, C.A., Stukenberg, P.T., Yu, H., and Gorbsky, G.J. (2016). The human SKA complex drives the metaphase-anaphase cell cycle transition by recruiting protein phosphatase 1 to kinetochores. eLife *5*.

Stucke, V.M., Baumann, C., and Nigg, E.A. (2004). Kinetochore localization and microtubule interaction of the human spindle checkpoint kinase Mps1. Chromosoma *113*, 1-15.

Stucke, V.M., Sillje, H.H., Arnaud, L., and Nigg, E.A. (2002). Human Mps1 kinase is required for the spindle assembly checkpoint but not for centrosome duplication. EMBO J *21*, 1723-1732.

Suijkerbuijk, S.J., van Dam, T.J., Karagoz, G.E., von Castelmur, E., Hubner, N.C., Duarte, A.M., Vleugel, M., Perrakis, A., Rudiger, S.G., Snel, B.*, et al.* (2012a). The vertebrate mitotic checkpoint protein BUBR1 is an unusual pseudokinase. Dev Cell *22*, 1321-1329.

Suijkerbuijk, S.J., Vleugel, M., Teixeira, A., and Kops, G.J. (2012b). Integration of kinase and phosphatase activities by BUBR1 ensures formation of stable kinetochore-microtubule attachments. Dev Cell *23*, 745-755.

Tang, Z., Bharadwaj, R., Li, B., and Yu, H. (2001a). Mad2-Independent inhibition of APCCdc20 by the mitotic checkpoint protein BubR1. Dev Cell *1*, 227-237.

Tang, Z., Li, B., Bharadwaj, R., Zhu, H., Ozkan, E., Hakala, K., Deisenhofer, J., and Yu, H. (2001b). APC2 Cullin protein and APC11 RING protein comprise the minimal ubiquitin ligase module of the anaphase-promoting complex. Mol Biol Cell *12*, 3839-3851.

Tang, Z., Shu, H., Oncel, D., Chen, S., and Yu, H. (2004). Phosphorylation of Cdc20 by Bub1 provides a catalytic mechanism for APC/C inhibition by the spindle checkpoint. Mol Cell *16*, 387-397.

Tang, Z., and Yu, H. (2004). Functional analysis of the spindle-checkpoint proteins using an in vitro ubiquitination assay. Methods Mol Biol *281*, 227-242.

Varma, D., Chandrasekaran, S., Sundin, L.J., Reidy, K.T., Wan, X., Chasse, D.A., Nevis, K.R., DeLuca, J.G., Salmon, E.D., and Cook, J.G. (2012). Recruitment of the human Cdt1 replication licensing protein by the loop domain of Hec1 is required for stable kinetochore-microtubule attachment. Nat Cell Biol *14*, 593-603.

Vleugel, M., Hoek, T., Tromer, E., Sliedrecht, T., Groenewold, V., Omerzu, M., and Kops, G.J. (2015). Dissecting the roles of human BUB1 in the spindle assembly checkpoint. Journal of cell science.

Vleugel, M., Tromer, E., Omerzu, M., Groenewold, V., Nijenhuis, W., Snel, B., and Kops, G.J. (2013). Arrayed BUB recruitment modules in the kinetochore scaffold KNL1 promote accurate chromosome segregation. The Journal of cell biology *203*, 943-955.

Wang, F., Dai, J., Daum, J.R., Niedzialkowska, E., Banerjee, B., Stukenberg, P.T., Gorbsky, G.J., and Higgins, J.M. (2010). Histone H3 Thr-3 phosphorylation by Haspin positions Aurora B at centromeres in mitosis. Science *330*, 231-235.

Wang, J., Wang, Z., Yu, T., Yang, H., Virshup, D.M., Kops, G.J., Lee, S.H., Zhou, W., Li, X., Xu, W.*, et al.* (2016). Crystal structure of a PP2A B56-BubR1 complex and its implications for PP2A substrate recruitment and localization. Protein Cell *7*, 516-526.

Waters, J.C., Chen, R.H., Murray, A.W., and Salmon, E.D. (1998). Localization of Mad2 to kinetochores depends on microtubule attachment, not tension. The Journal of cell biology *141*, 1181-1191.

Weir, J.R., Faesen, A.C., Klare, K., Petrovic, A., Basilico, F., Fischbock, J., Pentakota, S., Keller, J., Pesenti, M.E., Pan, D.*, et al.* (2016). Insights from biochemical reconstitution into the architecture of human kinetochores. Nature *537*, 249-253.

Welburn, J.P., Grishchuk, E.L., Backer, C.B., Wilson-Kubalek, E.M., Yates, J.R., 3rd, and Cheeseman, I.M. (2009). The human kinetochore Ska1 complex facilitates microtubule depolymerization-coupled motility. Dev Cell *16*, 374-385.

Welburn, J.P., Vleugel, M., Liu, D., Yates, J.R., 3rd, Lampson, M.A., Fukagawa, T., and Cheeseman, I.M. (2010). Aurora B phosphorylates spatially distinct targets to differentially regulate the kinetochore-microtubule interface. Mol Cell *38*, 383-392.

Wienken, C.J., Baaske, P., Rothbauer, U., Braun, D., and Duhr, S. (2010). Protein-binding assays in biological liquids using microscale thermophoresis. Nat Commun *1*, 100.

Williamson, A., Wickliffe, K.E., Mellone, B.G., Song, L., Karpen, G.H., and Rape, M. (2009). Identification of a physiological E2 module for the human anaphase-promoting complex. Proceedings of the National Academy of Sciences of the United States of America *106*, 18213-18218.

Yamagishi, Y., Honda, T., Tanno, Y., and Watanabe, Y. (2010). Two histone marks establish the inner centromere and chromosome bi-orientation. Science *330*, 239-243.

Yamagishi, Y., Yang, C.H., Tanno, Y., and Watanabe, Y. (2012). MPS1/Mph1 phosphorylates the kinetochore protein KNL1/Spc7 to recruit SAC components. Nat Cell Biol *14*, 746-752.

Yamaguchi, M., VanderLinden, R., Weissmann, F., Qiao, R., Dube, P., Brown, N.G., Haselbach, D., Zhang, W., Sidhu, S.S., Peters, J.M., *et al.* (2016). Cryo-EM of Mitotic Checkpoint Complex-Bound APC/C Reveals Reciprocal and Conformational Regulation of Ubiquitin Ligation. Mol Cell *63*, 593-607.

Yamamoto, T.G., Watanabe, S., Essex, A., and Kitagawa, R. (2008). SPDL-1 functions as a kinetochore receptor for MDF-1 in Caenorhabditis elegans. The Journal of cell biology *183*, 187-194.

Yang, M., Li, B., Liu, C.J., Tomchick, D.R., Machius, M., Rizo, J., Yu, H., and Luo, X. (2008). Insights into mad2 regulation in the spindle checkpoint revealed by the crystal structure of the symmetric mad2 dimer. PLoS Biol *6*, e50.

Ye, Q., Rosenberg, S.C., Moeller, A., Speir, J.A., Su, T.Y., and Corbett, K.D. (2015). TRIP13 is a protein-remodeling AAA+ ATPase that catalyzes MAD2 conformation switching. eLife *4*.

Zachariae, W., Schwab, M., Nasmyth, K., and Seufert, W. (1998). Control of cyclin ubiquitination by CDK-regulated binding of Hct1 to the anaphase promoting complex. Science *282*, 1721-1724.

Zaytsev, A.V., Mick, J.E., Maslennikov, E., Nikashin, B., DeLuca, J.G., and Grishchuk, E.L. (2015). Multisite phosphorylation of the NDC80 complex gradually tunes its microtubule-binding affinity. Mol Biol Cell *26*, 1829-1844.

Zaytsev, A.V., Sundin, L.J., DeLuca, K.F., Grishchuk, E.L., and DeLuca, J.G. (2014). Accurate phosphoregulation of kinetochore-microtubule affinity requires unconstrained molecular interactions. J Cell Biol *206*, 45-59.

Zhang, G., Kelstrup, C.D., Hu, X.W., Kaas Hansen, M.J., Singleton, M.R., Olsen, J.V., and Nilsson, J. (2012). The Ndc80 internal loop is required for recruitment of the Ska complex to establish end-on microtubule attachment to kinetochores. Journal of cell science *125*, 3243-3253.

Zhang, G., Lischetti, T., Hayward, D.G., and Nilsson, J. (2015). Distinct domains in Bub1 localize RZZ and BubR1 to kinetochores to regulate the checkpoint. Nat Commun *6*, 7162.

Zhang, G., Lischetti, T., and Nilsson, J. (2014). A minimal number of MELT repeats supports all the functions of KNL1 in chromosome segregation. Journal of cell science *127*, 871-884.

Zhang, G., Mendez, B.L., Sedgwick, G.G., and Nilsson, J. (2016). Two functionally distinct kinetochore pools of BubR1 ensure accurate chromosome segregation. Nat Commun *7*, 12256.

Zhu, T., Dou, Z., Qin, B., Jin, C., Wang, X., Xu, L., Wang, Z., Zhu, L., Liu, F., Gao, X., *et al.* (2013). Phosphorylation of microtubule-binding protein Hec1 by mitotic kinase Aurora B specifies spindle checkpoint kinase Mps1 signaling at the kinetochore. J Biol Chem *288*, 36149-36159.